Optimization of Minimum Quantity Cooling/Lubrication Machining of Composites through Flow Visualization

Youssef Iskandar

Department of Mechanical Engineering
McGill University, Montreal
April, 2013

A thesis submitted to McGill University in partial fulfillment of the requirements of the degree of Master of Engineering

Abstract

Modern machining involves more dependence on green manufacturing techniques. Minimum Quantity Cooling Lubrication (MQCL) of machining processes has replaced conventional flood cooling in many applications, involving various materials and cutting conditions. The use of this technique results in considerable reductions in the quantity of lubricant used, reducing manufacturing costs as well as the impact of the process on the environment. With the objective of achieving a fuller understanding of this technology, an interest has been taken in the properties of the aerosol, and their impact on machining performance. This study presents an attempt to understand these properties through the use of experimental and numerical flow visualization techniques, followed by machining experiments. The Particle Image Velocimetry study revealed how the MQCL nozzle geometry and the injection parameters (air and lubricant flow rates) which control the Sauter Mean Diameter (SMD) of the resulting droplets, affect the flow, and that droplets with smaller SMD are more capable of following the air flow. Computational Fluid Dynamics simulations showed that a single-phase (air only) simulation is sufficient in describing the flow, when comparing the simulation and experimental (real flow) PIV results. They also revealed that the potential thermal benefits of the air flow can be achieved if the nozzle orientation vis-à-vis a model tool is exploited. Comparisons of MQCL with conventional flood cooling and dry machining modes in milling of Carbon-Fibre Reinforced Plastics (CFRP) revealed that the benefit of MQCL (namely lower tool wear and higher geometric accuracy of the machined part), can be achieved if the atomization parameters are set for appropriate lubrication and SMD size.

Résumé

L’usinage moderne implique plus de dépendance des techniques de manufacture verte. La micro-lubrification (Minimum Quantity Cooling Lubrication) des processus d’usinage a remplacé l’arrosage conventionnel dans le cas de plusieurs applications, impliquant des matériaux et des conditions d’usinage variés. L’usage de cette méthode mène à des réductions considérables de la quantité de lubrifiant utilisé, réduisant ainsi les coûts de fabrication ainsi que l’impact du processus sur l’environnement. Un intérêt a été porté aux propriétés de l’aérosol, et leurs effets sur la qualité de l’usinage, ayant pour objectif une meilleure compréhension de cette technologie. Cette étude est une tentative de mieux comprendre ces propriétés à travers l’usage des techniques de visualisation de débit expérimentaux et numériques, suivis par des essais d’usinage. L’étude Particle Image Velocimetry (PIV) a démontré comment la géométrie de la buse el les paramètres d’injection (débits d’air et de lubrifiant) qui contrôlent la taille du diamètre moyen de Sauter (SMD) des gouttelettes résultantes, affectent le débit, mais aussi que les bulles ayants les tailles SMD les plus petites sont les plus efficace lorsqu’il s’agit de suivre le débit de l’air. Des essais numériques (Computational Fluid Dynamics) ont démontré que des simulations monophasiques (air seulement) sont suffisantes pour bien décrire le débit, en comparant avec les résultats du PIV (débit réel). Ils ont aussi démontré que les avantages thermiques de l’air peuvent être obtenus si la position de la buse vis à vis de l’outil est exploitée. Des comparaisons entre l’MQCL et de arrosage conventionnel et usinage à sec lors d’essais de fraisage de plastique à renfort fibre de carbone (PRFC) ont montré que les avantages de l’MQCL, notamment un usage réduit et une plus grande efficacité géométrique de la pièce usinée, peuvent être obtenus si les paramètres d’atomisation sont choisis pour une lubrification suffisante et taille SMD appropriée.

Acknowledgements

First and foremost, I would like to express my immense gratitude to my supervisors Dr. Helmi Attia and Dr. Vincent Thomson, for their support and guidance to me in this work. I feel incredibly lucky to have worked under Prof. Attia's supervision; his passion about his work will always continue to be my inspiration, in addition to his unending patience. His personal interest in the welfare of his students, and his personal mission in educating new researchers interested in creating knowledge, and capable of critical thinking, make him even more unique. An important part of my work was conducted under the supervision of Dr. Patrick Hendrick of Tecnolub Inc, in Brussels, Belgium. My flow visualization studies would not have taken place without his assistance and that of his student, Christophe Diakodimitris. Funding for this work was provided through the MITACS Accelerate program, in partnership with Tecnlub Inc. I would therefore like to thank them for this great opportunity and industrial experience.

I would also like to thank Prof. Attia for permitting me to perform my machining experiments at the Aerospace Manufacturing Technology Center of the National Research Council of Canada. The members of the Material Removal group always treated me as family. In particular, Ahmed Damir, who helped me take the first steps in machining research, spending much of his personal time. Mouhab Meshreki, whose critique and questioning always led me to more revelations and more questioning, and finally, Ahmed Sadek, whose knowledge of composites often provided me with much needed help. I must also give thanks to Nick DePalma and Patrick Tremblant, the machinists of the AMTC's Material Removal group; my CNC experiments would not have been realized without their help.

Last but not least, I would like to thank my parents. It is thanks to them that I am now capable of making an accomplishment such as this one. I hope to make of this work a celebration after years of guidance, patience and giving.

Table of Contents

List of Figures

List of Tables

Nomenclature

Capital Letter Symbols

C	Turbulent constant
C_p	Coefficient of pressure
D	Droplet diameter (μm)
E	Turbulent Yang-Shih term
Fx	Measured machining force in the X direction (N)
Fy	Measured machining force in the Y direction (N)
Fz	Measured machining force in the Z direction (N)
L	Characteristic length (m)
N	Tool rotational speed (rpm)
Nu	Nusselt Number
Oh	Ohnesorge number
P	Turbulence production
Pa	Atmospheric pressure (N/m^2)
Q	Second invariant of the vorticity tensor
Q_g	Volumetric gas flow rate (m^3/s)
Q_l	Volumetric liquid flow rate (m^3/s)
R_a	Average surface roughness (μm)
Re	Reynolds number
R_z	Surface roughness depth (μm)

S	Strain rate tensor
T	Turbulent time scale
Tz	Measured machining torque in the Zm direction (N/m^2)
Va, Q_g	Volumetric air flow rate (l/min)
V_B	Tool wear (µm)
Vc	Cutting speed (m/min)
V_f	Feed speed (mm/min)
V_{max}	Maximum droplet displacement velocity (m/s)
Vo	Volumetric oil flow rate (ml/min)
Vx	Stream-wise jet velocity (m/s)
We	Weber number
X	Rosin-Rammler parameter
Φ	Droplet volume fraction (m^3/m^3)
Ω	Vorticity tensor

Small Letter Symbols

c	Damping function constant
d	Droplet diameter (µm)
d_0	Liquid channel diameter (mm)
d_{32}	Sauter Mean Diameter (µm)
d_l	Liquid channel diameter (mm)
d_{max}	Maximum droplet displacement (m)
f,	Feed speed (mm/min)

f_μ	Yang-Shih damping function
h	Coefficient of convective heat transfer (W/m^2.K)
k_f	Coefficient of thermal conductivity (W/m.K)
I	Initial turbulence intensity (%)
m	Oil/air mass flow rate ratio
m_g, m_a	Gas mass flow rate (kg/s)
m_l	Liquid mass flow rate (kg/s)
q	Distribution width parameter
t	Time (s)
u_g	Gas exit velocity (m/s)
u_l	Liquid exit velocity (m/s)
u_r	Relative air-oil velocity (m/s)
ε	Turbulence kinetic energy dissipation (m^2/s^3)
θ	Angle (º)
κ	Turbulence kinetic energy (m^2/s^2)
μ	Dynamic viscosity (N·s/m^2)
ν	Kinematic viscosity (m^2/s)
ρ_a	Gas density (kg/m^3)
ρ_l	Liquid density (kg/m^3)
σ	Surface tension (N/m)
$\overrightarrow{\nu''}$	Velocity tensor (m/s)

Subscripts

a	Droplet size parameter
b	Droplet size parameter
i	Index for individual droplets
t	Turbulent quantities term
ε	Turbulence kinetic energy dissipation term
κ	Turbulence kinetic energy term

Abbreviations

GLR	Air/oil mass flow rate ratio (kg/kg)
SMD	Sauter Mean Diameter (μm)

Chapter 1 Introduction

Modern trends in manufacturing are steering the machining processes towards higher speeds, lower waste and improved product quality. Material removal rates between 150 – 1,500 cm^3/min can now be achieved for most materials. Tools and coatings with hardness up to 9,000 HV commercially exist, and the use of Computer Numerical Control (CNC) machines allows for accuracies down to 10 μm [1]. Adequate cooling and lubrication of high speed cutting processes is necessary due to the high thermal and physical stresses generated which have an impact on the tool life, the quality of the finished workpiece and the power consumption. In addition, as material is cut a fresh high energy surface is generated and quickly reacts with the surroundings like oxygen and water in humid air. The use of cutting fluids provides protection from these reactions, which may negatively affect the quality of the finished surface. A secondary function of cutting fluids is chip disposal [2].

The demand for greener manufacturing has been the primary drive for research on technologies that reduce cutting fluid consumption. The conventional method of heat disposal in machining with flood cooling/lubrication is becoming increasingly unacceptable, as it represents an economical and environmental burden. In addition to being a health hazard, it is estimated that the price of conventional cooling makes up to 17% of manufacturing costs, much higher than the cost of tooling estimated as 4% [1]. Dry machining along with the optimization of cutting tool design to fit specific operations has been employed as a solution to eliminate the need for cutting fluids. Near-dry or Minimum Quantity Cooling Lubrication (MQCL) machining has been observed to provide significant reduction in cutting fluid consumption compared to conventional flood cooling, as well as an increase in machinability when compared with dry machining. Cases where the heat generated in dry machining assists in reducing friction and forces through material softening exist, though the application is limited to non-ductile materials. Dry machining of ductile materials like some aluminum alloys results in high adhesive wear, due to the elevated temperatures. This is a case where completely dry machining is not possible, but where MQCL offers a middle solution with much less environmental impact. MQCL machining thus offers a link between conventional cooling and dry machining, and its application has been proved successful particularly in high speed machining [1, 3-8] .

1.1 Minimum Quantity Cooling Lubrication Design Considerations

MQCL machining involves a cutting fluid delivery method where the fluid, typically a straight biodegradable oil, is fed to the cutting zone in quantities between 0.2 and 30 ml/min [3], much less than conventional flood cooling where the flow rates usually range between 4 x 10^3 and 4 x 10^4 ml/min [9]. The fluid is fed either in the form of a rapid succession of droplets, or with the assistance of a transporting medium, i.e. air or CO_2, as an aerosol spray [10]. The delivery of the cutting fluids in near-dry machining can be achieved in two methods (Figure 1.1 and Figure 1.2):

1- Externally, via one or more nozzles directed at the cutting zone. External supply systems are more suitable in milling, turning, grinding and sawing operations when there are no obstructions to the flow close to the cutting zone, or when the tools are not equipped with internal supply channels [11]. This system has a low cost of installation in addition to its easier integration with existing machines.

2- Internally, via built-in channels in the tool, the chuck or the spindle. The internal supply system ensures the cutting fluid is available close to the cutting edge. This is useful in applications where external supply would be obstructed or inefficient, such as the cases of drilling, reaming, boring or tapping of holes of large length to diameter ratios (typically $\frac{Length}{Diameter} > 3$). These operations would normally require the tool to be withdrawn during the machining process to ensure adequate lubrication and/or cooling, interrupting the cutting and increasing the production time. In addition to the aforementioned advantages, the internal delivery eliminates the potential nozzle orientation errors, but the installation is more costly than in the case of external delivery and might not be possible for all machines. It also requires the development of special tools, which are more costly than conventional ones.

A second distinction could be made among MQCL systems; the supply of the lubricant to the nozzles can be fed via a single channel, containing the mixture of the gas and atomized fluid, or via two channels in which case the mixing occurs directly ahead of the tool (Figure 1.1) using an atomizer nozzle. Atomizer nozzles, such as Airblast nozzles have been studied extensively through their applications in fields outside of machining (e.g. internal combustion engines) [12], and correlations for predicting the flow characteristics exist for many of the nozzle geometries [13].

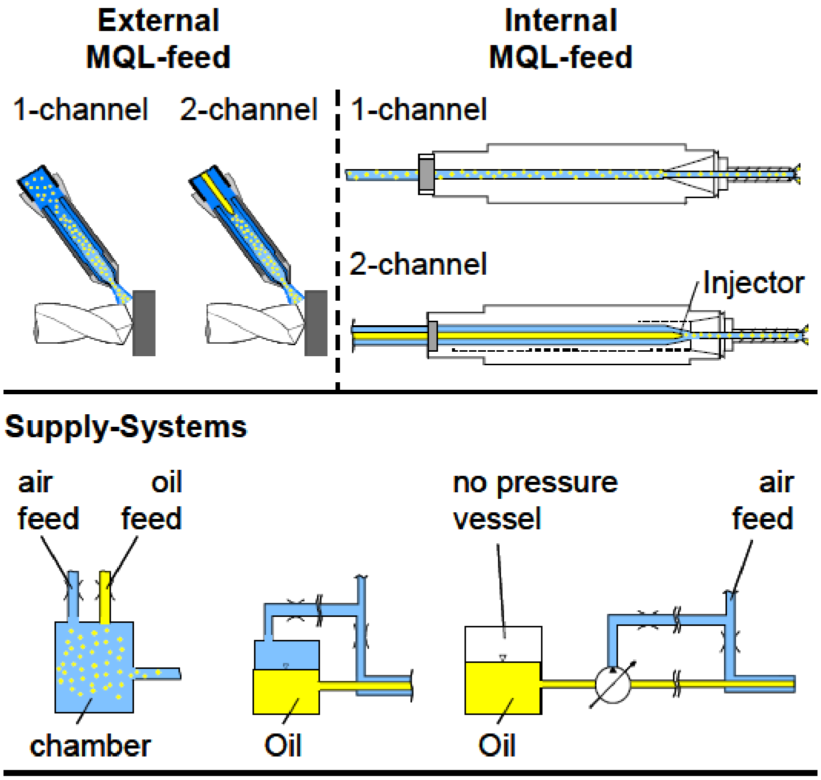

Figure 1.1 1-channel and 2-channel MQCL supply systems [3]

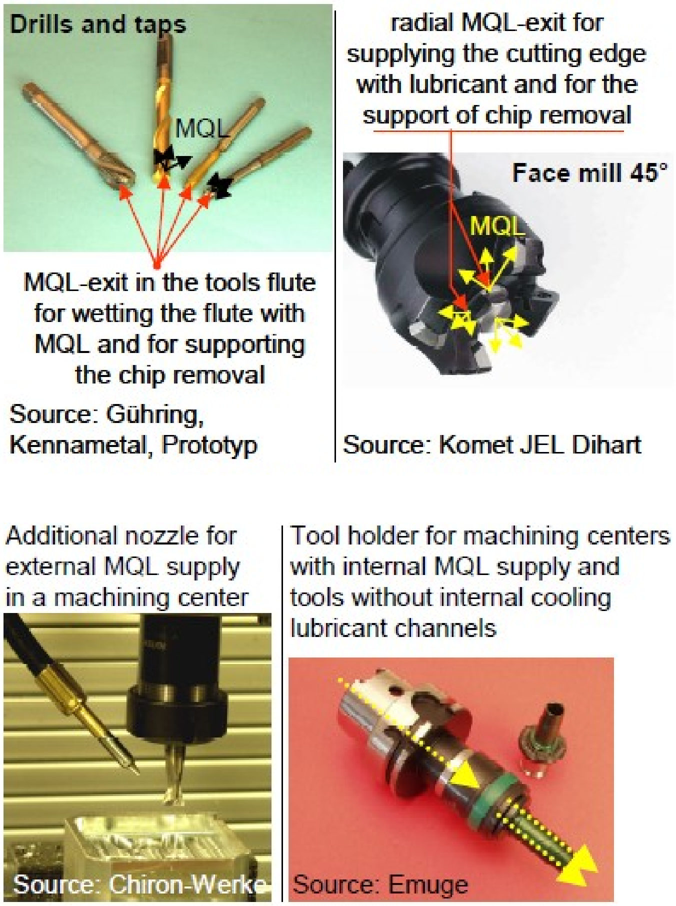

Figure 1.2 Different MQCL liquid delivery systems [3]

In the literature reviewed, nozzle and atomization characteristics are rarely considered [3], though it is easy to see how the properties of the aerosol droplets and the flow behaviour could have a major impact on MQCL application in machining. The variety in nozzle designs also dictates case-specific studies of its flow characteristics and the parameters that control them (pressures/flow rates).

1.2 Minimum Quantity Lubrication and Cooling

For conventional flood cooling, the cutting fluids are typically pure oils and emulsions of water and oil, dispensed at rates between 4 x 10^3 and 4 x 10^4 ml/min close to the tool-chip interface. They are often used in a cycle up to a point where the fluid loses its desired properties, due to oxidation or change in viscosity, becoming irreversibly contaminated with wear particles and chips [14].

The function of cutting fluids is dependent on the cutting speed. At low speeds, the fluid penetrates the tool-chip interface creating boundary lubrication, which reduces the effects of adhesive friction and wear as the contact area of the mating workpiece and tool is reduced. At high speeds, the penetration of the tool-chip interface might not be possible using flood cooling; the fluid simply carries away the heat generated in the cutting process through the removal of hot chips formed during cutting. The lubricating properties of flood cooling thus decrease with increasing cutting speeds since less fluid penetrates the tool-chip interface. Such effects are less pronounced in the case of MQCL, since the velocity of the droplets and the carrying air mixture is higher. The higher air-lubricant mixture velocity results in more lubricant/coolant presence near the interface, and thus compensates for the reduced amount of oil dispensed [3]. Furthermore, the high temperatures in the cutting zone might evaporate the liquid droplets, which in this case penetrate the tool-chip interface in vapor phase [2, 3, 15].

While lubrication is necessary in controlling friction and by consequence the heat generation, more cooling is required in cases where heat generation considerably affects the machining quality, and where more temperature control is needed. These high temperatures are due to the fact that nearly all work done in a machining process is transformed into heat. In a metal cutting operation, the primary heat source is the result of the plastic deformation work at the shear plane, the boundary between deformed and undeformed material. The secondary heat source is located at the tool-chip interface, as a result of the secondary plastic deformation work, as well as friction. A tertiary heat source could result from friction at the tool flank-workpiece interface, such as the case of a worn tool edge [2, 16, 17].

Pure oils, when used as the MQCL cutting fluid, reduce friction and adhesion between the tool and the workpiece due to their superior lubricating properties. This, of course, reduces the heat generated in the cutting process, but only to a certain limit [3]. In cases where cutting results in excessive heat generation, pure oils are replaced by emulsions; due to the higher water content they possess a higher heat capacity than pure oils. The near-dry lubrication process in this case is referred to as Minimum Quantity Cooling (MQC), making MQC distinct from Minimum Quantity Lubrication (MQL), where usually pure oil is used. Of the two distinctions, MQC remains largely unexplored even though it could provide solutions to processes with high heat generation [3].

The abundant presence of a gas also presents an enhancement to the MQCL process, as cutting fluids are not restricted to liquids. Humid air and oxygen can in some cases assume the function of the liquid cutting fluid, and this is essentially the case during dry machining. In metal cutting, oxygen can prevent the formation of a built-up edge (BUE) by contaminating the tool surface through adsorption [18]. The efficiency of MQCL fluids is also enhanced when their composition permits more adsorption on the tool and workpiece surfaces. Again, the abundant presence of gas in MQCL has an advantage as it was also found that oxygen improves the adsorption activity of certain lubricants (Figure 1.3) [11, 19, 20].

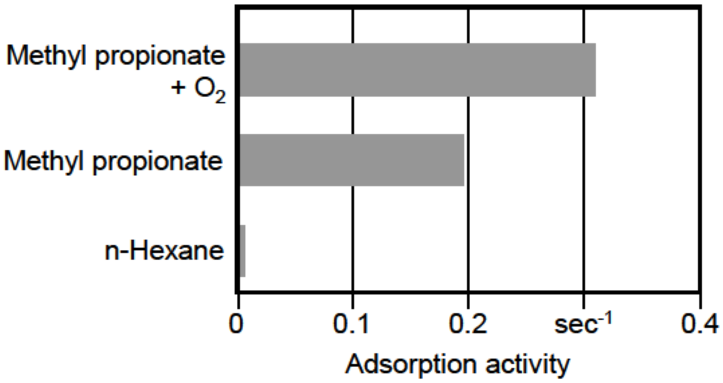

Figure 1.3 Effect of oxygen on the adsorption behaviour of lubricants [20]

Fatty alcohols, vegetable oils and synthetic esters are common MQCL lubricants and they are employed depending on the type of supply system, workpiece material and the process (Table 1.1) [3]. Additives to the cutting fluids are often introduced to enhance specific properties; anti-wear and extreme pressure (EP) additives, as well as the introduction of nano-sized particles to the cutting fluids (nano-fluids), are all currently being investigated for the use in MQCL machining [21-24]. Other studies exploit the solubility of some vegetable oils in CO_2, in an effort to enhance the use of high pressure vapor-phase lubricants in machining [25].

Currently, work is being done to optimize the use of cryogenic cooling, with liquid nitrogen as the cutting fluid (without a carrying gas), in MQCL machining operations. This has proved effective in maintaining the cutting temperatures below those of tool material softening, and it is particularly useful for cutting hard materials with low thermal conductivity, such as titanium alloys and Inconel [26].

Table 1.1 Areas of application of MQCL fluids [3]

Synthetic Esters	**Fatty Alcohols**
Applications in machining	
• Primarily reduction of friction • When high surface qualities are demanded • Adhesive workpiece materials (Built-up edge, apparent chips) • Low cutting speeds and high specific area load • Lubrication of supporting and/or guiding rails	• Primarily heat removal • Examples are: sawing, turning and milling of gray cast iron, machining of cast aluminum alloys

In addition to their tribological properties and effect on the cutting performance (i.e. adsorption behaviour, heat capacity…etc.), MQCL fluids are also selected based on their biodegradability (Table 1.2) [3]. From a practical point of view, the cutting fluids used in MQCL need to be storable for long periods of time, as they are only used in minimal quantities. In the storage containers, the temperatures can rise up to 70º C and therefore the fluids need to withstand this environment for long periods, without degradation. They also need to have a good oxidation resistance, so as to avoid the formation of an adhesive layer, in case they are left on the equipment.

Table 1.2 Properties of MQCL Fluids [3]

Synthetic Esters	**Fatty Alcohols**
• Chemically modified vegetable oils	• Long-chained alcohols made from natural raw materials or mineral oils
• Good biodegradability • Low level of hazard to water • Toxicologically harmless	
• High flash and boiling point with low viscosity • Very good lubrication properties • Good corrosion resistance • Inferior cooling properties • Vaporizes with residuals	• Low flash and boiling point, comparatively high viscosity • Poor lubrication properties • Better heat removal due to evaporation • Little residuals

Chapter 2 Critical Literature Review

It is clear that the applicability of near-dry machining will depend on the process, the cutting conditions (cutting speed, chip thickness), the tool material and geometry (insert, coating), the workpiece material, and the MQCL supply parameters (internal, external, flow rates, type of fluid). In high speed machining, wear regimes are either mechanically activated such as adhesion, abrasion, and fatigue, or thermally activated such as diffusion, all contributing to tool life reduction. Other forms of wear exist, such as erosion (chemical wear) and micro-chipping [24]. Although they are often present in combinations, the dominant wear regime varies with the aforementioned machining conditions.

The following sections review the recent studies on the application of MQCL machining in drilling, milling, turning, and grinding, comparing the MQCL machining performance with conventional flood lubrication and dry machining. The performance is evaluated by comparing cutting temperatures, cutting forces, tool wear, and machining quality under the different machining conditions. Unless otherwise specified, external MQL with pure oil is applied in all of the reviewed experiments.

2.1 Application of MQCL to Various Machining Processes

2.1.1 Drilling

In drilling operations, the cutting is performed at the lip of the drill bit using a chisel and two cutting edges, in the case of twist drills. The process is used to generate circular holes in the workpiece and the material removal rate varies with the cutting speed and axial feed of the tool. Similar processes like boring, tapping and threading have been performed with MQL as the lubrication technique [3].

Bhowmick et al. [23] compared the effects of distilled water and fatty alcohols with extreme pressure (EP) additives, as MQCL fluids (10 ml/h), in the short hole drilling ($\frac{Length}{Diameter} < 3$) of a magnesium alloy (AM60), at a speed of 50 m/min and a feed of 0.25 mm/rev, using HSS drills. They concluded that MQL drilling using the alcohol resulted in the lowest maximum torques, thrust forces and temperatures, followed by water (10 ml/h), emulsion (30 l/h) and dry drilling. The same trends were observed in the measurements of average surface roughness of the workpiece (Figure 2.1) [23], and of the amount of adhered magnesium on the tool surfaces. Furthermore, MQL machining with the fatty alcohol resulted in more uniform drilling torque and thrust curves than flood and dry cutting, due to the lower adhesion of magnesium.

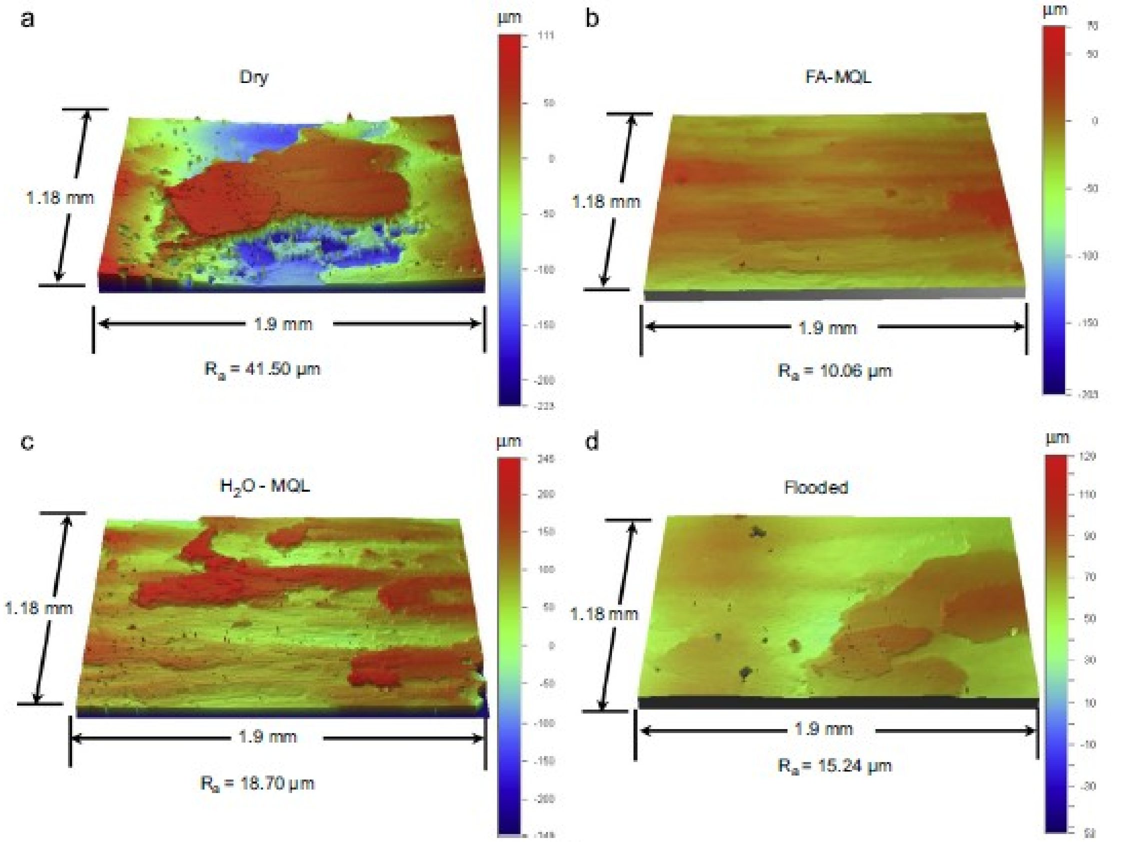

Figure 2.1 Three-dimensional optical surface profilometery images of typical surfaces for (a) Dry drilling; (b) MQL drilling (Fatty Alcohol); (c) MQC drilling (H_2O); (d) Flood cooled drilling [23]

Heinmann et al. [27] applied interrupted MQL (18 ml/h), MQC (18 ml/h), and dry deep hole drilling ($\frac{Length}{Diameter} = 10$) of carbon steel (0.45% carbon). The drilling was conducted at a cutting speed of 26 m/s and feed of 0.26 mm/rev, using uncoated HSS tools and HSS tools with TiN/TiAlN coatings. The effects of the different tribological environments on torque and tool life were examined. The lowest torque values were obtained with the TiAlN coated tool. It was also found that due to the elevated temperatures in dry drilling, a high hot hardness tool coating was necessary to reduce the excessive tool wear. Of the three types of fluids that were compared (ester, ester + alcohol, ester + water), the less viscous lubricant with higher water content (ester + water) was most efficient in reducing temperatures, while easily penetrating the cutting region.

Tasdelen et al. [28] examined the effect of internal/through spindle MQL flow parameters, in the short hole drilling of precipitation hardened steel, using a carbide tool. Flow rates of 5 ml/h, 15 ml/h and 23 ml/h were used, with air pressures of 6.2 bar, 5.2 bar and 4 bar, respectively. The cutting speed used was 155 m/min, and the feed was 0.11 mm/rev. The performance on MQL was compared with that of compressed air and flood cooled drilling. It was found that the use of flood emulsion resulted in lower cutting forces and torques as well as lower surface roughness (R_z) values than the cases of MQL or air, while MQL drilling with an oil flow rate of 23 ml/h resulted in the lowest tool wear.

Zeilmann et al. [29] compared the effects of internal and external application of MQL in the drilling ($\frac{Length}{Diameter} < 3$) of a titanium alloy (Ti-6Al-4V), at speeds between 10 and 50 m/min, feeds between 0.1 and 0.2 mm/rev, with coated and uncoated carbide tools (K10). The most stable behaviour of cutting temperatures was observed when applying conventional cooling internally, followed by internal MQL and dry cutting. The higher temperatures obtained when applying internal MQL had a positive effect in reducing the feed forces when compared with internally supplied flood cooling, but adverse effects were obtained with dry cutting due to excessive chip entanglement at high temperatures. However, the maximum temperatures obtained when applying internal MQL were 50% lower than those with external MQL.

Bhowmick et al. [30] used diamond-like-carbon-coated (DLC) drill bits in the drilling ($\frac{Length}{Diameter} < 3$) of an aluminum-silicon alloy (319 Al), at a speed of 50 m/min and feed of 0.25 mm/rev. They compared thrust force and torque values when machining dry, with distilled water as the MQL fluid (30 ml/h), and with emulsion flood cooling (30,000 ml/h). The results obtained showed comparable thrust force and torque values for flood cooling and MQL. Applying MQL in drilling resulted in considerably lower adhesion levels as well as more stable cutting forces, when compared with dry drilling. The results also highlighted the better performance of non-hydrogenated DLC coated drills, compared to hydrogenated DLC coated drills, in terms of thrust force, torque, and Buit-Up-Edge (BUE) formation, when water MQL is used.

Braga et al. [31] performed similar experiments comparing DLC coated and uncoated tools. An aluminum silicon alloy (SAE 323) was drilled under MQL with a mineral oil at a flow rate of 10 ml/h, air pressure of 4.5 bar, as well as under emulsion flood cooling at a flow rate of 2,400 l/h. The cutting speed was constant at 300 m/min, and the feeds varied between 0.1 and 0.2 mm/rev. It was observed that on DLC coated tools, the flank wear when using MQL was higher than with the use of flood cooling. The flank wear in the case of the uncoated carbide tool was similar, however, under both cooling systems. Finally, when comparing the hole quality, the holes drilled under MQL were of better or comparable quality to those obtained with flood cooling, regardless of the tool coating (Figure 2.2) [31].

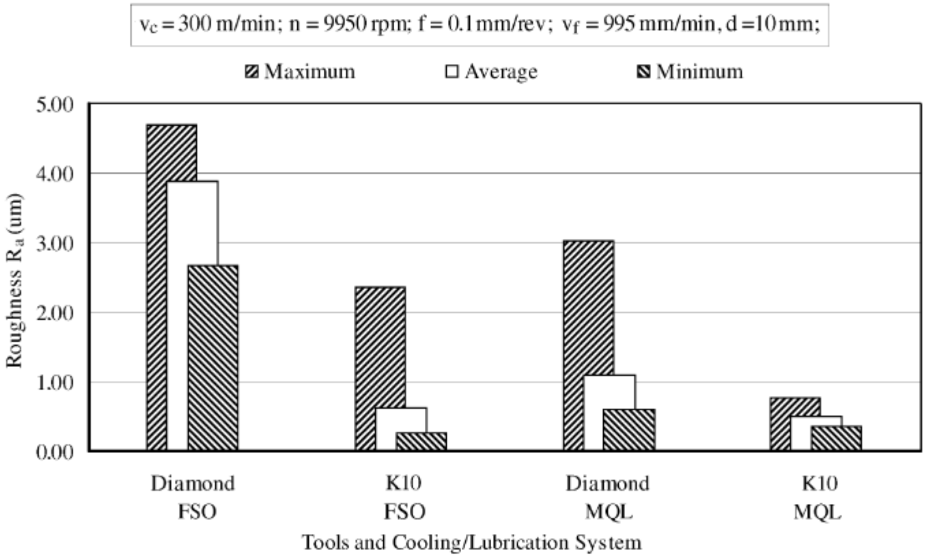

Figure 2.2 Comparison of the average surface roughness of the drilled hole surfaces under MQL and Flood Cooling [31]

2.1.2 Milling

Milling is a material removal process that applies to various operations such as planning, slotting, routing, and orbital drilling. In end-milling, the cutting is performed at the tip as well as the sides of the end-mill, thus the lubrication system must supply all these areas if adequate lubrication is necessary.

Yan et al. [32] investigated the significance of the MQL injection parameters on the milling of 50CrMnMo steel. Tests were conducted at a cutting speed of 220 m/min and a feed of 0.14 mm/tooth. The axial depth of cut used was 0.5 mm, and the radial depth of cut was 8 mm. The oil flow rate was varied between 13.9 and 58.4 ml/h, and the air pressure was varied between 2 and 6 bar. Within this range, the change in oil flow rate had negligible effects on flank wear, except at the lower levels. The increase in air flow rate led to a reduction in tool wear, reportedly due to better chip removal and the improved penetration of the flow to the cutting zone. Comparison of MQL with dry and flood cooling conditions showed that MQL produced the lowest tool flank wear (Figure 2.3) [32] and average roughness of the machined surface.

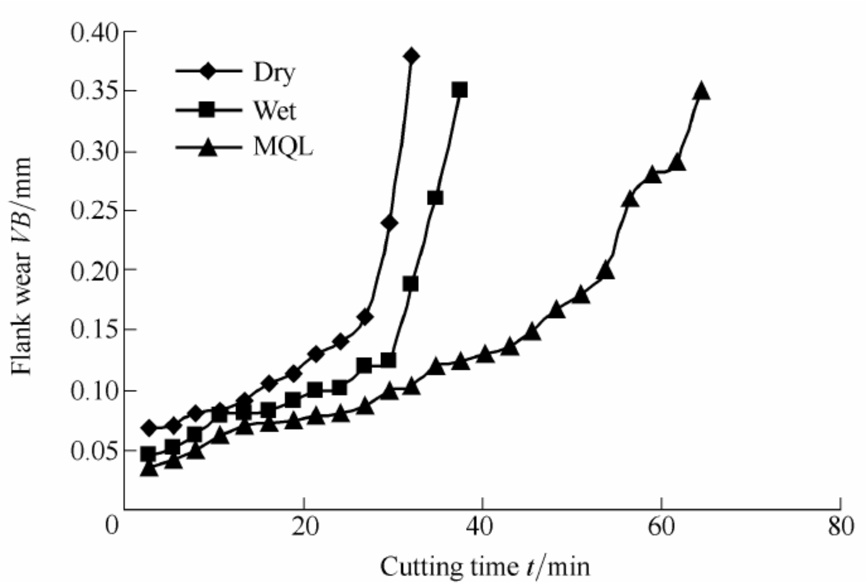

Figure 2.3 Increase of flank Wear V_B with cutting time under different lubrication environments (Vc= 219.8 m/min) [32]

Rahman et al. [33] applied MQL in low speed milling of steel (ASSAB 718 HH). In these tests, MQL was applied using a mineral oil with anti-wear and extreme pressure additives, at flow rate of 8.5 ml/h and air pressure of 5.2 bar. Tests were performed at a constant depth of cut (0.35 mm), with speeds in the range of 75 and 125 m/min, and feeds between 0.01 and 0.03 mm/tooth. Considerable reduction in cutting forces and thermal stresses in the case of MQL, compared to flood and dry cutting, was observed. No catastrophic tool failure occurred in the case of MQL, in contrast with flood cooled and dry cutting. In addition, the lowest amount of burr formation was obtained using MQL.

In a similar study, but at higher speeds, Liao et al. [6] used an oil flow rate of 10 ml/h and air pressure of 4.5 bar, as MQL flow parameters in the milling of hardened steel (NAK80). Tests with TiAlN and TiN coated carbide tools were conducted at speeds between 150 and 250 m/min, and feeds between 0.1 and 0.2 mm/tooth. The axial depth of cut and the radial depth of cut were 0.6 mm and 5 mm, respectively. The same conditions were used in tests with dry and flood coolant (20 l/min), in order to study the feasibility of MQL using biodegradable esters. The results showed that the lowest cutting forces were in the case of flood coolant, followed by MQL and dry cutting. The lowest tool wear values, however, were obtained under MQL, while flood cooling resulted in thermal cracking in the tool. The higher thermal wear in cutting tools at high speeds resulted in higher surface roughness values in the workpiece, when flood cooling was used. This trend was reversed at lower speeds, where flood cooling proved superior than MQL, making MQL a more suitable cooling method for high speed machining.

Kishawy et al. [24] applied MQL (synthetic ester with EP additives) in milling of cast aluminum-silicon alloy (A356). Tests were conducted at speeds up to 5,225 m/min, using diamond coated and uncoated carbide inserts. The study was aimed at comparing MQL with flood and dry machining, in terms of tool life, cutting forces, and machined surface quality. The results showed that the cutting forces in the case of MQL and flood cooling were similar up to a speed of 2,000 m/min, beyond which flood cooling becomes superior in reducing cutting forces. As expected, dry machining exhibited the highest cutting forces. MQL cutting minimized the difference in the chip thickness ratio between sharp and worn tools. Also the lowest volume of adhered aluminum was obtained in the case of the MQL environment.

Hwang et al. [34] evaluated the machinability of aluminum (Al6061) in milling tests using MQL (vegetable oil) and flood as the mode of lubrication. Analysis of Variance (ANOVA) was used to evaluate the importance of the different parameters on the surface roughness and cutting forces. The results showed that the cutting forces were largely dependent on the cutting parameters, as opposed to the mode of lubrication. The surface roughness values, however, were dependent on all the cutting conditions. Little difference in cutting forces was found, but the roughness values were lower in the case of MQL, consistent with previous studies.

Sun et al. [35] compared tribological environments using titanium (Ti-6Al-4V) as the workpiece material. Tests were conducted using dry, flood, and vegetable oil MQL with flow rates between 2 and 10 ml/h and air pressure of 5.2 bar. All tests were carried out at speeds between 40 and 140 m/min, feeds of 0.05 to 0.2 mm/rev, axial depth of cut of 0.5 mm, and radial depths of cut between 2 and 8 mm. The MQL supply was efficient in reducing the tool adhesion levels, which was the main wear mechanism, and was strongly dependent on the coolant supply method. MQL led to significantly longer tool life, particularly at higher speeds, while flood cooling was ineffective even when compared to dry cutting (Figure 2.4) [35]. The use of MQL also resulted in lower levels of thermal cracking in the tool, compared to flood and dry machining, due to the lower temperature gradients which were significant in the case of flood cooling. The lower tool wear rate in the case of MQL also had a strong impact on reducing the cutting forces.

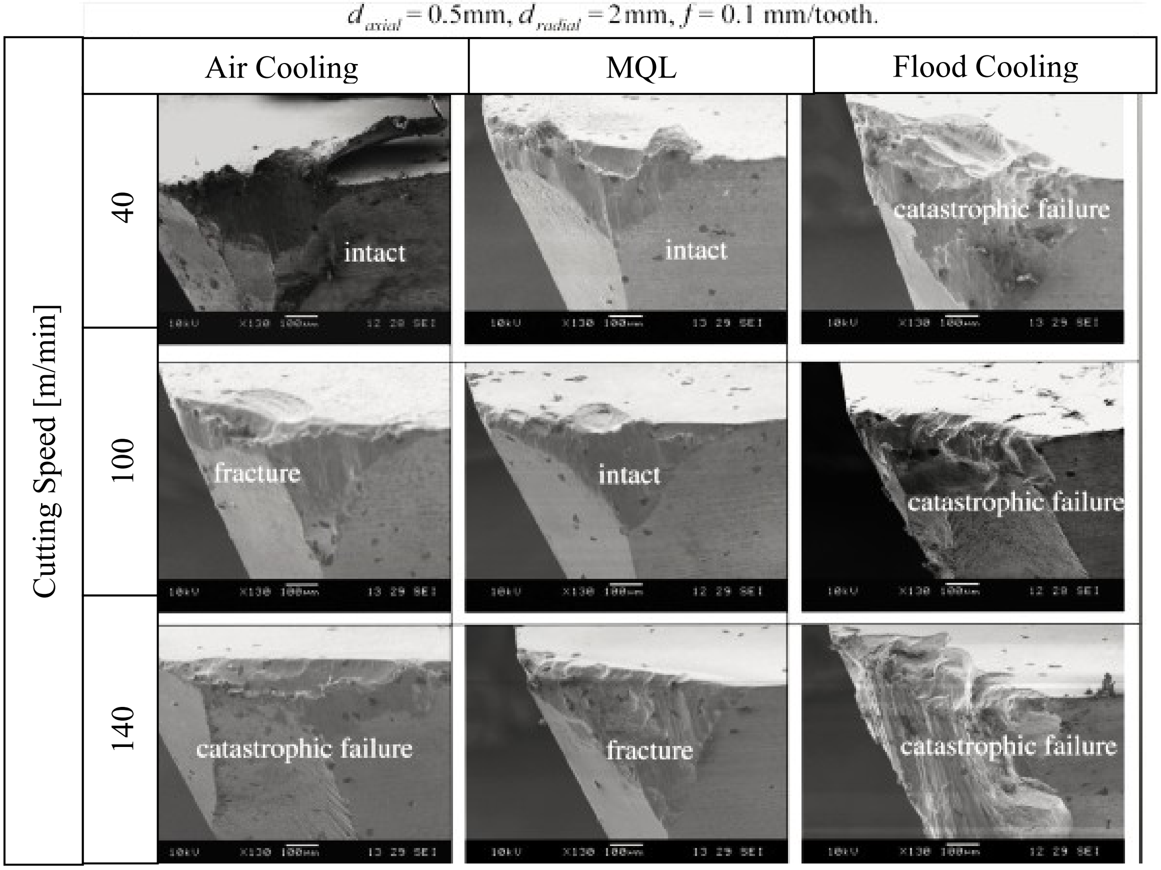

Figure 2.4 Scanning Electron Microscopy (SEM) images of carbide tool edges for varied cutting speeds and coolant supply methods when milling Ti-6Al-4V [35]

2.1.3 Turning

The turning operation is performed by a single point cutting edge in contact with a rotating workpiece. Because of the geometry of the process, it represents the lowest challenge to the applicability of MQL techniques due to the exposed tool tip and workpiece surfaces.

Khan et al. [5] applied external vegetable oil MQL in turning of steel (AISI 9130) using an uncoated carbide inserts. Tests were conducted with a 1 mm depth of cut at cutting speeds between 223 and 483 m/min and feed rates in the range of 0.1 to 0.18 mm/rev. The pure oil MQL flow rate was 100 ml/h with an air pressure of 6 bar. The performance of MQL was compared with that of dry machining and flood cooling at a rate of 360 l/h. It was found that MQL provided a 10% reduction of temperatures compared to flood cooling. This effect was more prominent at higher speeds, producing smoother and brighter chips and preventing any BUE formation. MQL also showed significant reduction in flank wear due to lower abrasion, adhesion, and diffusion wear regimes (Figure 2.5) [5]. The reduction in tool wear, in turn, led to an overall improvement in surface finish.

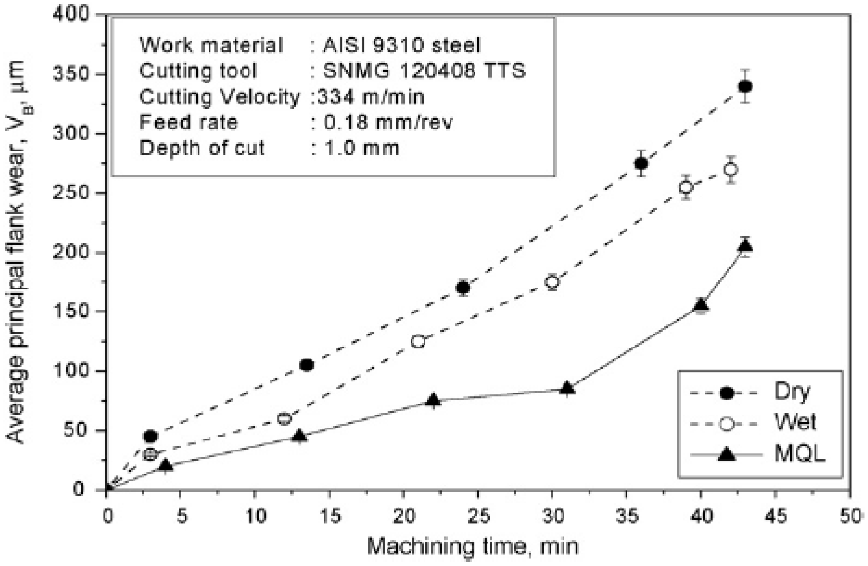

Figure 2.5 Growth rate of average flank wear with time under dry, wet and MQL conditions when turning steel at 334 m/min [5]

Kamata et al. [36] studied the effect of the MQL air pressure on high speed finish-turning of Inconel 718, using a biodegradable synthetic ester. It was found that when using external MQL with an oil flow rate of 16.8 ml/h and an air pressure of 4 bar, the tool wear obtained was consistently lower than with flood cooling (3.7 L/min) or dry machining. An increase in air pressure from 4 bar to 6 bar yielded higher tool wear, similar to dry cutting. It was suggested that increased oxidation, due to the more abundant oxygen, was the reason. The possibility that the excess air resulted in excessive atomization of the MQL fluid, thus not reaching the cutting zone, was not considered. When applying argon as the carrier gas, at a pressure of 4 bar, the tool life was in fact shorter than that with air or under dry conditions. This is likely due to the lower specific heat and thermal conductivity of argon, compared to air. An increase in lubricant supply from 16.8 ml/h to 31.8 ml/h caused an increase in tool life, without a significant improvement in the machined surface finish.

In a similar study [15], Obikawa et al. examined the effects of MQL flow parameters on the cutting temperature and tool wear. Internal application of MQL (7 ml/h with vegetable oil; 3 bar and 7 bar air pressures) was used in grooving experiments on 0.45% carbon steel, using uncoated and triple coated tools (TiN/TiCN/TiC). Tests were conducted at high speeds of up to 300 m/min, and a constant feed of 0.12 mm/rev. The internal MQL supply (through the tool) proved to be more effective in reducing tool wear, when compared with the external MQL, as it enhanced the concentration of the oil supply in the cutting zone. A decrease in maximum temperature and tool wear were observed when the MQL air pressure was increased, for a fixed oil flow rate. This indicated a potential effect of the injection parameters on the atomization of the lubricant, and consequently its effect on machining. The observed temperature reduction using MQL was also strongly dependant on the tool wear.

Varadarajan et al. [37] applied MQC (mineral oil with 60% water coolant) in turning of hardened steel (AISI 4310) with a triple coated insert (TiN/TiC/TiCN).

The MQC emulsion flow rate was 120 ml/h and the air pressure was 200 bar. All experiments were conducted at a constant depth of cut of 1.25 mm. The cutting speeds were varied between 40 and 120 m/min, and the feeds were between 0.05 and 0.14 mm/rev. Comparing the MQC machining results with flood and dry machining showed that lower cutting forces and shorter chip contact lengths were observed in the case of MQC. This was attributed to the successful penetration of the fluid to the cutting edge and the contamination of the tool chip interface, owing to the small size and high velocity of the fluid particles. Consistently, lower cutting temperatures were also observed for the entire cutting speed and feed range, when using MQC (Figure 2.6). MQC machining also resulted in lower surface roughness (R_a) over a longer period of cutting time, than in the case of flood and dry machining. The resulting chips were also short and tightly coiled, which is practically more acceptable (i.e. no interference with machining process, entanglement, or safety hazards).

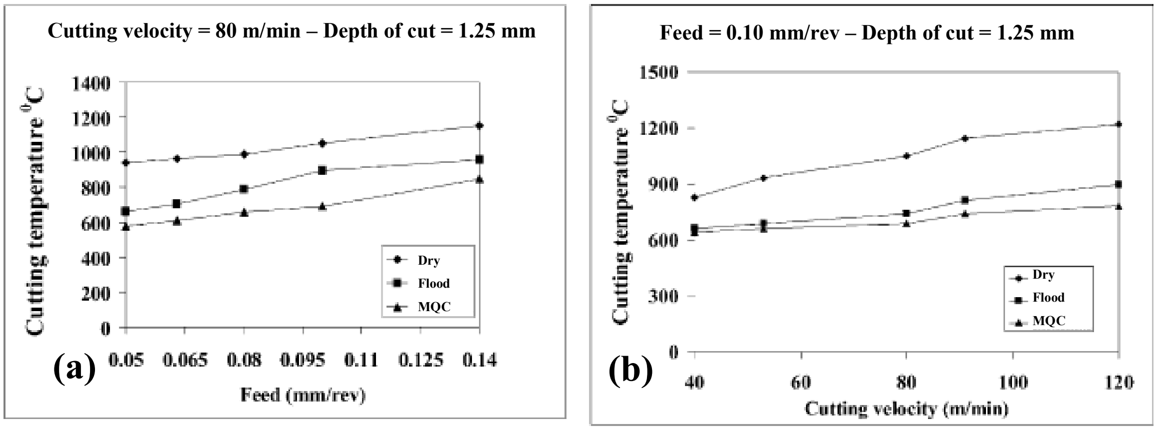

Figure 2.6 Variation of cutting temperature during dry, wet and MQC turning of steel. (a) Effect of feed; (b) Effect of cutting speed [37]

Dhar et al. [38] used uncoated carbide inserts in turning steel (AISI 1040), with MQL, at an oil flow rate of 60 ml/h and air pressure of 7 bar. Tests were conducted at a constant depth of cut of 1 mm, a speed range of 64 to 130 m/min, and feeds range between 0.1 to 0.3 mm/rev. A reduction of the average tool-chip interface temperatures, which maintained a sharp tool edge for a longer cutting length, was observed when comparing MQL with flood or dry cutting. Short, curled chips were formed when using MQL, facilitating a quicker release of the heat generated in cutting. MQL turning also led to higher dimensional accuracy due to the slower tool wear progression. The same conclusions were observed when turning AISI 4340 steel (Figure 2.7) [39].

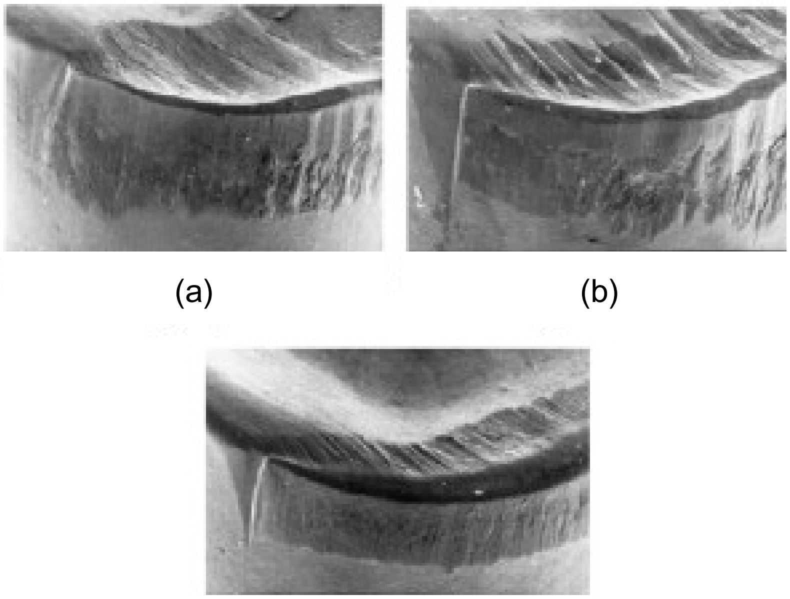
(a) (b)

(c)

Figure 2.7 SEM views of tool tips when turning steel under different lubrication environments (a) Dry; (b) Flood Cooling; (c) MQL [39]

Using AISI 1045 steel, Jayal et al. [40] studied the effects of different esters with EP additives in the application of MQL, and compared the results with flood cooling. Turning tests were conducted at a speed of 400 m/min, a feed of 0.35 mm/rev, and 2 mm depth of cut, using tools of different coatings and geometries. The MQL flow rate and air pressure were fixed at 30 ml/h and 6 bar, respectively. The study showed lubrication was not apparent in the case of MQL. In the case of tools with chip-breaking grooves, which serve to ease the access of cutting fluids, rapid crater formation with MQL with EP additives was observed, possibly due to an excess of the additives on the surface of the tool. Comparison of tool life under the different lubrication conditions also showed that MQL with and without EP additives performed worse than flood cooling.

Itoigawa et al. [41] experimented with Oil film on Water droplets (OoW), in the turning of a highly ductile aluminum-silicon alloy (Al-Si-5). A nozzle composed of three concentric channels delivers water droplets coated with an oil film (Figure 2.8) [41]. This technique provides additional cooling to what normally would be an MQL system, due to higher latent heat of vaporization of the water. The system was compared with a regular 2-fluid MQL system (both at the same synthetic ester flow rate, with 3,000 ml/h of water for the OoW system). Polycrystalline diamond (PCD) and a carbide tool (K10) tools were used. The application of MQL with OoW resulted in improved machining performance by lowering friction, adhesion, and tool wear, compared to standard MQL and emulsion flood cooling. The primary function of the water in OoW MQL was preserving the coherence of the boundary lubricant film, through the cooling effect of water.

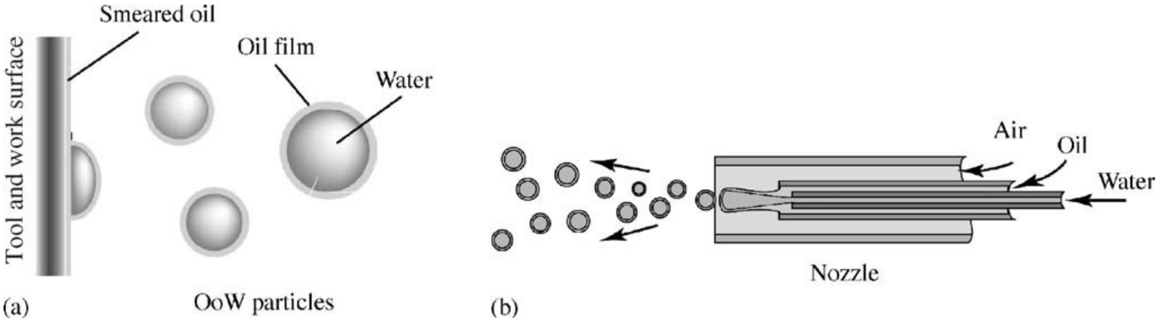

Figure 2.8 Concept of Oil film on Water (OoW) atomizer nozzle [41]

Gaitonde et al. [42] used an L_9 Taguchi array to optimize the application of MQL on the turning of brass (Cu-Zn39-Pb3), using a carbide (K10) tool. Tests were conducted at cutting speeds between 100 and 400 m/min, feeds between 0.05 and 0.15 mm/rev, and oil flow rates between 50 and 200 ml/h. Analysis of variance (ANOVA) was conducted to determine the importance of different parameters, as well as the two-level interactions present on the cutting forces and finished surface roughness (R_a). The ANOVA showed that at lower speeds, the quantity of lubricant tends to be less significant. The feed rate was found to be the most dominant parameter, followed by the cutting speed, in terms of effects on forces and surface roughness. Interactions between the quantity of lubricant dispensed and the cutting speed were present, particularly at higher flow rates, while no significant interactions between the machining parameters were found.

2.1.4 Grinding

Grinding is a finishing material removal process used when high precision and surface smoothness are required, it is also an example of machining process with a geometrically undefined cutting edge. Considerably fewer studies have been performed on grinding with MQCL.

Sadeghi et al. [43] used MQL at rates between 20 and 140 ml/h, and 4 bar air pressure, to compare the effects of the tribological conditions when grinding titanium (Ti-6Al-4V). Aluminum oxide (Al_2O_3) wheels were used at a wheel speed of 15 m/s, work speed of 40 m/s, and depth of cut of 0.007 mm. Considerable reduction in cutting forces was obtained when applying MQL, as compared to cutting with flood cooling. In addition, better performance was obtained when the MQL fluid was synthetic oil, than a vegetable oil. In terms of surface roughness, MQL grinding can achieve similar results as flood cooling. Flood cooling slightly outperformed MQL, however. The comparison of different MQL oil flow rates showed that an optimal flow rate exists; 60 ml/h, in the present case.

Tawakoli et al. [8] used an Al_2O_3 wheel in grinding soft and hardened steels, at removal rates in the range of 0.21 and 1.04 mm^3/mm.s, with MQL at 66 ml/h and air pressure of 4 bar. The comparison of MQL, flood and dry cutting conditions showed that at high removal rates, the tangential force is the lowest for MQL grinding for both types of steel. Grinding with MQL resulted in the lowest roughness values in the case of hardened steel, and comparable roughness values (to flood cooling) in the case of soft steel. This trend is reversed at lower removal rates (Figure 2.9 and Figure 2.10) [8]. Examination of the machined surface indicated that the use of MQL resulted in a different cutting mechanism (shearing and fracturing), than the cases of dry and flood (grain pull-out, deformation and ploughing).

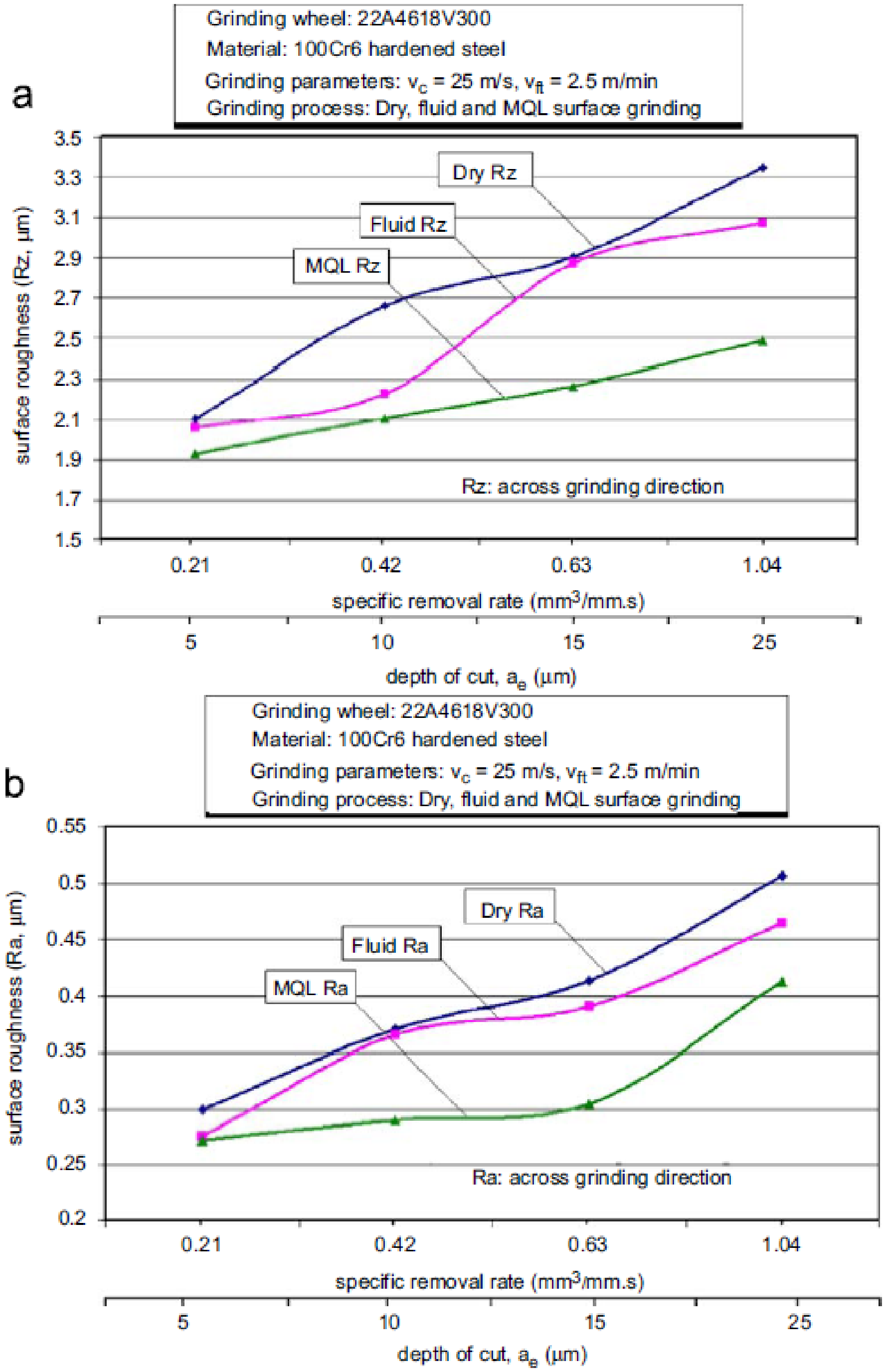

Figure 2.9 Surface roughness measurements of (42CrMo4) steel across grinding direction: (a) Rz; (b) Ra [8]

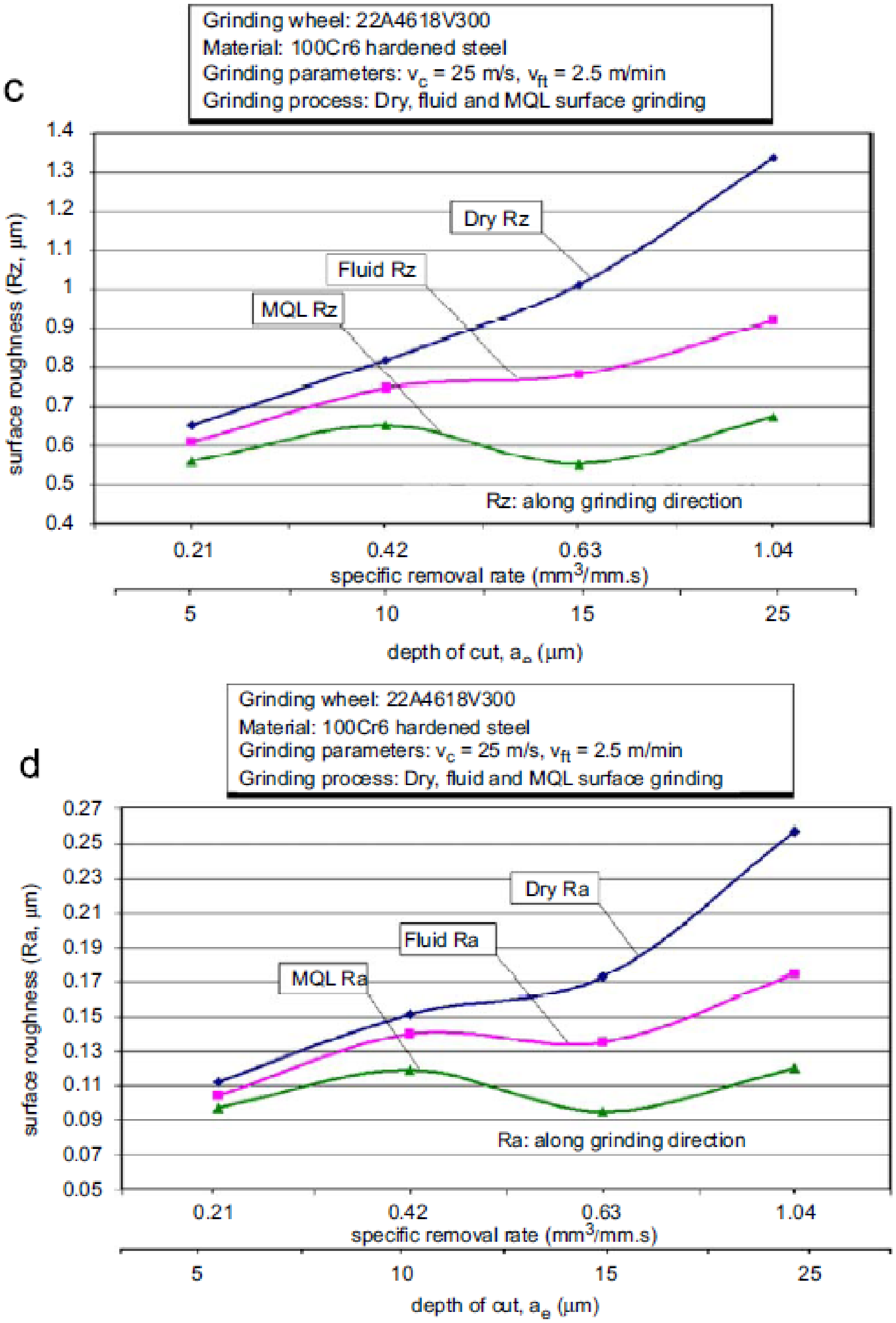

Figure 2.10 Surface roughness measurements of (42CrMo4) steel along grinding direction: (c) Rz; (d) Ra [8]

2.2 Literature Analysis and Thesis Structure

The previous review of studies performed on machining with MQCL showed promising results. The technology appears to have a niche of applications where it would prove beneficial in terms of quality and savings, in addition to the environmental benefits. It can also be concluded that there is a good understanding of the beneficial chemical and tribological effects on machining. A critical literature review shows, however, that there has been limited knowledge of the flow mechanisms through which MQCL functions. All studies mention gas pressures and lubricant flow rates, but fail to provide any information on the MQCL flow itself. The presence of different techniques of atomization has a great impact on the nature of the aerosols generated; MQCL systems present in the industry operate at different pressure ranges (2 to 200 bar) and use different nozzle geometries. The characteristics of the aerosol flow (velocity distribution, shape) and the properties and size of the droplets could also impact the MQCL application in machining. Such characteristics are seldom considered in the literature, but their understanding would be necessary for further investigations e.g. on the thermal aspects of MQCL.

Table 2.1 shows the parameters used in MQCL applications reported so far. It can be seen that the provided information is not sufficient in describing the flow characteristics, since each of the systems used was different; the air pressures and the lubricant flow rates are not indicative of the velocities at the nozzle exit. The shape, design and positioning of the nozzles also have an impact, and are therefore important parameters for process optimization.

While no experimental flow visualization study has been performed on MQCL thus far, a few numerical studies are present [44, 45]. A numerical or an experimental flow visualisation could assist in gaining knowledge of the parameters that most influence the flow behaviour. This in turn could be used to understand the influence of these parameters on machining.

Table 2.1 Parameters of MQCL application to processes reported in this review

Operation	Workpiece Material	Air Pressure (bar)	Oil Flow Rate (ml/h)	Coolant Type	MQCL Type
Drilling	AM60	-	10	Fatty Alcohol	External
	Carbon Steel	-	18	Ester/Water/Alcohol	External
	Hardened Steel	4-6.2	5-23	-	Internal
	319 Al	-	30	Distilled Water	External
	SAE 323	4.5	10	Mineral Oil	External
Milling	ASSAB 718 HH	5.5	8.5	Mineral Oil	External
	50CrMnMo	2-6	13.9-58.4	-	External
	NAK80	4.5	10	Biodegradable Ester	External
Turning	Inconel 718	4-6	16.8-31.8	Synthetic Ester	External
	Carbon Steel	3-7	7	Vegetable Oil	Internal
	AISI 4310	200	120	60% Water-Mineral Oil	External
	AISI 1045	6	30	Ester	External
	Cu-Zn39-Pb3	-	50-200	-	External
Grinding	Ti-6Al-4V	4	20-140	Synthetic/Vegetable Oil	External

For the MQCL technology to further penetrate machining practice, its application needs to be expanded to other materials. MQCL machining of difficult to cut materials such as Inconel and Carbon Fibre Reinforced Plastics has not had its share of investigation. Many machining-related ambiguities still remain; there is lack of understanding of the speeds/material removal rates at which MQCL machining is more effective than flood cooling, the predominant effect of MQCL at high speeds (cooling vs. lubricating) is also unclear.

The objective of this thesis is to obtain a basic understanding of the atomization parameters which most significantly influence the machining process, when MQCL is applied. The approach followed in this thesis is:

1- An experimental visualization of the MQCL nozzle's external aerosol flow, using Particle Image Velocimetry, with the purpose of understanding the effects of air and lubricant flow rates on the nozzle spray. This investigation is presented in Chapter 3.

2- A numerical simulation of the MQCL nozzle’s internal and external air flow, with the purpose of visualizing the flow in Computational Fluid Dynamics (CFD) models which better simulates the machining environment. The details of this study are presented in Chapter 4.

3- An experimental investigation of the effect of the MQCL parameters on the performance of Caron-Fibre Reinforced Plastic machining, will be carried out. The details of this study are presented in Chapter 5.

4- Conclusions and comments on the overall results of this investigation, as well as recommendations for future research, are presented in Chapter 6.

Chapter 3 MQCL Flow Visualization

3.1 Introduction

While it is clear that an atomization of cutting fluids could benefit the machining process, there is less understanding of what makes a good aerosol jet. Thus far, a definition of a good atomization exists only for older and more common applications, like internal combustion. Machining applications are still lacking this knowledge. The characteristics of the flow behaviour and the effects of particular flow parameters on machining itself also remain unknown. Furthermore, the atomization techniques vary greatly and their details are seldom mentioned in literature discussing MQCL. Such details are often commercial trade-secrets and thus not available in open literature. Finally, in many practical and research-based cases, the MQCL parameters are not even considered, and the manufacturer’s nominal parameters are used. This study aims at understanding the properties of an MQCL flow, in preparation of finding the effects of these properties which benefit machining. For this visualization study and the machining investigation that follows, a novel 2-channel airblast MQCL system was supplied by Tecnolub Inc. The MQCL nozzles of this system are commercially available and used in industrial practice.

The visualization of continuous external flows can be performed through a variety of techniques, depending on the application and the information required. An atomized flow is a two-phase flow (liquid and gas), which adds the burden of understanding the droplet characteristics (shape and size distribution), in addition to understanding the properties of the flow field. Particle Image Velocimetry (PIV) is a commonly used technique for visualizing jets. The reason is that PIV typically relies on reflective particles seeded in the flow to track the flow. For MQCL nozzles, oil droplets already present in the nozzle jet serve as the trackers for the measurement system, without the need of introducing additional trackers which could affect the flow behaviour.

A disadvantage in using PIV to visualize aerosols is its inability to provide droplet information, but simply velocity information on the gas and liquid mixture. It could thus be useful to supplement it by performing Laser Doppler Anemometry (LDA), a technique which could provide the missing droplet information. The LDA technique was, however, beyond the scope of this research.

Various correlations for the droplet size distribution, and the mean droplet size in an atomization process, have been developed for different nozzles [13]. These correlations offer a good agreement with experiments, though none could be generalized to all nozzles. The most widely used correlation for droplet size distribution is the Rosin and Rammler correlation [46]:

$$1 - \Phi = \mathrm{e}^{-(\frac{\mathrm{D}}{\mathrm{X}})^{\mathrm{q}}} \qquad 3.1$$

where $1-\Phi$ is the fraction of droplets of the total volume of droplet material having diameter greater than *D*, and *X* is a size parameter defined as the value of *D* for which $1-\Phi = e^{-1}$. The exponent *q* is a distribution width parameter, it provides a measure of the uniformity of the spray; the higher the value, the more uniform the spray is. The values *q* can take vary between 1.5 and 4 though can reach up to 7 [13].

In many applications, it is convenient to use only a mean or an average diameter instead of the complete droplet size distribution. This concept has been generalized as follows [47]:

$$d_{ab} = \left(\frac{\sum_i N_i {d_i}^a}{\sum_i N_i {d_i}^b}\right) \qquad 3.2$$

where *a* and *b* are constants which may take on different values depending on the application.

The diameter d_{32}, referred to as the Sauter Mean Diameter (SMD), can properly indicate the fineness of a spray from an atomization quality point of view. The SMD can be defined as the diameter of a drop which has the same volume/surface area ratio as the entire jet. It can be calculated as follows, based on equation 3.2 [47]:

$$d_{32} = \left(\frac{\sum_i N_i {d_i}^3}{\sum_i N_i {d_i}^2}\right) \qquad 3.3$$

This property is relevant from a lubrication and thermal exchange perspective, commonly arising in machining applications. The SMD was thus utilized as a practical parameter for comparisons.

3.2 PIV Technique Background

Particle Image Velocimetry is a technique that relies on seeding particles to determine the flow behaviour. The particles seeded are assumed to follow the fluid flow without interfering with the fluid itself. A thin pulsating laser light sheet illuminates a cross section of the flow, as a high speed Charge-Coupled Device (CCD) camera captures successive images of the particles. These images which capture the illuminated tracers in the flow are then treated to extract the flow properties (Figure 3.1) [48].

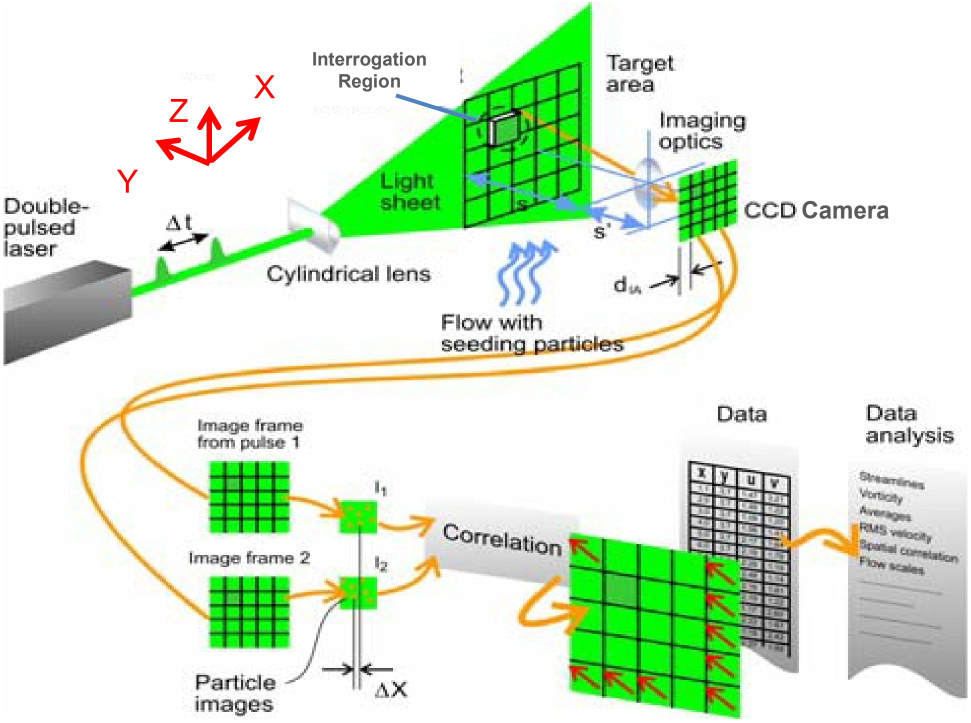

Figure 3.1 Typical Particle Image Velocimetry setup [48]

If the time between two pulses is *Δt*, then the velocity of the particle for a displacement of d_{max} is [49]:

$$V_{max} = \frac{d_{max}}{\Delta t} \qquad 3.4$$

The captured PIV images are divided into small regions called “interrogation regions” (Figure 3.1 and Figure 3.2), the dimension of which determines the resolution of the measurement. The interrogation regions can be either adjacent to each other, or overlap with their neighbours. Although PIV can be performed using multiple exposure images, the preferred PIV method captures two images on separate frames. A cross-correlation analysis is then performed to extract the direction and magnitude of the flow. A computational algorithm is then used to obtain the information from the many tracer particles in the interrogation regions, and outputs the most probable statistical values for the velocity’s magnitude and direction. Interrogation regions for cross-correlation are commonly 32 by 32 pixels. In order to maintain good accuracy and low noise in the measurements, a rule of thumb is to ensure that within the time *Δt* between two pulses, a particle travels only a third of the interrogation region in the sheet plane (X-Z), and a third of the light sheet thickness in the out of plane (Y) direction [49].

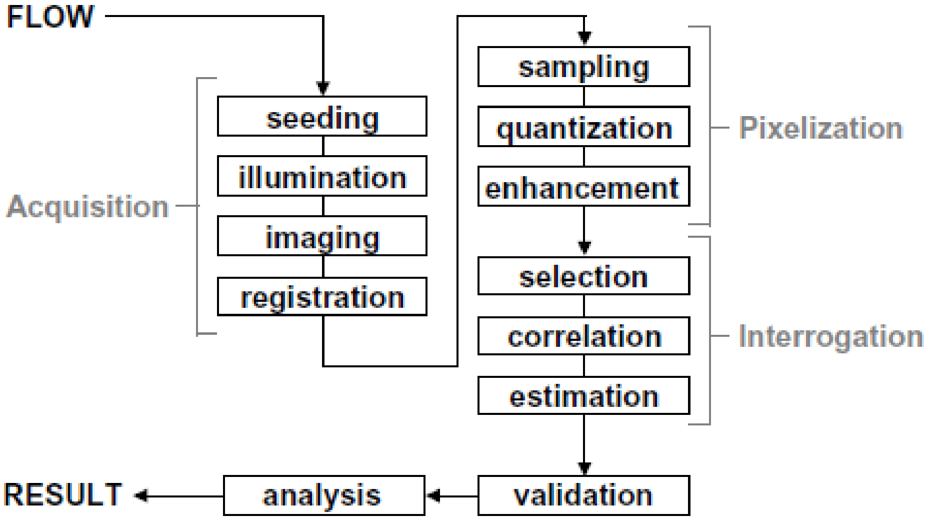

Figure 3.2 PIV analysis procedure [49]

The use of a single camera to capture the images permits the deduction of the flow components in the X and Z directions only (the components within the light sheet plane), and thus is not suitable for highly turbulent flows. The use of a second camera (Stereoscopic-PIV) permits the expansion of PIV measurements to three dimensions.

A typical PIV system, such as the one used in the experiments carried out in this thesis, consists of a laser light source, along with the necessary optical hardware to generate the light sheet, a high speed camera, and a computer with the appropriate post-processing software. Most PIV systems consist of dual-cavity Nd:YAG lasers, which give pulses of about 10 ns in duration at frequencies between 5 and 30 Hz. Charge-Coupled Device cameras (used for cross-correlation of particle displacement) with resolutions up to 2,000 by 2,000 pixels are available, with framing rates up to 30 Hz. PIV relies on a thin light-sheet to capture the images of seeding flows, and as a consequence, large errors can occur if there exists a large velocity component in the out of plane direction, such as in highly turbulent flows. In addition, noise in the captured images is inevitable because of the background or other particles that might exist in the captured image. For PIV, the seeding particle density is typically 10 to 20 particles per interrogation region, with diameters between 1 and 50 μm [50].

3.3 Experimental Setup

Atomization can occur by orienting a gas flow at an angle with the liquid flow direction; in this case the relative velocity between the gas and the liquid is the main driver of the atomization process. A special case of twin-fluid atomizers is the Airblast atomizers. They use a higher air mass flow rate, but at a lower speed (<100 m/s) than in the general case of twin-fluid atomizers, commonly referred to as Air-Assist. The current Tecnolub Inc. design is composed of two coaxial cylindrical channels, the liquid flows in the inner channel while the gas flows in the outer channel. This is an Airblast type nozzle, with an oil channel exit diameter of 0.25 mm and air channel internal and external diameters 2.75 mm and 4.25 mm respectively. The inner oil channel length was 0.5 mm longer than the outer air channel.

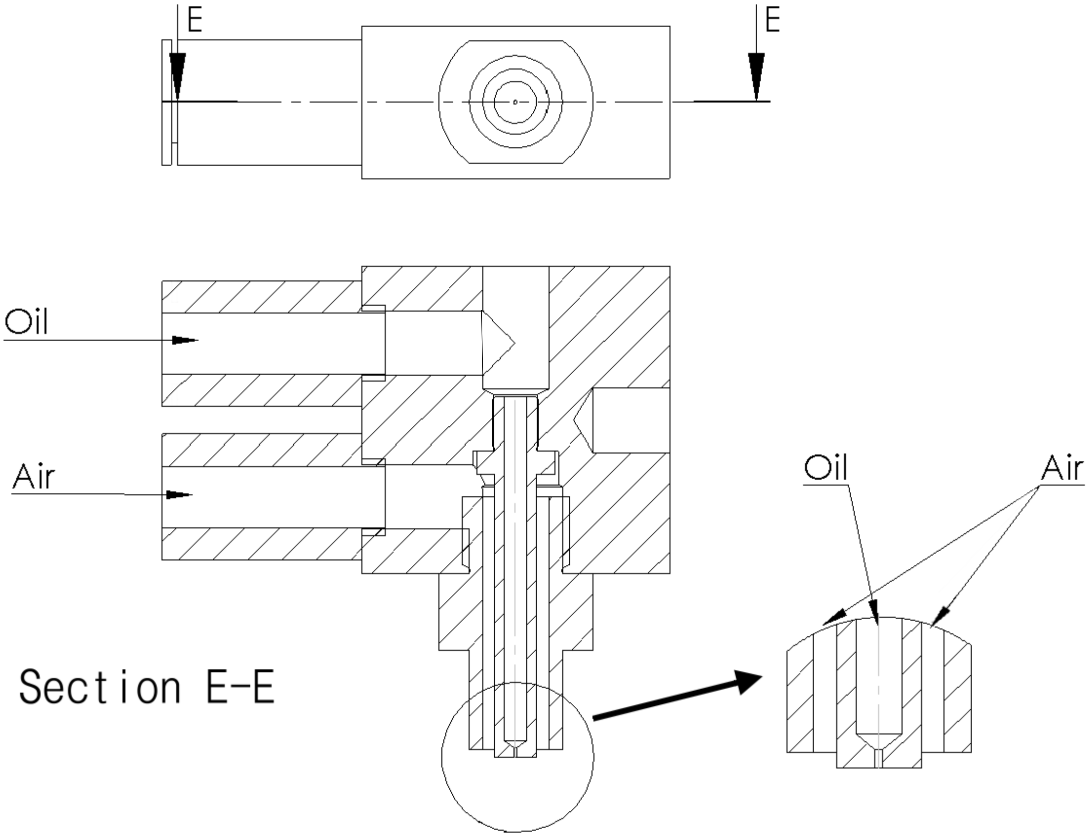

Figure 3.3: MQCL nozzle geometry

The PIV setup (provided by The Royal Military Academy, Belgium) used was a typical setup as described above; the MQCL nozzle was fixed at the same height of the CCD camera lens, and its flow axis was parallel to the plane of the captured image. The laser sheet was oriented to be in the center of the jet flow, in the same plane of the nozzle axis (Figure 3.4). The nozzle was supplied with two separate channels for the air and oil, and the flow rates in each channel were adjusted prior to each experiment. An air compressor fed the air channel with filtered air, and a pump supplied the oil channel from a reservoir tank (Figure 3.5).

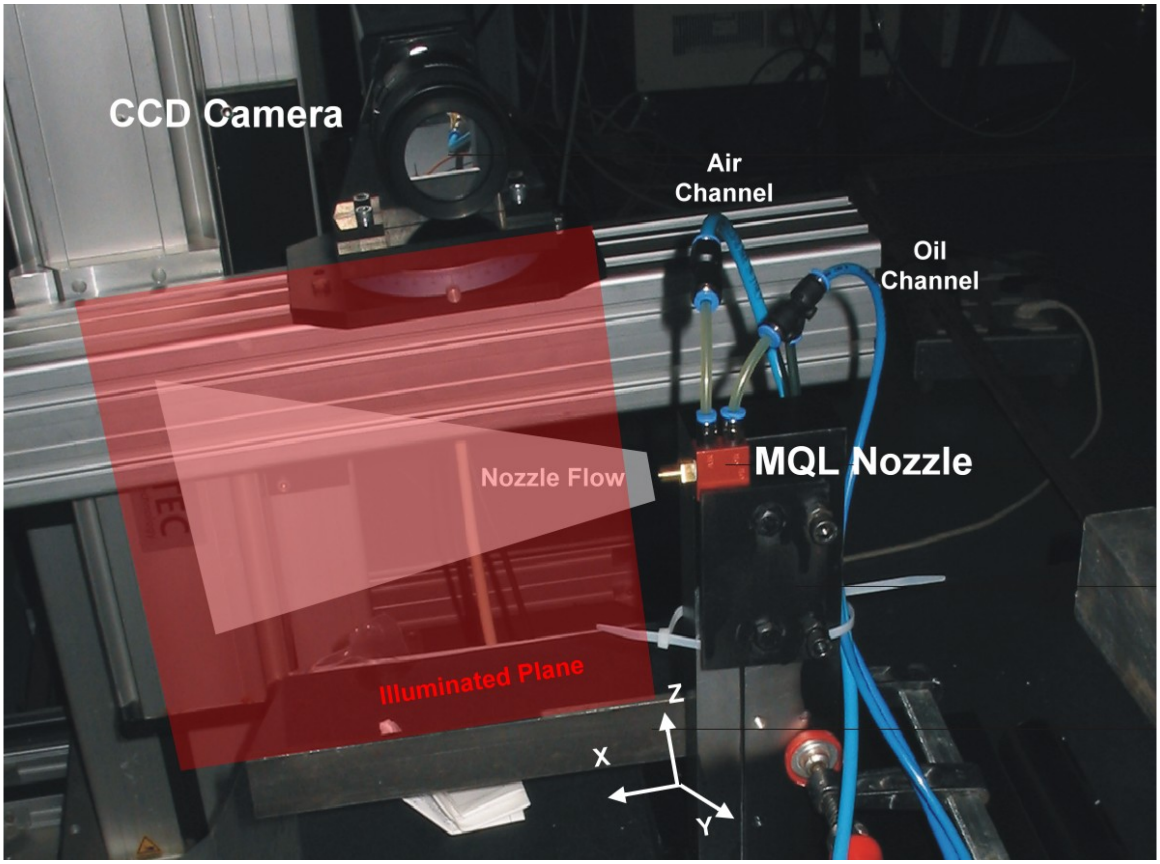

Figure 3.4: PIV Setup showing nozzle position and measurement region

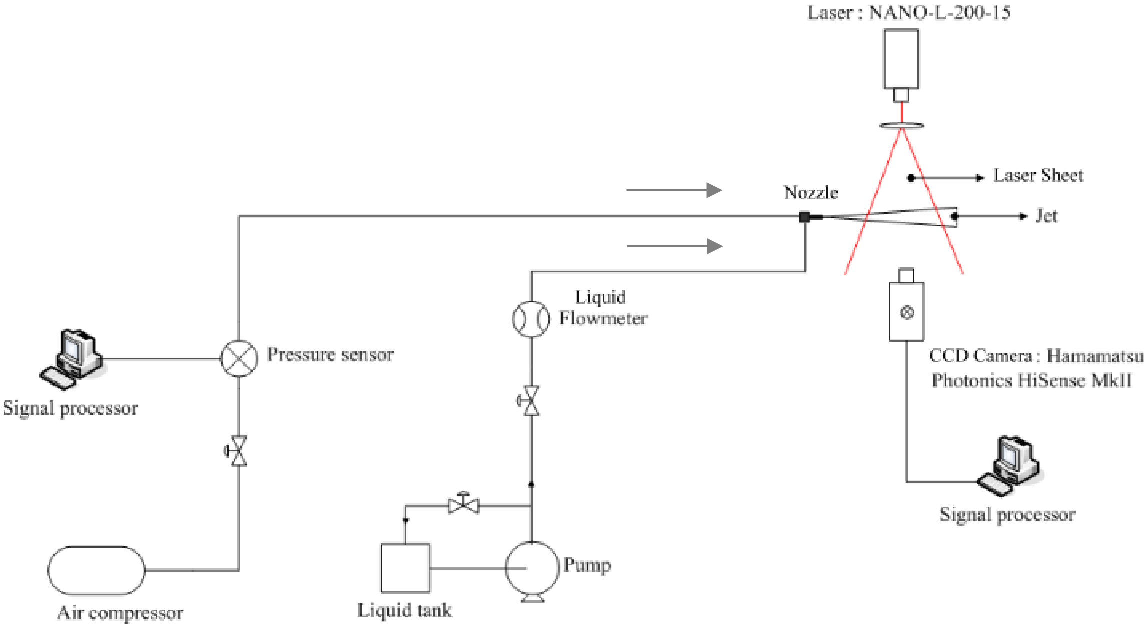

Figure 3.5 PIV setup diagram

Four air flow rate levels between 20 l/min and 31 l/min, and 3 oil flow rate levels between 10 ml/min and 24 ml/min, were tested in a full factorial design, as shown in Table 3.1:

Table 3.1 PIV Experiment Conditions and Parameters

Test	Oil Flow Rate	Air Flow Rate
1	10 ml/min	20 l/min
2	10 ml/min	25 l/min
3	10 ml /min	28 l/min
4	10 ml /min	31 l/min
5	17.5 ml /min	20 l/min
6	17.5 ml /min	25 l/min
7	17.5 ml /min	28 l/min
8	17.5 ml /min	31 l/min
9	24 ml /min	20 l/min
10	24 ml /min	25 l/min
11	24 ml /min	28 l/min
12	24 ml /min	31 l/min

3.4 Results and Discussion

The geometry of the nozzle used by Tecnolub Inc. resembles the geometry of the nozzle by Hai-Feng Liu [51]. The correlation for the SMD is given by:

$$SMD = 685.8(u_g - 3.297u_l)^{-0.4813}m^{0.3665} + 0.1824d_l m \qquad 3.5$$

where u_g is the gas velocity in m/s, u_l is the liquid velocity in m/s, d_l is the liquid channel exit external diameter in mm, m is the oil/air mass flow rate ratio, and SMD is the resulting Sauter Mean Diameter in microns. Other correlations for the SMD exist for different speed ranges and nozzle geometries, they are given in Table 3.2. It is worth noting, here, that increasing the nozzle diameter reduces the SMD for a given oil flow rate; although d_l increases, u_l will decrease making the first component of the correlation much smaller.

Table 3.2 Various correlations for predicting the Sauter Mean Diameter

Study	Type	Air Velocity	Correlation
Sakai et al. [12]	Air-Assist-Internal	>100 m/s	$SMD = 14\,.\,10^{-6}\,.\,d_0^{0.75}\,.\,(\frac{m_l}{m_a})^{0.75}$
Inamura and Nagai [12]	Air-Assist-External	>100 m/s	$\frac{SMD}{t} = \left(1 + \frac{16850\,.\sqrt{Oh}}{We\,.\left(\frac{\rho_l}{\rho_g}\right)}\right).\,(1 + \frac{0.065}{(\frac{m_l}{m_g})^2})$
Elkotb et al. [12]	Air-Assist-External	>100 m/s	$SMD = 51 d_0 Re^{-0.39} We^{-0.18} (\frac{m_l}{m_g})^{0.29}$
Nukyama and Tanasawa [47]	Airblast-Internal	<100 m/s	$SMD = 0.585\sqrt{\frac{\sigma}{\rho_l u_r^2}} + 53\left(\frac{\mu_l^2}{\sigma\rho_l}\right)^{0.225} (\frac{Q_l}{Q_g})^{1.5}$
Lorenzetto and Lefebvre [47]	Airblast-Internal	<100 m/s	$SMD = 0.95\left(\frac{(\sigma m_l)^{0.33}}{\rho_l^{0.37}\rho_g^{0.30}u_r}\right)(1 + \frac{m_l}{m_g})^{1.70} + 0.13\sqrt{\frac{\mu_l^2 d_0}{\sigma\rho_l}}(1 + \frac{m_l}{m_g})^{1.7}$
Rizk and Lefebvre [12]	Airblast-Internal	<100 m/s	$SMD = 0.48 d_0\left(\frac{\sigma}{\rho_a u_r^2 d_0}\right)^{0.4}(1 + \frac{1}{GLR})^{0.4} + 0.15 d_0\sqrt{\frac{\mu_l^2}{\sigma\rho_l d_0}}(1 + \frac{1}{GLR})$
Hai-Feng Liu et al. [51]	Airblast-External	<100 m/s	$SMD = 685.8(u_g - 3.297u_l)^{-0.4813} GLR^{0.3665} + 0.1824 d_l GLR$

Figure 3.6 shows the Sauter mean diameters predicted according to correlation 3.5. With the fact that u_l is always lower that u_g in mind, it can be observed that an increase in the air flow rate reduces the SMD for a fixed oil flow rate. The increase of the air flow rate only causes the relative velocity of the two fluids to increase; this, in turn, favors more breakups in the fluid surface and forms finer droplets. Increasing the oil flow rate while fixing the air flow rate results in the opposite effect; the lower relative velocity favors less liquid surface breakup and the formed droplets are coarser. The largest value of SMD is thus

obtained using the lowest air flow rate combined with the highest oil flow rate, and the smallest SMD is obtained using the highest air flow rate and the lowest oil flow rate.

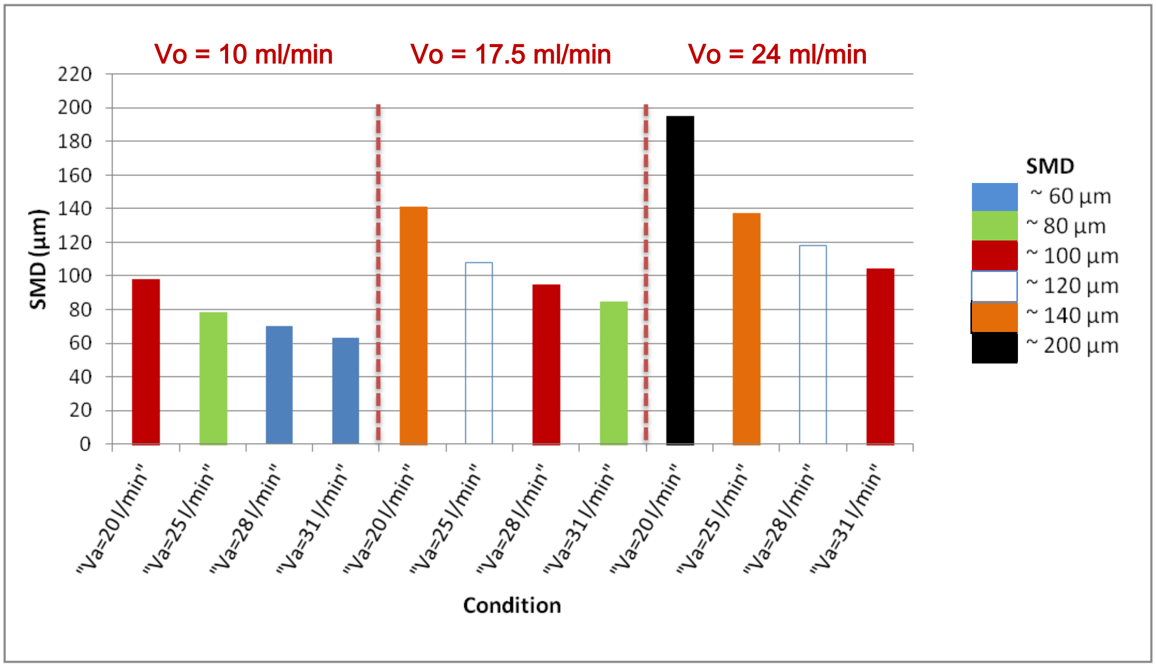

Figure 3.6 Predicted Sauter Mean Diameters

From a machining perspective, both cooling and lubrication are often required. An MQCL flow with a low SMD should therefore be more effective in penetrating the cutting zone. The appropriate amount of cooling and lubrication would be determined on the basis of the machining application and the liquid lubricant characteristics. The air flow rate would then be adjusted to maintain the necessary SMD. Put differently, the “capacity” of a flow to carry the lubricants is increased through an increase in the air flow rate. It can be expected, however, that there exists a limit to that capacity based on the nozzle geometry; if the flow at the nozzle exit is highly turbulent due to an insufficiently sized nozzle exit area, excessive atomization could occur and no jet would be formed (i.e. shapeless oil mist and air). If on the other hand, the air flow rate is not adequately high, less atomization would be occurring and the flow might not penetrate to the cutting zone, despite the appropriate cooling and lubricating capacity of the dispensed oil volume.

The air and oil flow rates were picked to be around the manufacturer's recommended values in practical machining applications. The combinations fall within the requirement of preventing incomplete or excessive atomization from occurring. Of these combinations, similar SMD values across the three oil flow rate levels were predicted (shown in pairs of the same color in Figure 3.6). For the analysis, instantaneous measurements extracted from the CCD camera images were averaged over 500 to 1,000 instantaneous shots, depending on the predicted SMD.

Figure 3.7 shows the images captured by the CCD camera and the corresponding stream-wise velocity field of the air. The images and the velocity fields display the flow in the X-Z plane, 22 mm away from the nozzle exit in the X direction. The image shows a decrease in droplet diameter and finer atomization with the increase of the volumetric air flow rate. From the velocity distribution, it can be observed that an increase in the flow rate of the air leads to an increase of the air velocity in the jet region. It can also be observed that there exists a deviation in the flow towards the positive Z direction; the jet axis deviates from the nozzle exit axis (horizontal) for all air and oil flow rates combinations. This deviation indicates a strong velocity gradient inside the nozzle channel, prior to the exit. The decrease in the slope of this deviation with the increasing air flow rate can be better observed in the velocity vector plots in Figure 3.8.

It can be observed that the velocity in the jet region 20 mm on the X axis (40 mm from the nozzle exit) vary between 10 and 30 m/s, depending on the flow rates. Away from the jet axis, a mild flow with a speed between 5 and 10 m/s exists (green). This flow is a result of noise in the captured image, and is completely erroneous. It will be reviewed in a following section. The velocity vectors in Figure 3.8 show signs of circulation above and below the jet exit, which become less pronounced as the air flow rate increases, for the same oil flow rate.

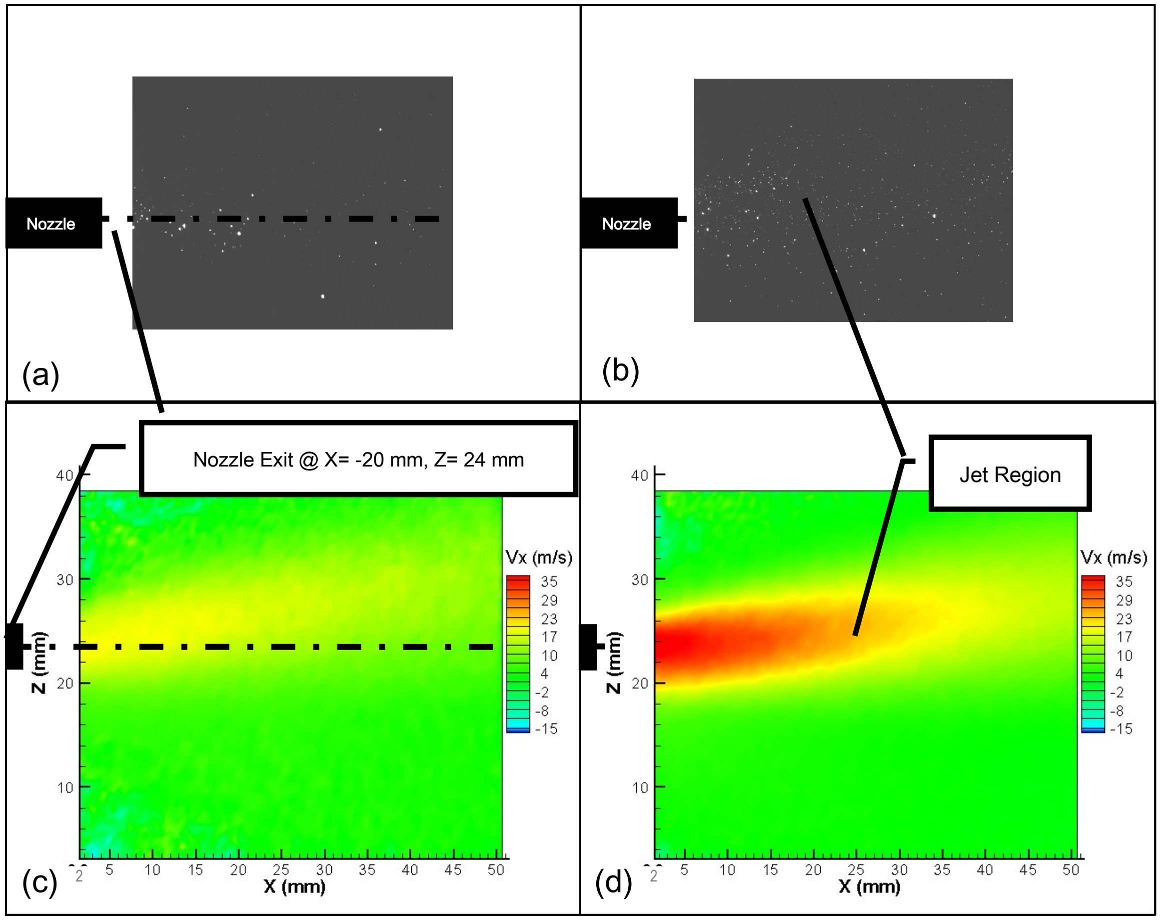

Figure 3.7 Top: CCD image of the flow when Vo= 10 ml/min ((a) Va= 20 l/min; (b) Va= 31 l/min); Bottom : Stream-wise velocity distribution when Vo= 10 ml/min ((c) Va= 20 l/min; (d) Va= 31 l/min)

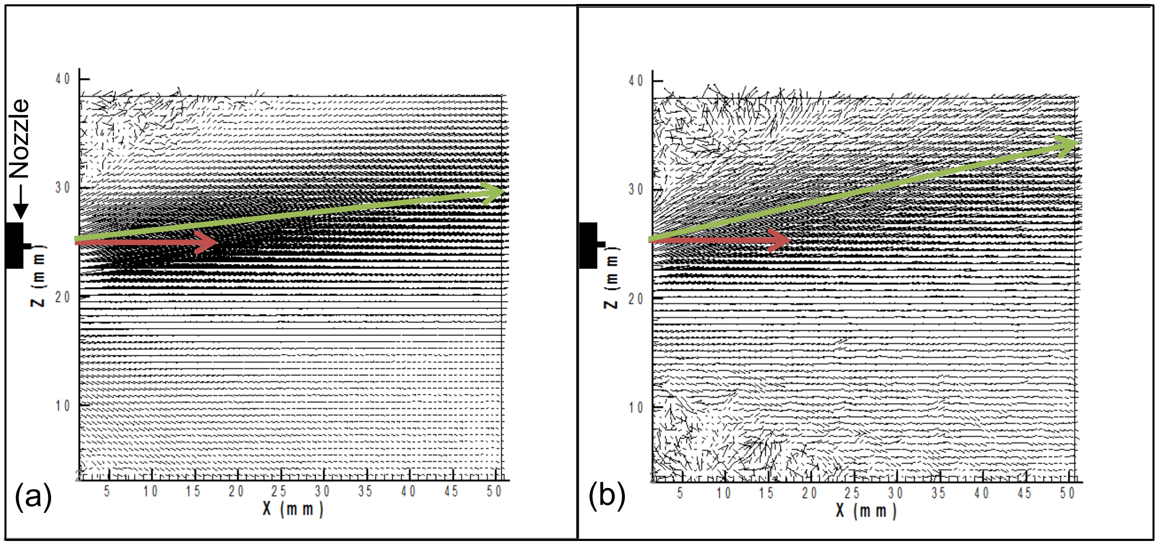

Figure 3.8 Velocity vectors for Vo= 10 ml/min: (a) Va= 31 l/min; (b) Va= 20 l/min

To better examine the flow profile, the vorticity (defined as the curl of the velocity field [52]) was calculated across the flow field. The plots in Figure 3.9 show the vorticity when the oil flow rate is 10 ml/min. The behaviour of the vorticity varied depending on the location in the jet. Vortices above the jet cone were of larger magnitude in the case of the lower air flow rates. The magnitude of the vorticity at that location decreases with the increasing air flow rate Va. Vorticity in the jet region was higher at elevated air flow rates. The same behaviour was observed across the air flow rates for the other two oil flow rates.

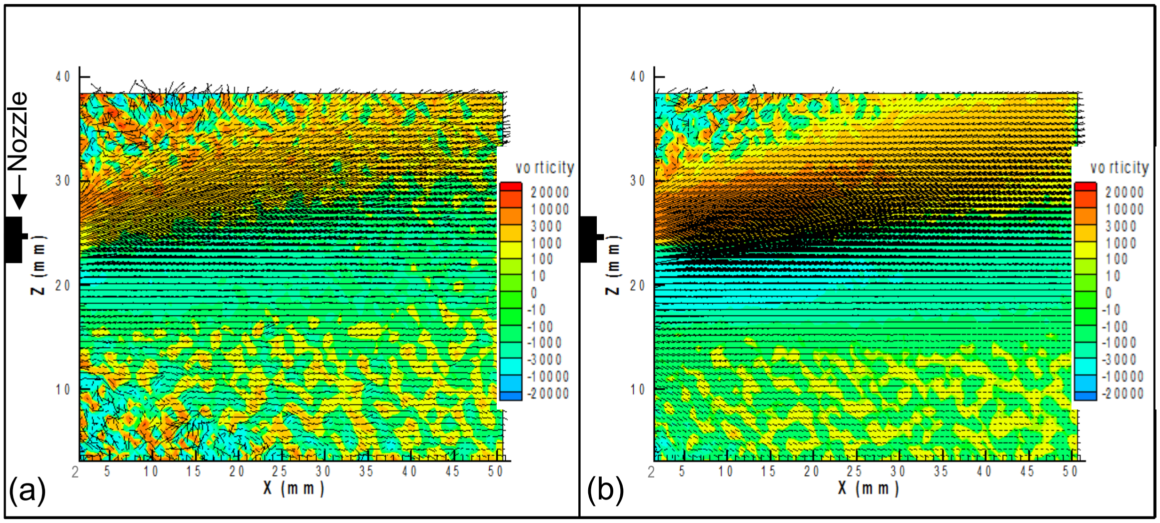

Figure 3.9 Vorticity field and velocity vectors when Vo= 10 ml/min: (a) Va= 20 l/min; (b) Va= 31 l/min

In many cases, the magnitude of the vorticity is not adequate for determination of vortex cores, therefore the Q-Criterion was used. The Q-Criterion defines a vortex core as the region where the vorticity magnitude is higher than the strain-rate magnitude, or equivalently, when the second invariant *Q* of the velocity tensor is positive [53]:

$$Q \equiv \frac{1}{2}(\|\Omega\|^2 + \|S\|^2) > 0 \tag{3.6}$$

where *Ω* is the vorticity tensor and *S* is the strain-rate tensor. Figure 3.10 shows the plots of *Q* in the region of the jet cone for the extreme air flow rates, when the oil flow rate is equal to 10 ml/min. Vortex cores, according to the Q-Criterion, are displayed as the yellow/green patches in the image field. It can be seen that vortices become more abundant in the jet region with the increase of the air flow rate. Vortices of lower magnitude are present in the vicinity of the nozzle exit. The Q-Criterion confirms the initial observation that the number of vortices present in the jet region slightly increase with the increasing air flow rate, for a fixed oil flow rate.

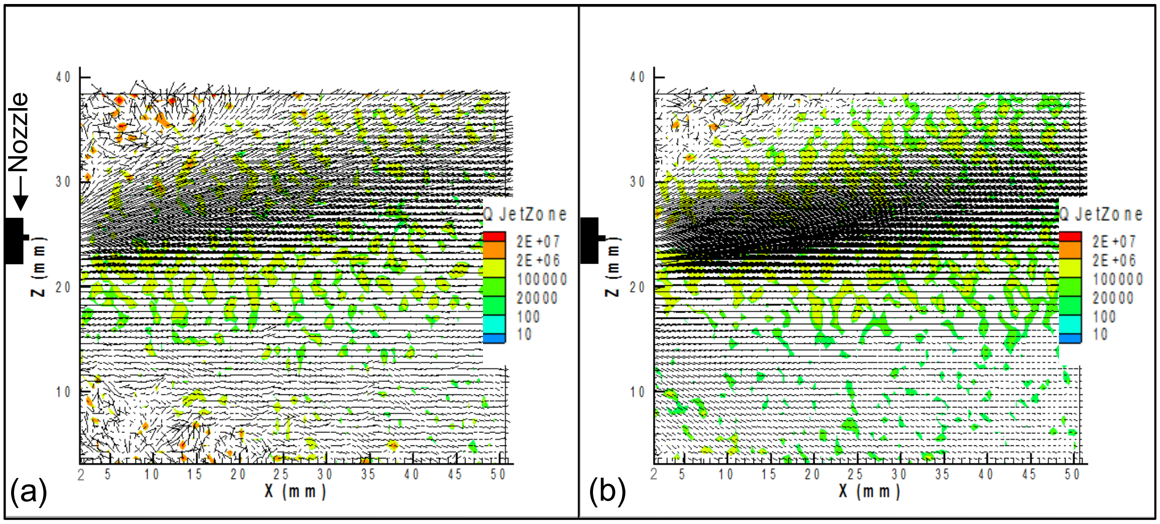

Figure 3.10 Calculation of the second invariant of the velocity tensor, *Q*, in the flow field and velocity vectors when Vo=10 ml/min: (a) Va=20 l/min; (b) Va= 31 l/min

The oil flow rate had little effect on the stream-wise velocity field in the jet region, as can be seen in Figure 3.11. The effect on the lateral shape and deviation of the cone along the flow direction was also minimal. Circulation in the regions above and below the jet axis became more prominent with the increase of the oil flow rate, for a fixed air flow rate. Comparison between the stream-wise velocity fields at the various air flow rates showed that this circulation was more sensitive to the oil flow rate, when the air flow rate is low. This can be observed in the predicted values of the SMD in Figure 3.6; the rate of increase of the SMD for the lowest air flow rate with the increase of the oil flow rate, is highest when the air flow rate is minimum (Va = 20 l/min).

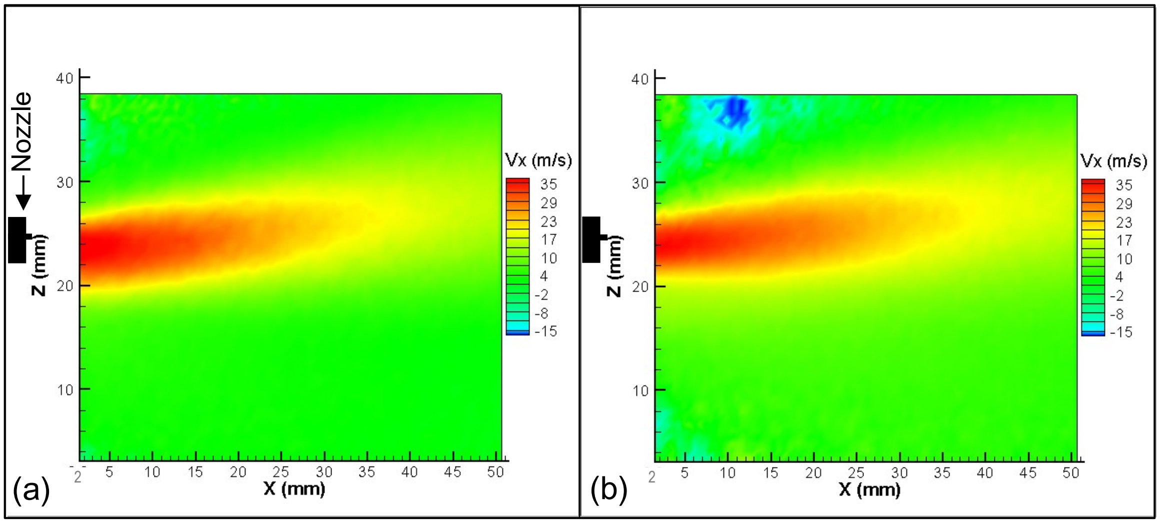

Figure 3.11 Stream-wise velocity distribution when Va= 31 l/min: (a) Vo= 10 ml/min; (b) Vo= 24 ml/min

The plots in Figure 3.12 show the Q-Criterion results for the highest air flow rate (Va= 31 l/min), as the oil flow rate is increased. It can easily be noted that the intensity of the vortices just above and below the nozzle exit increases with the increase of dispensed oil, with no change in the amount of vortices in the jet region. This indicates the more prominent interference of the oil with the air flow, and is a sign of inadequate atomization.

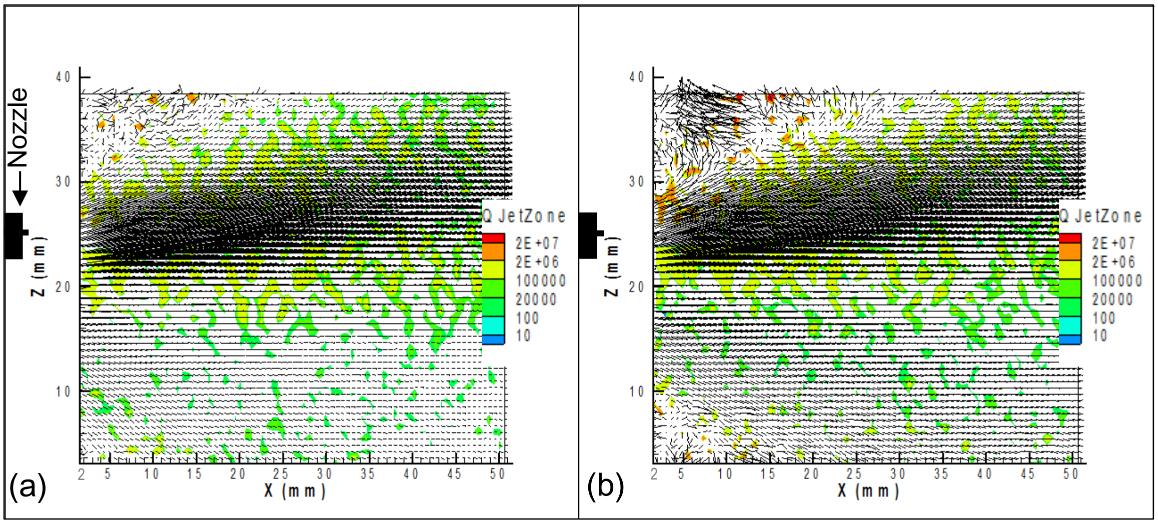

Figure 3.12 Calculation of the second invariant of the velocity tensor, *Q*, in the flow field and velocity vectors when Va= 31 l/min: (a) Vo=10 ml/min; (b) Vo= 24 ml/min

With the effect of the increase of the air flow rate on vortices taken in perspective, these observations show the interaction between the air and oil flow rates. An excess in the number and intensity of vortices above the jet exit indicate inadequate atomization when the oil flow rate is increased, across all air flow rate levels. On the other hand, the number of vortices in the jet region increases with the air flow rate, across all oil flow rate levels, indicating the turbulence in the air flow. The air-induced vorticity, in addition to the increased fluid relative velocities, results in better atomization quality. At lower air flow rates the atomization can be severely affected if the oil flow rate is too high. It can be concluded, then, that the volumetric, or equivalently, the mass flow rate ratio of the two fluids is important from an atomization point of view. This conclusion indicates the importance of the SMD as a predictor of the atomization quality.

Flows of comparable SMD were examined for changes in the flow behaviour. Figure 3.13 shows the stream-wise velocity and velocity vectors for 2 pairs of the experimental conditions. It shows that the flow behaviour across the different flow parameters is strikingly similar. This further underlines the importance of the SMD as a predictor for the flow behaviour.

A final PIV test was conducted for comparison of various tests with Va = 31 l/min. In Figure 3.14 (a) only the air channel was used, and the tracking was conducted using finer pre-atomized liquid particles seeded in the air channel, no atomization at the nozzle exit was occurring. These finer particles of 2 to 5 μm in diameter are designed to better follow the air flow.

The first plot in Figure 3.14 shows the stream-wise velocity contours of the flow along with the velocity vectors, using the pre-atomized particles. The vectors show no signs of circulation, this was validated using the Q-Criterion; no positive values were obtained away from the jet zone (This can be seen in Appendix D). The middle and right plots in Figure 3.14 (using oil) show the substantial amount of noise in the measurements with the minimum and maximum oil flow rates, as compared with the measurements with the finer pre-atomized droplets. The generally coarser droplets generated with the MQCL airblast nozzle do not follow the air flow, and were the cause of these errors. In addition, the absence of atomization occurring at the nozzle exit prevented any circulation from occurring in the zones directly above and below the exit (the seeded particles were atomized prior to entering the air channel and not using the MQCL nozzle itself).

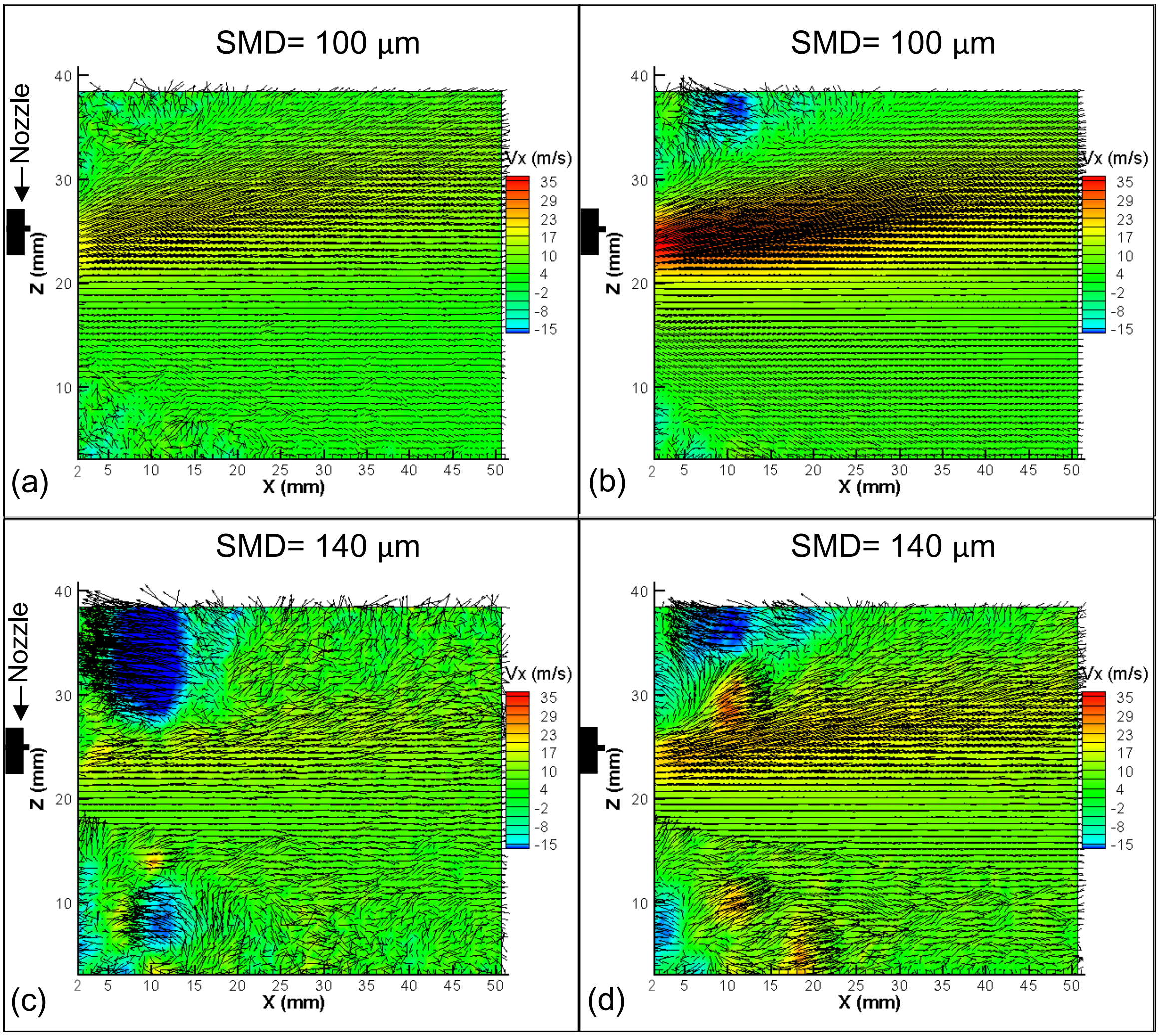
SMD= 100 µm

SMD= 100 µm

SMD= 140 µm

SMD= 140 µm

Figure 3.13 Stream-wise velocity distribution and velocity vectors for 2 pairs of conditions of comparable SMD: Top: SMD= 100 µm: (a) Va= 20 l/min; Vo= 10 ml/min; (b) Va= 31 l/min; Vo=24 ml/min. Bottom: SMD= 140 µm: (c) Va= 20 L/min; Vo= 17.5 ml/min); (d) Va= 25 L/min; Vo= 24 ml/min

The deviation of the flow was also less prominent in the PIV flows with oil. This could be explained by the fact there is less or negligible deviation in the flow axis of the **oil** nozzle; all the PIV results with oil represent a mixture of the oil and air flows, since the PIV system is tracking the oil droplets in the measurements.

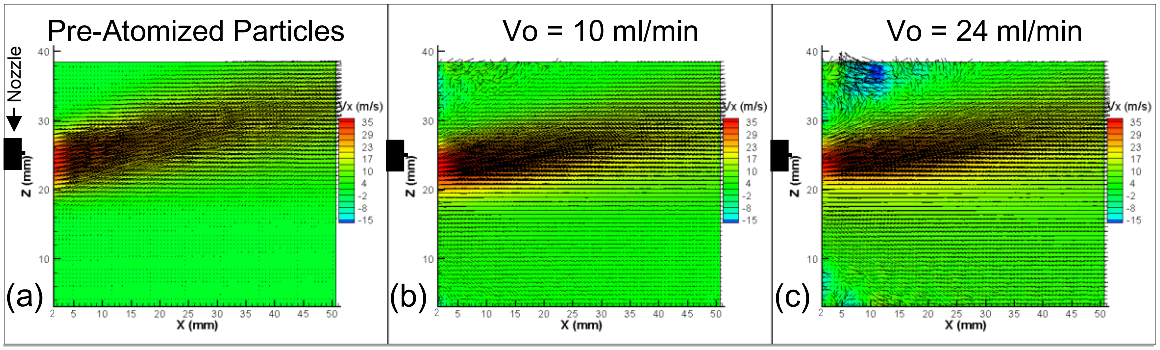

Figure 3.14 PIV stream-wise velocity distribution for Va= 31 l/min:
(a) With pre-atomized particles; (b) Vo= 10 ml/min (SMD= 60 μm); (c) Vo= 24 ml/min (SMD= 100 μm)

3.5 Conclusions

In summary, the nozzle behaviour is accentuated at the extreme air and oil flow rates. The predicted Sauter Mean Diameter controlled by these two flow parameters had the most impact on the flow behaviour. Jets of comparable SMD values had almost identical flow behaviour. When a large SMD was predicted, the coarser droplets increased the vorticity above the jet exit, indicating inadequate atomization. At low air flow rates, less vortices were present in the jet zone but the atomization quality was greatly affected if the oil flow rate was increased; the larger velocity in the Z direction of the larger droplets (as predicted by the SMD) is manifested in the form of vorticity in that region. At higher air flow rates, the higher air velocity at the exit allows the maximum atomization (low SMD) but the air flow becomes more turbulent in the jet region. This could be an indication of excessive atomization. An excessive atomization represents a loss in the quantity of lubricant effectively delivered to the cutting zone, despite the fact that the quantity that gets delivered is adequately atomized. Without a proper accounting of the quantity the lubricant dispensed through the jet, it cannot be concluded whether all the jet combinations effectively deliver all the dispensed oil. This was beyond the scope of this study, but can be verified through machining experiments. This is the subject of chapter 5.

Furthermore, the velocity measured by PIV is the velocity of the tracers, i.e. the oil droplets. It can be observed, however, that an increase in the exit velocity of the oil through an increase in the oil flow rate does not affect the measured stream wise velocity, for a fixed air flow rate. This implies that the measured velocity in PIV is the velocity of the combined jet, and that the jet flow velocity is predominantly the air velocity (since it is not affected by an increase in Vo). These experiments can, thus, be useful to validate a single-phase (air only) numerical model of the flow. This model could then be modified to describe the cutting environment more accurately than in PIV experiments. This advantage is not present in PIV since the flow zone has to be exposed in order to properly capture images of the flow, in addition to the cost and speed factors. The single phase model also has the advantage of the lower computational requirement in terms of power and time, as opposed to a more sophisticated two-phase numerical design, without loss of velocity information, but droplet distribution would still be unavailable. This is the subject of chapter 4.

Chapter 4 Computational Fluid Dynamics Simulations

4.1 Introduction

The experimental visualization of the MQCL nozzle flow allowed the observation of the external flow of the air and oil mixture. An important conclusion was the low effect of the oil flow rate on the flow stream-wise velocity in the jet region (droplet sizing and flow away from the jet region notwithstanding). This conclusion permits the construction of a numerical model of the nozzle air flow only, without any loss of the flow information. This model will then allow visualizing the external flow when a modification in the flow environment is present, without the need for further experimentation. It will also allow for simulating flow environments which are not possible to replicate in PIV experiments. By simply examining the air flow behaviour, the droplet behaviour can be predicted since the particles follow closely the air flow. The sizing of the droplets could then be predicted based on information available in the open literature on similar nozzles. Furthermore, this model will permit the visualization of the air flow inside the nozzle itself. This was not possible through PIV. With the combined knowledge of the droplet behaviour and the air flow behaviour when a machining environment is simulated, more information becomes available for analyzing actual machining results.

To begin, a model of the unobstructed internal and external flow of the nozzle was designed. This initial model allowed the validation of the model idealization and the accuracy of computation, with the use of the PIV flow results. The model was then modified to simulate a simplified machining environment, using stationary and rotating objects (simulating the tool and workpiece) under different air flow rates. Computational Fluid Dynamics (CFD) is a numerical technique used to solve the governing equations describing the fluid flow. The computations are performed at a finite number of points, rather than the entire flow field. The design and density of the meshing thus had to be carefully refined to obtain the maximum possible definition, without excessive computational time.

4.2 Mathematical Model

FINE™/Hexa, the software used in this study relies on hexahedral unstructured grids generated by the accompanying software HEXPRESS™ [54]. The mathematical model used was the Turbulent Navier-Stokes model with the κ-ε extended wall function. The κ-ε models implemented in HEXSTREAM™ are linear, that is, the turbulent Reynolds stress tensor is related to the mean strain tensor in a linear fashion through the Boussinesq assumption [55]. For a fluid with velocity tensor $\overrightarrow{\nu''}$:

$$-\left(\rho\overrightarrow{\nu''} \times \overrightarrow{\nu''}\right) = \mu_t \left[2S - \frac{2}{3}\left(\vec{\nabla}.\overrightarrow{\nu''}\right)I\right] - \frac{2}{3}\rho\kappa I \tag{4.1}$$

where ρ is the fluid density, μ_t is the turbulent eddy-viscosity, S is the mean strain tensor, κ is the turbulent kinetic energy, and I is the identity matrix:

$$S = \frac{1}{2}(\vec{\nabla} \times \overrightarrow{\nu''} + \left(\vec{\nabla} \times \overrightarrow{\nu''}\right)^T) \tag{4.2}$$

Two transport equations, written in their conservative form, are solved for the turbulent kinetic energy κ and the turbulent dissipation ε:

$$\frac{\partial\rho\kappa}{\partial t} + \vec{\nabla}.\left(\rho\mu\kappa - \left(\mu + \frac{\mu_t}{\sigma_k}\right)\vec{\nabla}\kappa\right) = P - \rho\varepsilon \tag{4.3}$$

$$\frac{\partial\rho\varepsilon}{\partial t} + \vec{\nabla}.\left(\rho\overrightarrow{\nu''}\varepsilon - \left(\mu + \frac{\mu_t}{\sigma_\varepsilon}\right)\vec{\nabla}\varepsilon\right) = \frac{1}{T}(C_{\varepsilon 1}P - C_{\varepsilon 2}\rho\varepsilon) + E \tag{4.4}$$

where μ is fluid viscosity, σ is the fluid surface tension, P is the turbulence production. In Equation 4.4, T is the turbulent time scale and E is a term specific to the Yang and Shih model [56], $C_{\varepsilon 1}, C_{\varepsilon 2}$ are the turbulent constants, to be discussed after. Denoting the trace of a matrix product by Tr, the production term is defined by:

$$P = Tr(-(\rho\overrightarrow{\nu''} \times \overrightarrow{\nu''}) \cdot S) \tag{4.5}$$

where $-(\rho v" \times v")$ is the turbulent Reynolds stress tensor, and S is the mean flow strain tensor. In the HEXSTREAM™ code, the incompressible formulation of the production is considered, even when compressible flows are simulated. This assumption guarantees that the production term never becomes negative, since $\nabla . v = 0$. The turbulent time scale T and the term E in Equations 4.3 and 4.4 are defined according to Yang and Shih [56] as follows:

$$T = \frac{\kappa}{\varepsilon} + (\frac{\nu}{\varepsilon})^{0.5} \tag{4.6}$$

$$E = \nu\mu_t(\vec{\nabla} \cdot S)^2 \tag{4.7}$$

where ν is the kinematic viscosity. The turbulent constants in Equation 4.4 are those given by Launder and Spalding [57]:

$$C_{\varepsilon 1} = 1.44; C_{\varepsilon 2} = 1.92;\ \sigma_\kappa = 1.0\ \sigma_\varepsilon = 1.3$$

The turbulent eddy viscosity is defined by a Kolmogorov-Prandtl type formula:

$$\mu_t = \rho C_\mu f_\mu \kappa T \tag{4.8}$$

where $C_\mu = 0.09$. The damping function is defined by Yang and Shih [56] as a function of the Reynolds number based upon the distance to the wall y with:

$$f_\mu = \sqrt{1 - e^{(-c_1 Re_y - c_2 Re_y^3 - c_3 Re_y^5)}},\ with\ Re_y = \frac{\rho\sqrt{k}y}{\mu} \tag{4.9}$$

where the constants are:

$$c_1 = 1.5 \times 10^{-4};\ c_2 = 5.0 \times 10^{-7};\ c_3 = 1.0 \times 10^{-10}$$

In this model, the turbulent equations 4.3 and 4.4 are not solved in the first layer of cells next to the wall. The κ and ε variables are defined by using wall functions derived from Direct Numerical Simulation (DNS). This wall function κ-ε model differs from the standard one (Launder and Spalding) [57], since different wall functions are used for κ and ε. Moreover, the turbulent time scale and the turbulent viscosity are defined in the same way as in the Yang and Shih model presented above. This model allows the user to obtain accurate results on fine meshes, contrary to the standard high Reynolds κ-ε model.

4.3 Meshing and Boundary Conditions

The air channel of the Tecnolub Inc. nozzle was modeled using a CAD software based on the real nozzle design. Figure 4.1 shows the modeling of the nozzle's internal channel. The oil channel was modeled as a cylinder that extends outside the air nozzle's exit (as it is the case with the real nozzle). The model was then imported to HEXPRESS™ for the remaining part of the modeling and meshing. Since the purpose was to simulate the flow inside and outside of the nozzle, a rectangular parallelepiped was added at the exit of the air nozzle (Figure 4.1).

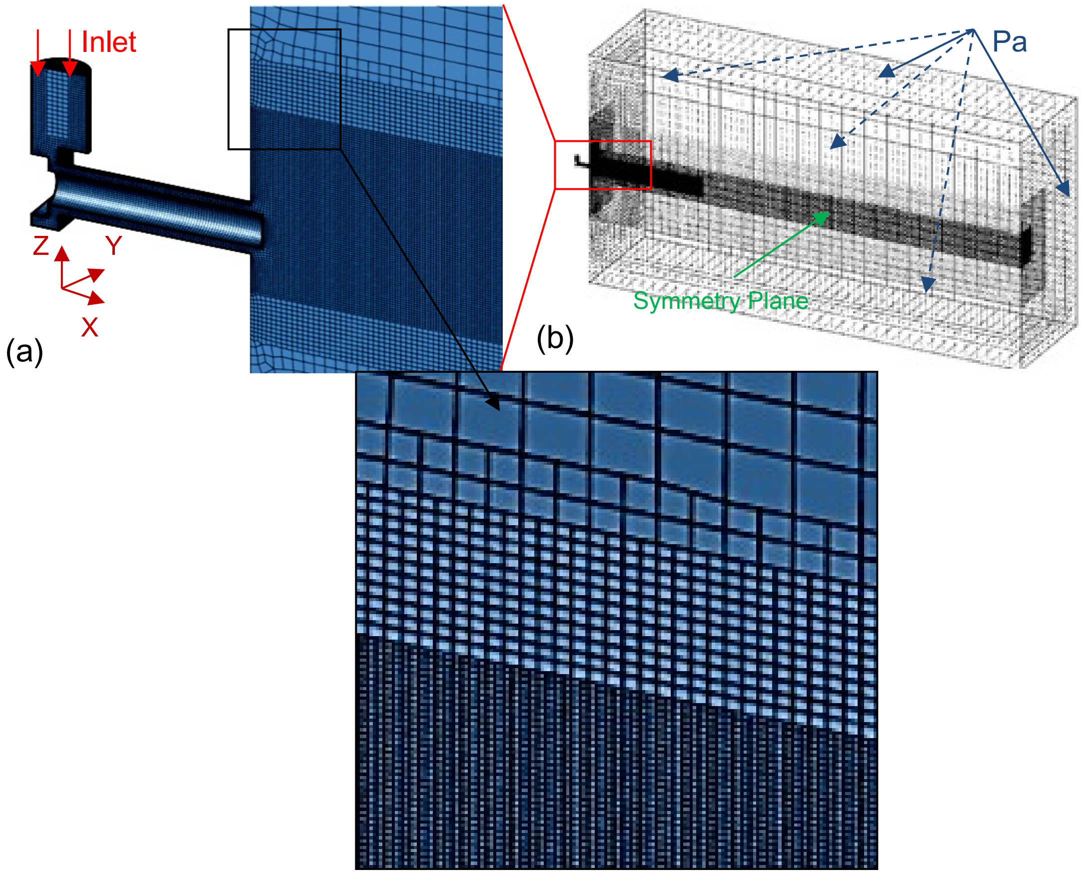

Figure 4.1 (a) Close-up of nozzle meshing showing air nozzle inlet and annular cross-section; (b) Meshing of external environment and boundary conditions, the darker regions contain denser meshes

This parallelepiped had the purpose of simulating the outer environment, in order to visualize the external flow. All the sides of the parallelepiped had an atmospheric boundary condition (Pa = 101.3 kPa). In addition, they did not permit any back-flow into the computed environment (Figure 4.1 (b)). Evidently, a dense mesh results in a larger number of points over which the calculations take place. The result is a more accurate and detailed solution at the expense of calculation time and required computational power. The compromise was achieved by making use of symmetry around the X-Z plane, since the flow was expected to be symmetrical along that plane. Because of the geometry of the nozzle, the flow was not expected to be symmetrical along the X-Y plane, as confirmed by the PIV experiments. In addition, the mesh was refined for denser grid in locations where a high velocity variation was expected, such as the case of a viscous boundary layer. A coarser grid was made where the solution is expected to change more gradually. Another important parameter in the solution quality is the grid structure.

4.4 CFD Model Description and Validation

Figure 4.2 (a-c) shows the stream-wise velocity within the nozzle cross section. It can be observed that the velocity is not uniform throughout the annular cross-section of the air channel. As the air exits the nozzle, a region of high circulation is present; this is the location where the atomization occurs (Figure 4.2 (d)). Figure 4.3 shows the misalignment of the flow cone axis with the nozzle axis, a noticeable deviation of the flow upwards can be observed. This deviation is consistent with velocity behaviour obtained in the PIV experiments. The cause of this deviation can be seen in Figure 4.2 (c), the 90° elbow of the nozzle's internal channel results in a visibly higher velocity in the lower region of the horizontal annular channel. This velocity gradient remains until the exit of the nozzle, resulting in the jet deviation. It is, thus, expected that a straight internal channel could eliminate this deviation and render the nozzle jet more symmetric. A longer annular channel could also lead to a more uniform flow at the exit.

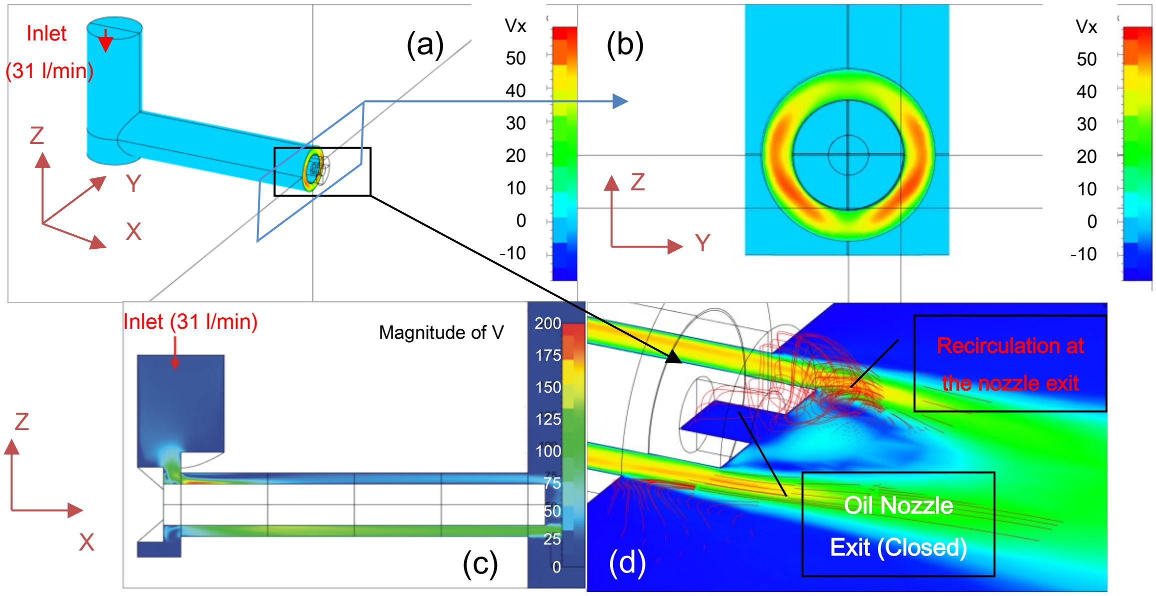

Figure 4.2 (a) Isometric view of the complete nozzle geometry; (b) Stream-wise velocity at the exit of the nozzle; (c) stream-wise velocity of the internal flow of the nozzle when Va= 31 l/min; (d) Isometric view of the recirculation at the nozzle exit, in the vicinity of the oil nozzle exit

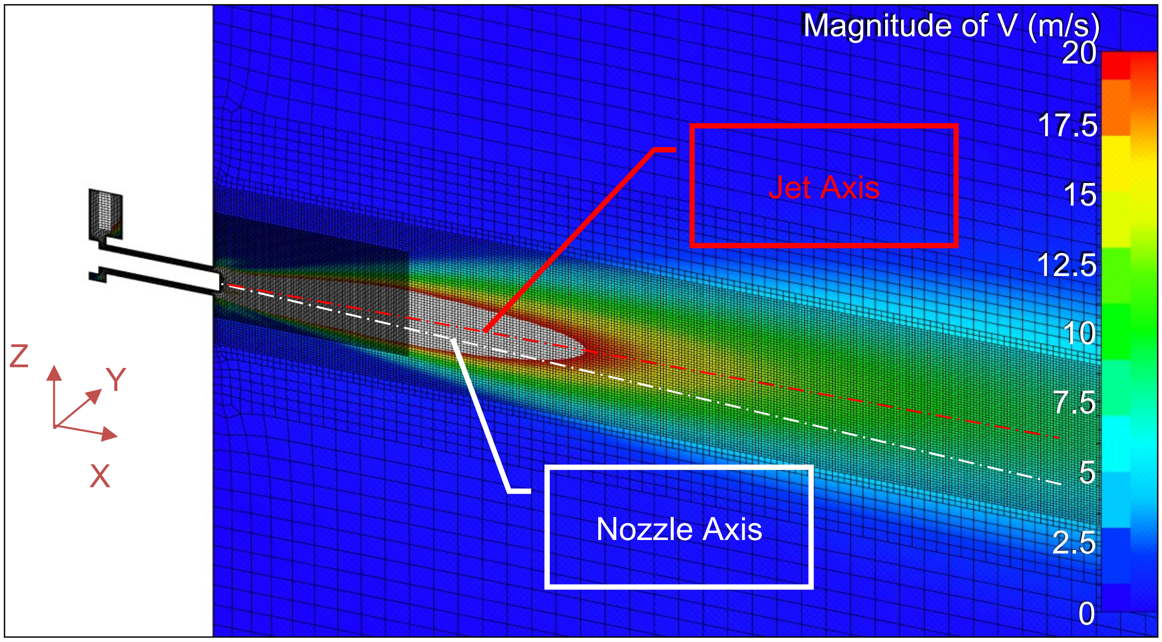

Figure 4.3 Magnitude of the velocity when the air exits the air nozzle into the external environment, Va= 31 l/min (velocities above 20 m/s were masked for better visualization)

For validation, the stream-wise velocity of the flow in the plane of the jet axis was compared with the mean experimental (PIV) stream-wise velocity (Va= 31 l/min). The comparison was performed over 150 points located at 4 distances from the nozzle exit. The velocity profile of the pre-atomized particle flow (PIV) was initially picked to exclude any effect the larger oil droplets could cause, however irrelevant. Comparisons with the oil flow were later performed. Figure 4.4 compares the mean experimental and the computed stream-wise velocity of the air at different distances from the nozzle exit. It can be seen that the velocities match with very little error just outside the nozzle exit. The deviation between the computed and the experimental flow axes then increases as the distance from the exit is increased, though the slope of the jet remains constant.

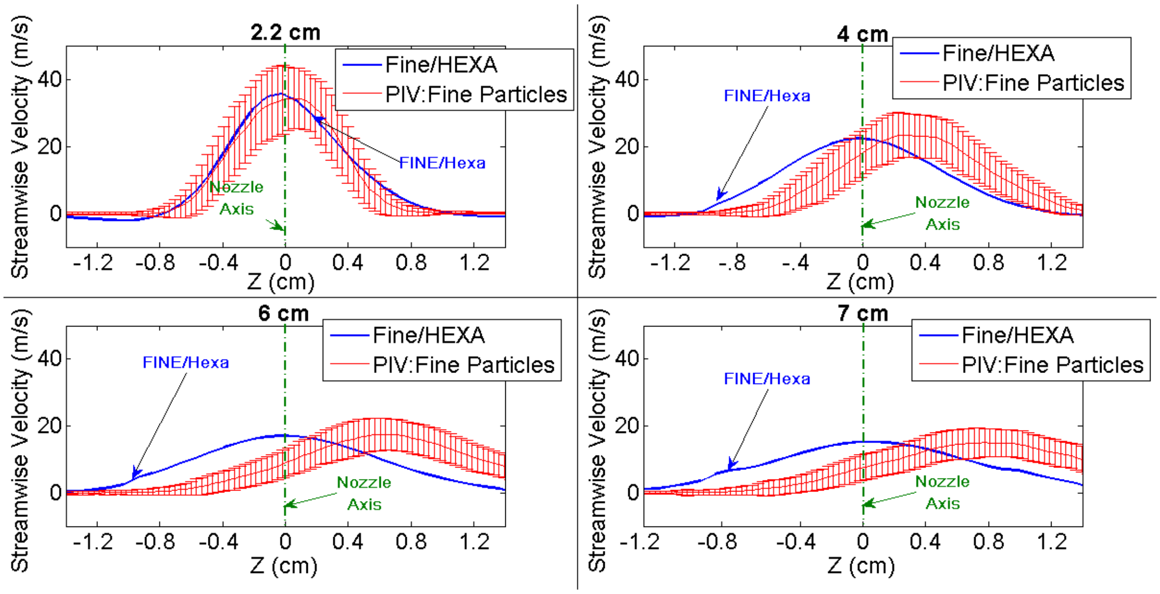

Figure 4.4 Comparison of computed and the mean experimental (Pre-Atomized Particles) stream-wise velocities of the air when Va= 31 l/min at different distances from the nozzle exit

The velocity distributions of the experimental and the computed flows are, however, shifted by about 5 mm. This shift could be explained by a physical misalignment of the MQCL nozzle with respect to the horizontal plane during the experiments; at a very close distance from the exit the deviation caused by an angular misalignment is minimal, as the distance is increased the effect of a small angular misalignment becomes more pronounced. It can easily be shown that a misalignment of only 4° could result in this shift. In addition, because the real MQCL nozzles are meant to be coaxial, any misalignment in the air nozzle with respect to the oil nozzle implies an annular cross-section of non-uniform thickness; this could increase the velocity gradient inside the nozzle since one side of the annular section will be thinner than the other. It is worth noting, however, that the error in the peak velocities is only 3.8% at 2.2 cm from the nozzle exit, and decreases to 2.1% at 7 cm from the nozzle exit. The errors of the peak velocities will be discussed further in a following section.

The numerical model was then compared with the oil PIV measurements with different oil flow rates. Figure 4.5 compares the computed and experimental mean stream-wise velocities at different distances from the exit, for the same air flow rate (Va= 31 l/min). The peak velocities match well again at close distance from the exit, then the deviation in the jet axis becomes more prominent downstream of the flow. With the exception of the peak velocities at 4 cm, all other peak velocities do not show any significant error in the calculation.

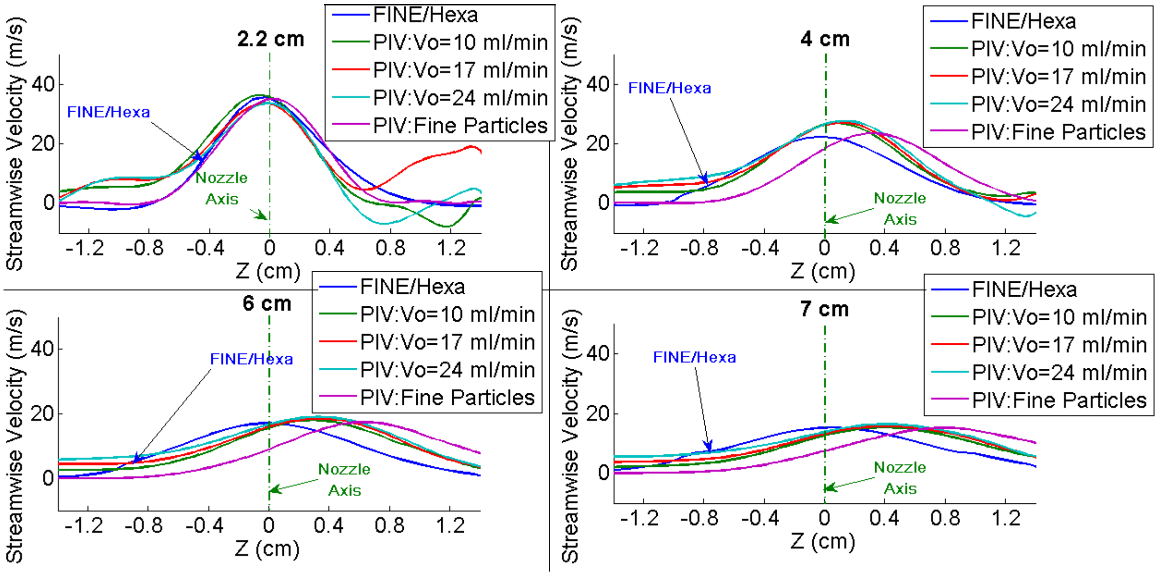

Figure 4.5 Comparison of computed and the mean experimental (Oil) stream-wise velocities of the air (Va= 31 l/min) at different distances from the nozzle exit

From these results it was concluded that the numerical model was valid for further analysis and development. The same model was, thus, used to simulate the flow of the remaining 3 air flow rates used in the PIV experiments. The computed and measured stream-wise velocities when the air flow rate is minimum (20 l/min) are shown in Figure **4.6**.

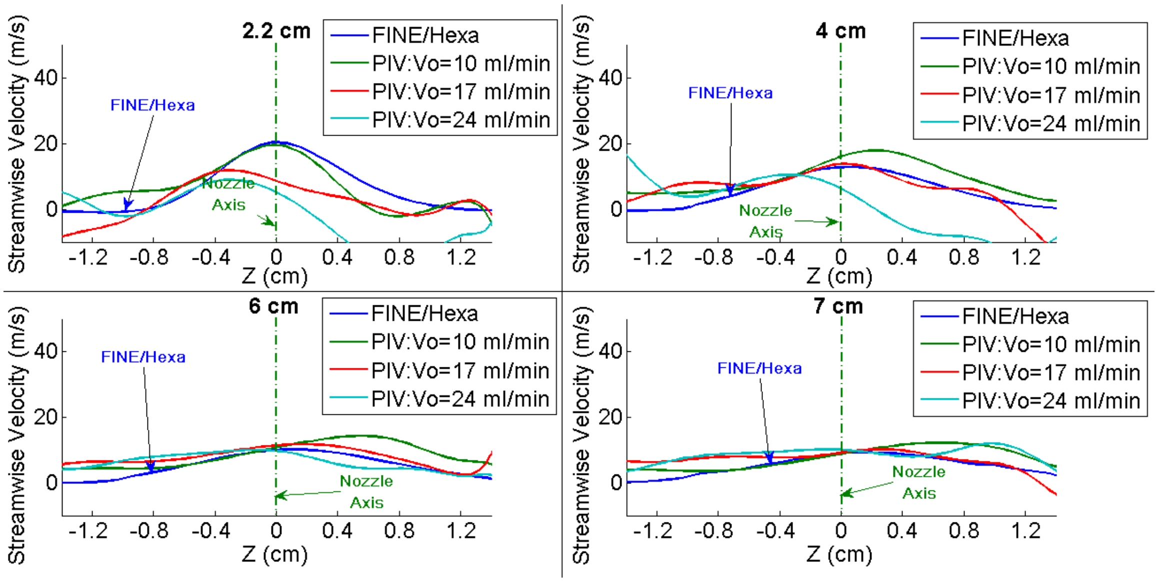

Figure 4.6 Comparison of computed and the mean experimental (Oil) stream-wise velocities of the air (Va= 20 l/min) at different distances from the nozzle exit

Approximately the same behaviour observed in the case of the maximum air flow rate is present in this case as well. An important observation, however, is that even at a close distance from the exit only the lowest oil flow rate results in a match between the computed and measured stream-wise velocities. This is the result of the inadequate atomization (large SMD) when the air flow rate is low while the oil flow rate is increased. Throughout all 4 simulations, there existed an appropriate match between the peak velocities in the jet cone, this observation was visible throughout all predicted SMD's in the PIV experiments with oil. Table 4.1 shows the errors when the computed peak velocities of the jet are compared with the experimental ones.

Table 4.1 Error of peak velocities when comparing simulation with experimental mean stream-wise velocities with different predicted SMD's

Distance from Nozzle Exit	PIV (Va= 31 l/min; Pre-Atomized Particles)	PIV (Va=31 l/min; Vo=10 ml/min) SMD = 63.5 μm	PIV (Va=20 l/min; Vo=24 ml/min) SMD = 195.3 μm
2.2 cm	3.78%	5.83%	128.24%
4 cm	4.06%	15.81%	23.34%
6 cm	2.75%	2.91%	10.00%
7 cm	2.09%	2.09%	9.78%

The largest error was obtained with the largest predicted SMD very close to the nozzle exit, in the vicinity of the atomization region. The lowest errors were equivalently obtained when the predicted SMD was lowest, and furthest away from the exit (7 cm). The causes of these errors can be attributed both to the proximity to the atomization region and to the size of the droplets. It is, thus, confirmed here that larger droplets are less efficient in following the air flow. In addition, the flow in the proximity of the nozzle exit would not have a proper atomization quality for machining application, since the atomization is still incomplete in that region.

4.5 Flow Behaviour over Stationary Obstacles

A smooth cylinder was placed in the nozzle jet region to simulate the effect of an obstruction present in a machining environment (Figure 4.7 (a)). Two cylinder diameters were used. The smaller diameter (1/4”) could simulate a small cutting tool while the larger diameter (3/4”) could simulate a larger tool or a cylindrical workpiece. Each tool was placed at two distances from the nozzle exit (38 mm and 170 mm), again to simulate various locations the nozzles could take. The 4 configurations were tested when the air flow rates were 20 l/min and 31 l/min. For the maximum air flow rate and the shortest cylinder distance, the Reynolds number expected for the flow over the smaller diameter tool was ~18,500, while it was ~35,000 for the larger diameter tool.

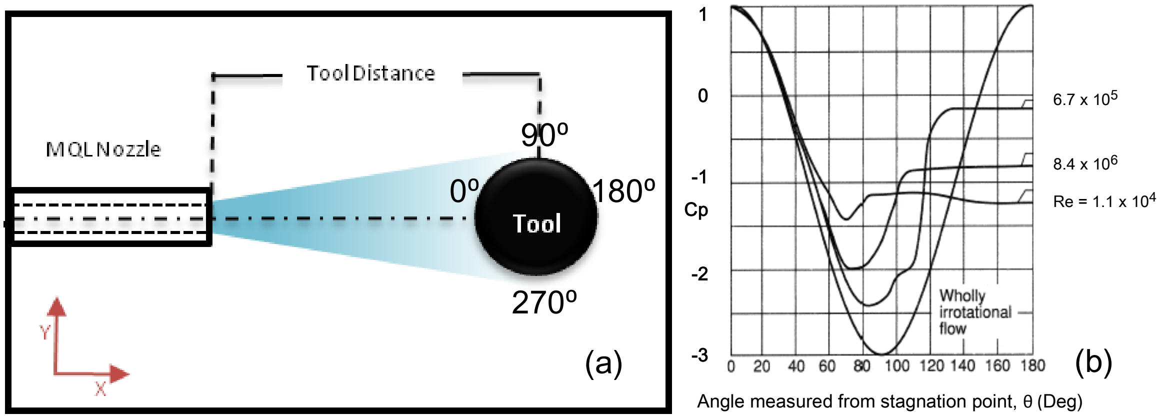

Figure 4.7 (a) Configuration of the simulated setup when a cylinder is introduced in the jet region; (b) Expected variation of the coefficient of pressure around the tool surface for different Reynolds numbers [52]

The Reynolds number is defined as follows:

$$Re = \frac{\rho v L}{\mu} \tag{4.10}$$

where ρ is the fluid's density, v is the fluids mean velocity, L is the characteristic length (the cylinder's diameter in this case) and μ is the fluid's dynamic viscosity. These Re values mean that a laminar boundary layer is expected around the cylinder surface, with a turbulent wake in the second half of the cylinder. For cylinders in uniform cross flow, the pressure is expected to drop around the point where the boundary layer separates from the cylinder surface, as shown in Figure 4.7 (b) [52]. Figure 4.8 shows the pressure distribution around the 1/4" diameter tool at close distance from the nozzle exit. The pressure at 80º from the

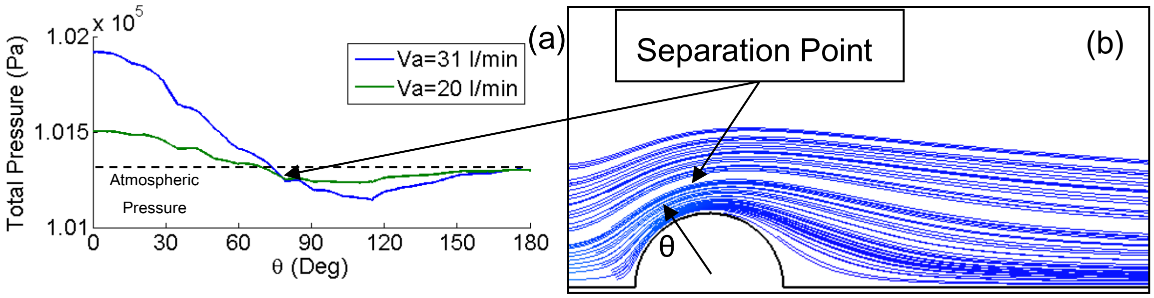

Figure 4.8 (a) Total pressure around 1/4" cylinder surface, at 38 mm from the nozzle exit; (b) Streamlines of the flow and the location of the separation point

stagnation point drops to below the atmospheric pressure indicating the flow separation. This pressure distribution is qualitatively in agreement with the Cp drop in Figure 4.7 (b), for the case of Re = 1.1 x 10^4.

Figure 4.9 shows the tangential velocity of the air flow around the cylinder surface for all the conditions tested. Here the separation of the flow and the wake region can be observed in the form of negative velocities right around the 80º – 90º region. A lower tangential velocity can be observed in the case of the larger diameter cylinder at close distance from the exit. The flow at 170 mm from the exit shows no difference in behaviour around the tool, but the velocities are too low for practical use. For a fast delivery of the lubricant to the cutting zone, a faster tangential velocity is desired. A faster tangential velocity will encourage more convection with the carried lubricant, as well as with the air flow itself.

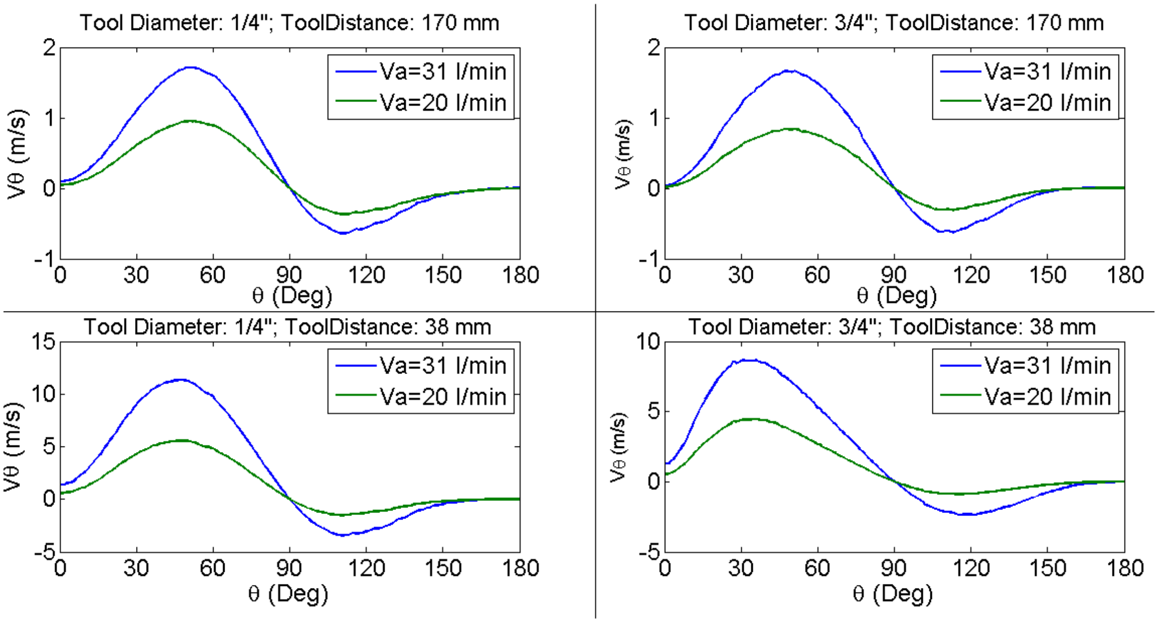

Figure 4.9 Tangential velocity of the air flow around the cylinder surface for all the conditions tested

4.6 Flow Behaviour over Rotating Obstacles

To observe the effect of a moving obstacle on the flow, a rotating cylinder was introduced in the jet region to simulate a rotating tool or workpiece. When a cylinder is rotated in a cross flow, the turbulent wake and boundary layer are expected to shift in the direction of the cylinder rotation (Figure 4.10 [58]). The CFD mesh was redesigned to include the full geometry of the flow region, which would not be symmetric in the case of a rotating cylinder.

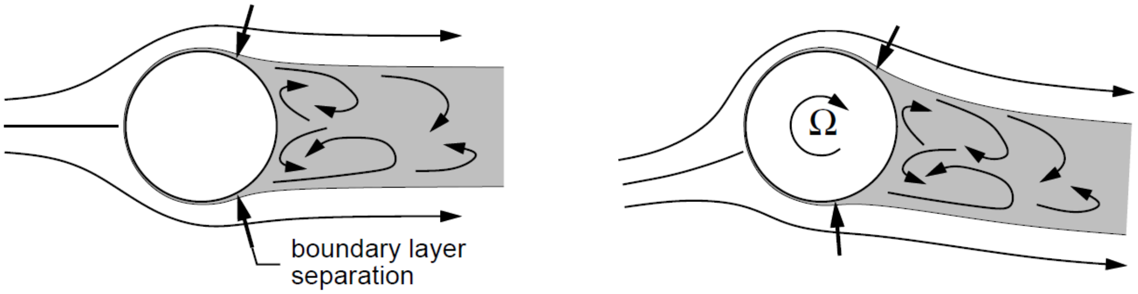

Figure 4.10 Effect of rotation on a uniform flow for Re≥10^4 [58]

Figure 4.11 shows the tangential velocity of the air around the 1/4” tool, when the rotational speed is varied between 5,000 and 15,000 rpm. The effect of the rotational speed can be observed in the higher tangential velocity in the second half of the tool section (i.e. downstream of the tool). The location of the flow separation point is slightly shifted under the effect of the rotational speed, though only by 1º to 4º for each rotational speed increase of 5,000 rpm. It can

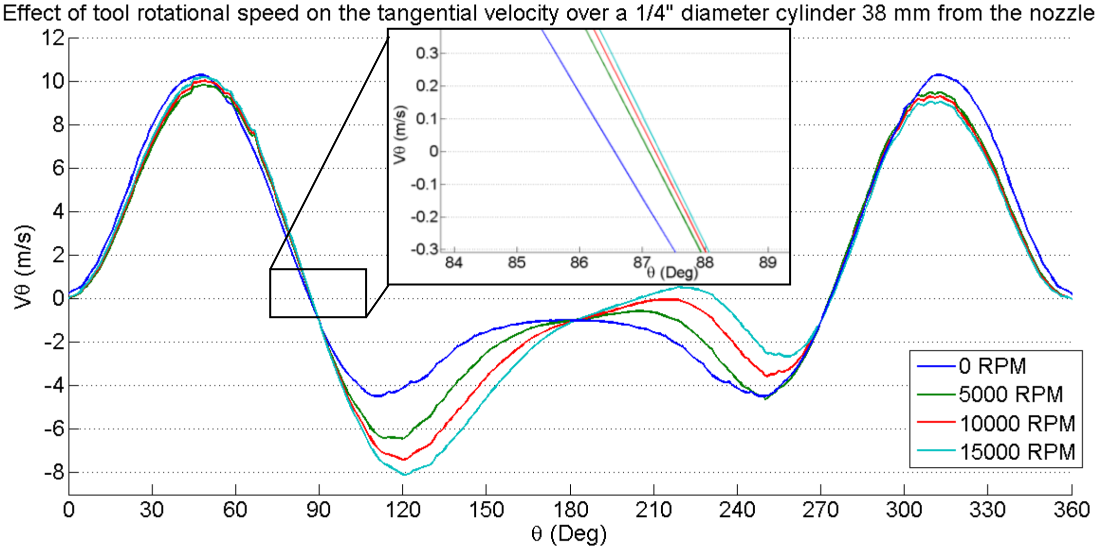
Effect of tool rotational speed on the tangential velocity over a 1/4" diameter cylinder 38 mm from the nozzle exit

Figure 4.11 Tangential velocity of the air around a 1/4” cylinder as the rotational speed is varied between 5,000 rpm and 15,000 rpm. The velocities around the stationary cylinder were projected for comparative purposes.

thus be concluded that, for the aforementioned range of tool speeds, little change in the behaviour of the flow around a rotating tool is expected. Therefore, for a real atomized flow with sufficiently low SMD, the oil droplets are expected to follow the tool rotational direction.

4.7 Flow Behaviour over Rotating and Heat Generating Obstacles

For a non-rotating cylinder in cross flow, the local Nusselt number varies over the surface of the cylinder. The Nusselt number is a dimensionless parameter representative of the convective heat transfer occurring, it is defined as:

$$Nu = \frac{hL}{k_f} \qquad 4.11$$

where h is the convective heat transfer coefficient, L is the cylinder's characteristic length (the cylinder's diameter in this case) and k_f is the fluid's coefficient of thermal conductivity. Figure 4.12 [58] shows the local Nusselt number variation for a non-rotating cylinder in uniform cross flow, and Reynolds number between 7,800 and 219,000. For a rotating cylinder, the behaviour of the Nusselt variation changes depending on the Re and the rotational speed. It is, therefore, expected that the maximum Nu shifts in the direction of the rotation.

To further simulate the machining environment, a uniform heat generating boundary condition was added to the cylindrical surface. The purpose was to simulate the heat generated during the cutting operation, and to investigate the presence of a heat transfer variation around the periphery of the tool surface. Such variation could be exploited for maximum heat transfer to the air, if the nozzle is positioned appropriately. The same model used in the stationary and rotating tool simulations was used again, only with the additional heat generating boundary condition of 10 W/m^2 (Figure 4.13). The estimate for the heat generated was calculated based on typical machining parameters.

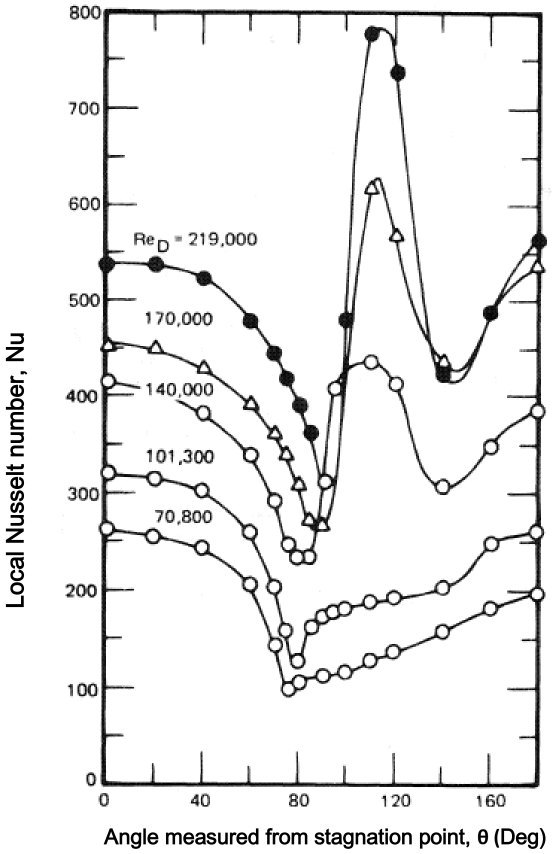

Figure 4.12 Local Nusselt number over a stationary cylinder surface [58]

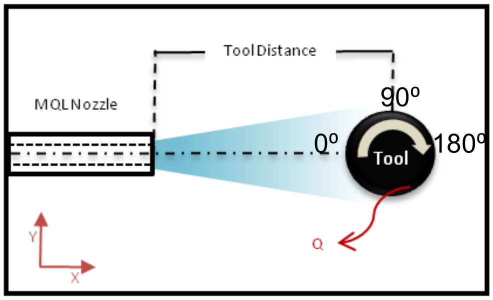

Figure 4.13 Configuration of the simulated setup when a rotating cylinder with heat generation is introduced in the jet region

Figure 4.14 shows the resulting Nusselt number distribution over the surface of the tool. A major and a minor peak can be observed in the second half of the cylinder, between 220° and 250°, indicating increased heat exchange with the air jet.

The peaks fall in the wake region of the cylinder, where high circulation is present. This observation implies that, in this region, more heat exchange is occurring with the air. This could prove beneficial in machining; in a milling operation the heat output will be cyclic (due to the intermittent cutting effect) and the maximum heat generation will occur at the point with the maximum chip thickness. If the nozzle is oriented such that the maximum heat exchange occurs in that point, the heat transfer with the nozzle air will be more prominent, and could help reduce the cutting temperatures.

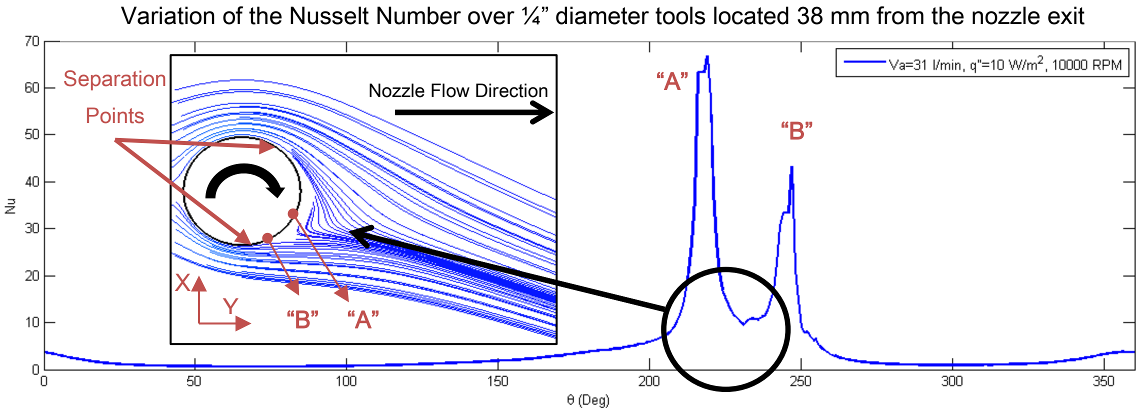

Figure 4.14 Resulting local Nusselt number distribution over the surface of the rotating cylinder (10,000 rpm), when Va= 31 l/min

4.8 Conclusions

The comparison of the single-phase numerical model with the PIV experimental flow results indicated a strong resemblance in the flow behaviour, despite the absence of the liquid droplets from the model. The fact that a single-phase model was reliable in predicting the flow allowed the use of the numerical model to further simulate the machining environment, without resorting to a more complex 2-phase model.

It was shown that the effect of the increase in air flow rate results in the same velocity profiles as in the PIV experiments with oil droplets. This resemblance decreases in the case of excessively high predicted SMD (~140 μm). With the knowledge that the oil droplets follow the air flow as was shown in Chapter 3, the behaviour of the air-oil mixture can be visualized with great accuracy.

The presence of a tool in the jet region caused the air flow to follow the tool surface; the tangential velocities decreased with the tool diameter. A short cylinder distance was observed to show higher tangential velocities, since the flow weakens far away from the nozzle exit and would not be suitable for practical use in machining.

When the tool is rotating, the separation point is shifted in the direction of rotation. This shift increases with the increase in rotational velocity. As heat is generated on the tool surface, the temperature of the ambient air flow increases; the local Nusselt number was shown to vary with the location around the tool, peaking at 220º (taken in the direction of rotation) from the nozzle flow direction for a Va of 31 l/min and tool rotational speed of 10,000. This observation could prove useful in machining, where the MQCL jet could be oriented for a maximum heat transfer from the tool and workpiece surface. The best location for the nozzle with respect to the cutting direction must therefore be considered when using the MQCL nozzle. The effect of the direction of chip generation must also be considered in practice, as chips could highly interfere with the nozzle flow.

Chapter 5 Machining Experiments

5.1 Introduction

The flow visualization trials, reported in Chapter 3 and Chapter 4, investigated the effect of the MQCL flow parameters on the atomization and the air flow behaviour. In this chapter, these parameters were investigated for their effect on the machining of carbon-fiber-reinforced plastic (CFRP) composites.

Three sets of experiments with MQCL were designed in order to study the effect of the flow parameters (namely lubricant and air flow rates and coolant or lubricant type), and nozzle parameters (namely the nozzle orientation, and nozzle diameter), on the routing of CFRPs. Routing is a machining process commonly applied in the manufacturing of aerospace CFRP components. It is a subcategory of slotting, where the axial depth of cut is equal to or greater than the workpiece thickness.

The first set of experiments was composed of a number of tests seeking to determine the most suitable nozzle position vis-à-vis the cutting direction, by investigating various nozzle positions. The second set sought an understanding of the effect of different tribological environments during prolonged cutting, by comparing various MQCL conditions with conventional alternatives. Finally, the third set aimed at finding the significance of the MQCL flow parameters in the machining of CFRP laminates, in terms of their effects on the machining quality and tool wear. A total of 60 tests were performed.

5.2 Experimental Setup

The routing experiments were performed on a 5-axis DMU 100P duoBLOCK® CNC milling machine (28 kW; 18,000 rpm max). A practical problem in the machining of CFRPs is the NC machines' vulnerability to the abrasive dust, resulting in the process. The experimental setup, therefore, needed to allow a rapid collection of the CFRP dust generated, without intervening with the collection of the data, such as temperatures and forces (Figure 5.1). Furthermore, the developed setup was designed to allow a flexible positioning of the MQCL nozzle to ensure its functionality for future applications, such as different cutting directions.

The test sample was mounted vertically to an aluminum fixture bolted to the horizontal dynamometer (Kistler 9255B, with a linearity error of ±1% and a cross-talk error of ±1%, see Appendix C), which rested on the CNC machine table (Figure 5.1). The height of the test sample was limited by the allowable measurement height permitted by the dynamometer's manufacturer (120 mm). The forced were measured with the dynamometer and the data was recorded using data acquisition hardware (Kistler 5070 8-Channel Charge Amplifier, and National Instruments PCI4472, 24 bit resolution, 102.4 kS/s sampling rate).

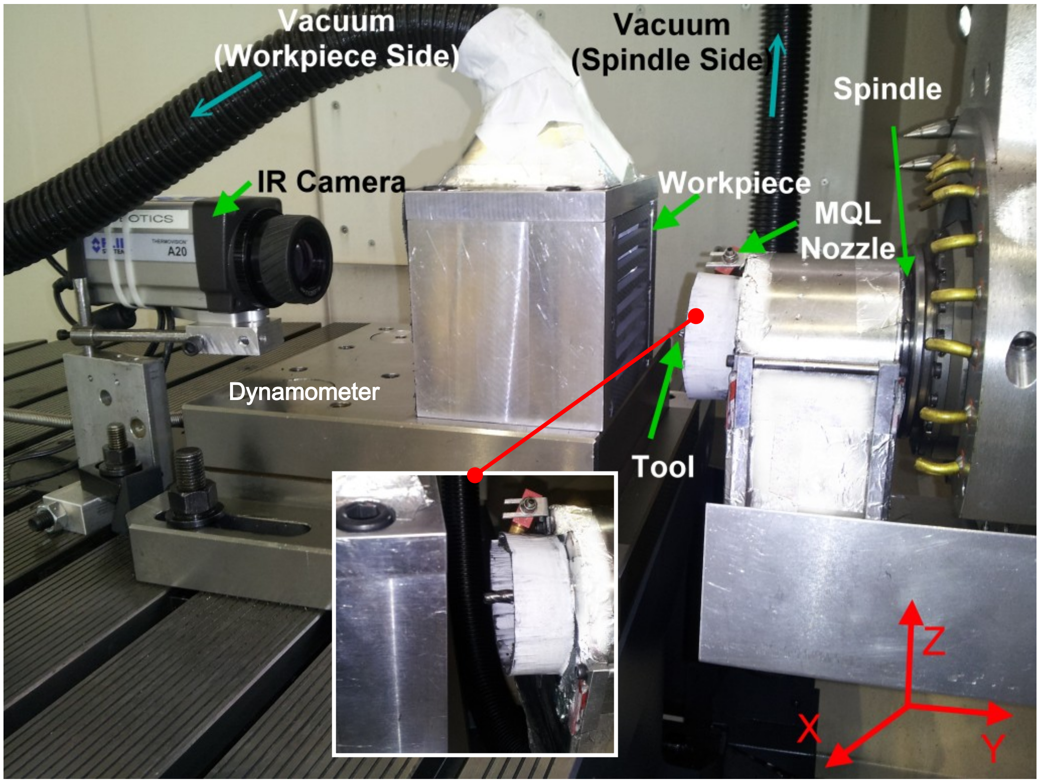

Figure 5.1: Overview of the experimental setup used in the machining experiments

An infrared camera was used to measure the tool temperature. Although less accurate than using a thermocouple device, it is more appropriate given the potential for CFRP to delaminate if a thermocouple was inserted. Instead, a FLIR ThermoVision® A20 infrared camera, located behind the workpiece, was used to capture the temperature of the tool throughout each test. The camera was fixed on the CNC machine table and directed towards the workpiece as shown in Figure 5.2 (a). The data acquisition software had to be calibrated in order to properly obtain the emissivity of the measured surface (the carbide cutting edge), for the temperature range of cutting. This value was obtained by preheating the tool to different temperatures using a torch, and comparing the IR camera's measured temperature of the tool surface with thermocouple readings, until the proper emissivity is obtained. The temperature measurement error expected was ±15º, between 100º and 200º C (see Appendix C).

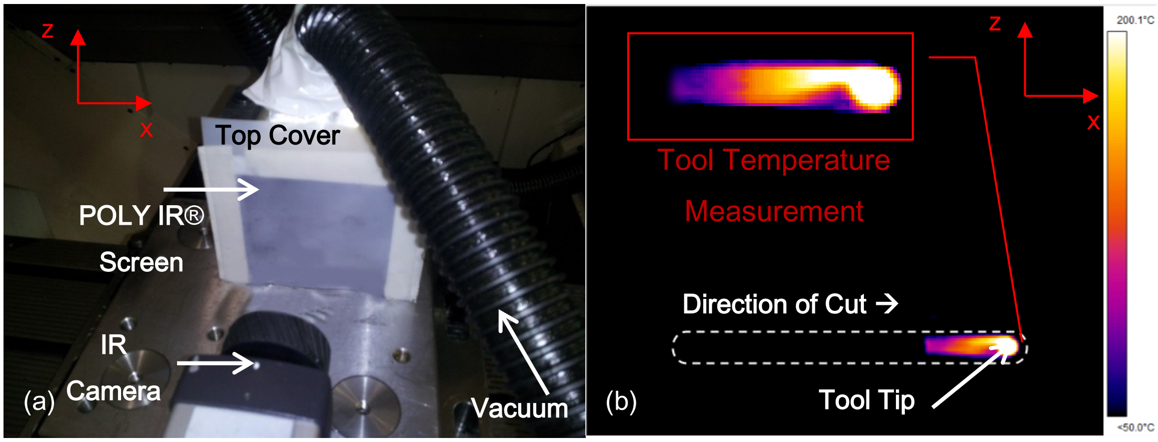

Figure 5.2: (a) View from the back of the experimental setup showing the Top Cover, the IR Camera, and the protective polymeric screen; (b) Typical IR Camera visual output showing the cut outline and the measured maximum temperatures in the measurement window

To avoid the obstruction of the temperature measurement, a special polymeric screen (POLY IR® 2) was used in the casing behind the workpiece. This polymer was transparent to the infrared light in the wavelength range used by the camera, but it was found that a recalibration of the camera was still necessary. The emissivity of the tool behind the screen was found to be 0.23, as opposed to 0.55 in the absence of the screen. Figure 5.2 (b) shows the temperature output of the camera with the screen at the end of the cut.

During the routing process, CFRP dust is generated on both sides of the machined laminate. To prevent any machine damage, the CFRP dust was collected in these two locations; behind the workpiece, via a top cover leading to the vacuum (Figure 5.2 (a)), and on the spindle side, with the assistance of a cover that enclosed the machining area close to the tool (Figure 5.3).

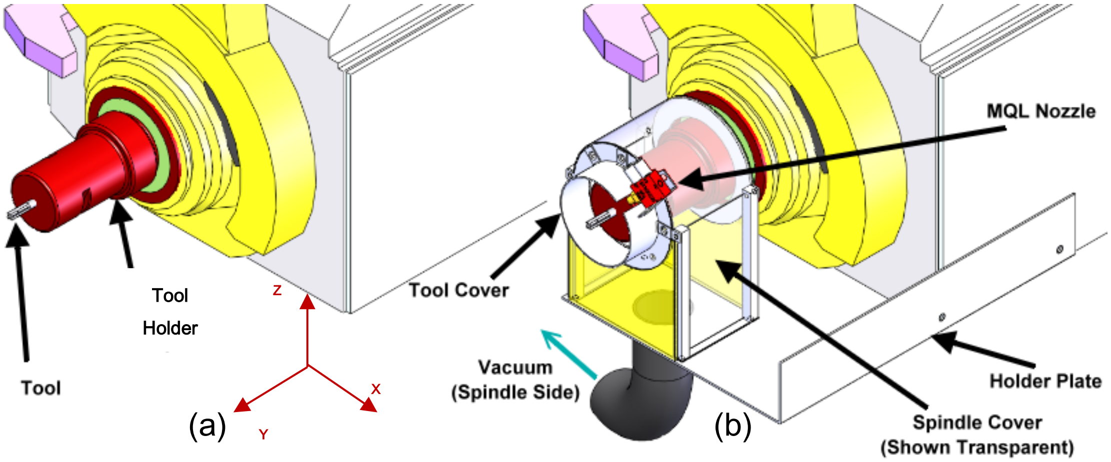

Figure 5.3: CNC Machine spindle head with the experimental machining setup. (a) Spindle head with setup unmounted; (b) Spindle head with setup mounted

The spindle cover was resting on a holder plate attached to the spindle head. A tool cover, on the perimeter of the front opening, covered the periphery of the tool for close collection of the chips as they are generated. The tool cover allowed 7 mm of the tool to penetrate the workpiece, and contained an opening for the MQCL nozzle. A clearance between the tool cover and the workpiece prevented the setup from touching the workpiece and introducing error in the dynamometer measurements. Further measures were taken in order to prevent the vacuum channels from touching the dynamometer during the tests.

The most suitable direction for the MQCL nozzle with respect to the cutting direction was to be determined in the first set of experiments. A nozzle fixture was developed to allow eight positions radially around the tool, with 45º of spacing between each two adjacent positions, as shown in Figure 5.4 (a). The nozzle holder, mounted on the nozzle fixture, allowed four degrees of freedom for further radial and vertical positioning of the nozzle. This was necessary for the nozzle's fine-positioning and flexibility.

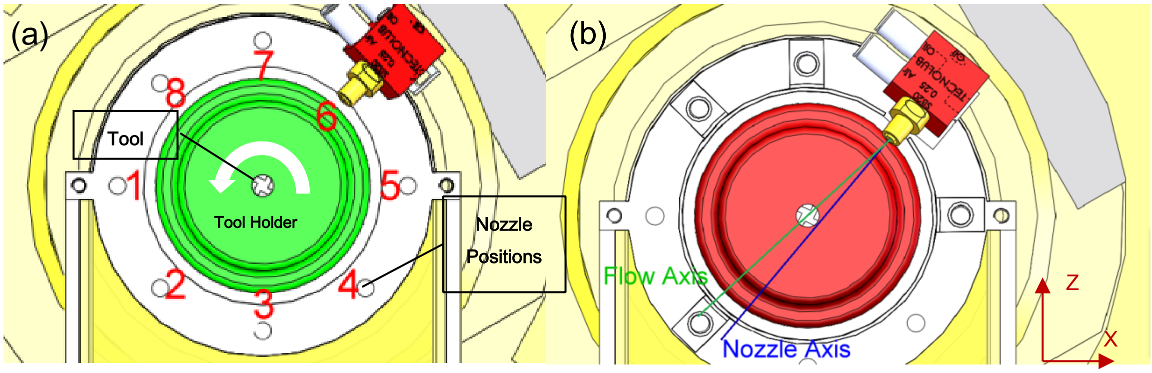

Figure 5.4: (a) Front view of setup cover showing 8 possible nozzle positions, nozzle in position #6; (b) Nozzle fine-positioning by flow axis

Both the PIV and the CFD results showed a deviation between the flow axis and the nozzle axis. This was compensated for by rotating the nozzle counter-clockwise, to radially align the actual flow axis with the tool axis (Figure 5.4 (b)). The nozzle was also positioned so that its axis is at an angle with the X-Z plane (Figure 5.5). This angle permitted the shortest cutting distance before the lubricant could physically contact the midpoint of the cutting edge, where the maximum effect of lubrication is assumed.

As mentioned earlier, the MQCL system provided by Tecnolub Inc. was a two-channel Airblast external system; an outer pressurized air nozzle provided the necessary kinetic energy to atomize the cutting fluid exiting the inner channel. The coolant/lubricant used was MECAGREEN 550 for all pure oil (MQL) and emulsion (MQC) tests. It has the same physical characteristics as the lubricant used in the PIV experiments (EMULTEC VG). Two lubricant nozzle diameters were used throughout these experiments. The system was fitted with an electronic air flowmeter at the inlet of the system's air channel to measure the air flow rate supplied to the nozzle.

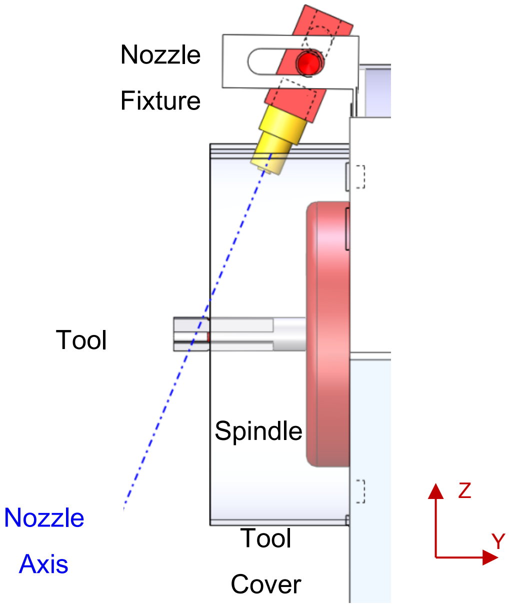

Figure 5.5: MQCL nozzle axis fine-positioning with respect to the X-Z plane

Due to the low liquid flow rates used in MQCL, suitable liquid flow meters were not available commercially. In order to control the liquid lubricant flow rate, a pressure sensor was mounted at the inlet of the liquid channel, and an empirical pressure-flow rate relationship was developed for each nozzle and coolant type used (Figure 5.6). This characteristic relationship was used to correlate the measured pressure at the channel inlet, with the flow rate at the nozzle exit. The maximum errors expected for the oil and air flow rates are ±8.5% and ±3%, respectively (see Appendix C). This MQCL setup was identical to the one used during the PIV experiments in the previous study.

The orthotropic properties of CFRP materials have implications on the machining process. Due to the large number of variables already involved in these experiments, measures were taken in the material selection to limit its orthotropic effects. A stacked multidirectional (0º-45º-90º-45º) woven laminate was therefore selected in order to best mimic isotropic material properties (see Appendix B). The laminate had a thickness of 6.35 mm and was cut into plates 125 mm x 112 mm, with 6 countersunk clear-holes to prevent the mounting screws from interfering with the tool cover.

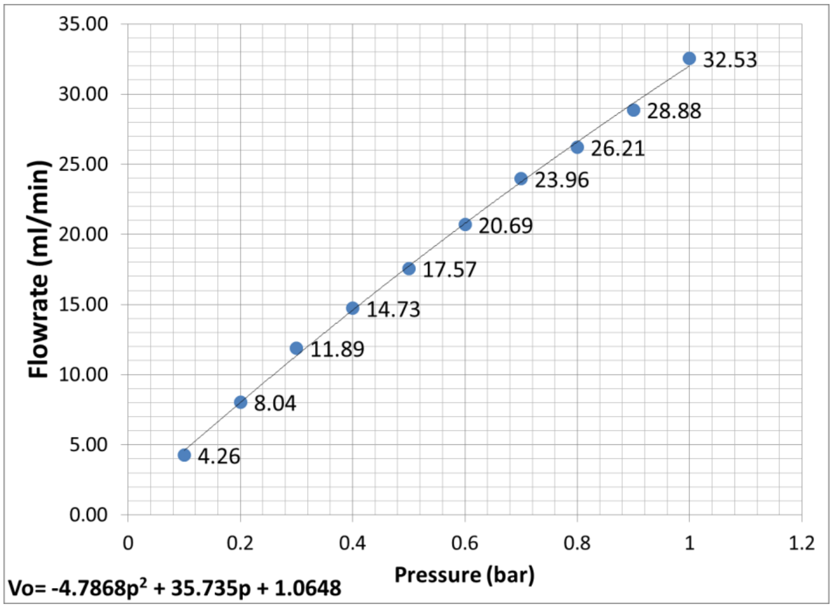

Figure 5.6: Pressure-Flow rate characteristic for 5% Mecagreen 550 emulsion.

Each workpiece had space for 8 horizontal routing slots, 90 mm in length each (Figure 5.7). The distance between each two adjacent cuts was 6.35 mm. A pilot hole was first drilled at each cutting location to permit tool to penetrate the axial depth of cut in the Y axis (i.e. the workpiece thickness), before the routing along the X axis began. This was to ensure that the tool cover on the spindle side was flush with the workpiece. The result was avoiding an initial dispersion of cutting dust, when the spindle is not close enough to the workpiece for the vacuum to be efficient. The pilot holes also permitted keeping the side cutting edges of the tools intact prior to the start of the routing process, during entry.

All cuts in the experiments were performed using helical 4-flute 1/4” uncoated tungsten-carbide endmills (SGS-30131). The selection criterion was to combine the elevated hardness of tungsten-carbide with the moderate cost compared to coated carbide tools. Uncoated carbide tools are also more commonly used in the industry. A total of 29 tools were used in all tests, an additional tool was used to pre-drill the pilot holes on the samples.

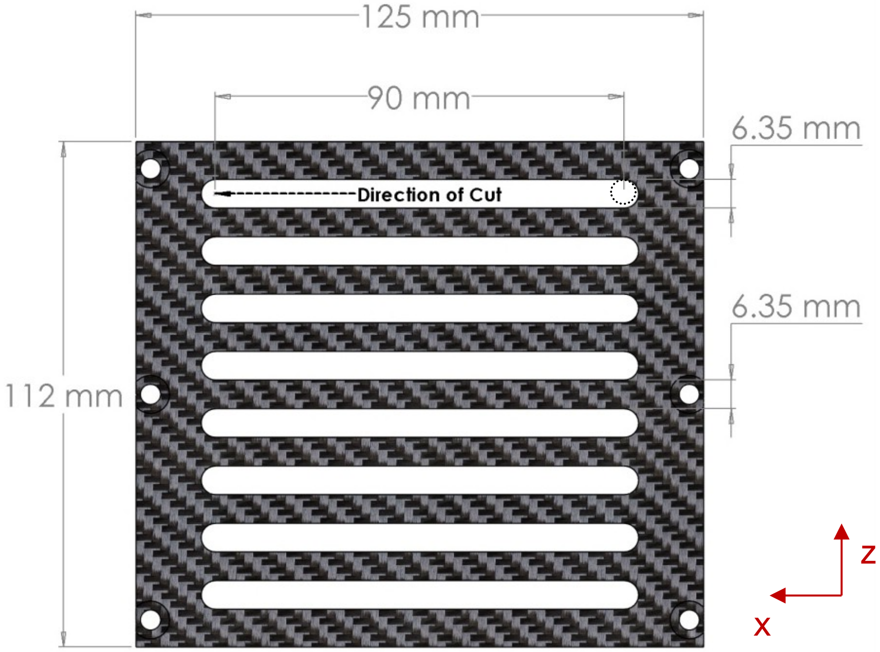

Figure 5.7: Front view of workpiece layout showing a sample pilot hole (dotted)

5.3 Results and Analysis

5.3.1 Study of the Effects of the Nozzle Orientation (Experimental Set-1)

The flow visualization study in section 4.7 has revealed a variation in the Nusselt number around the periphery of the tool surface (Figure 4.14). It was further shown that when the tool was rotated, this variation underwent a rotation relative to its position when the tool was stationary. The maximum heat transfer to the air, when the tool is rotating, was predicted to be about 220º (taken in the direction of rotation) from the nozzle flow direction, for a Va of 31 l/min and tool rotational speed of 10,000. Depending on the nozzle position, this location could be aligned with different geometric features in the cut, such as the cut direction. It was therefore necessary to determine the most suitable nozzle position, which would allow the maximum exploitation of the coolant/lubricant use, as well as this Nusselt variation, if it is indeed significant.

A two-step set of experiments was designed to first test 8 different nozzle positions around the spindle/tool, with constant cutting and MQCL flow parameters. The resulting temperature, force and tool wear measurements were used as a basis for the selection of two most appropriate positions. This was followed by prolonged cutting using the two selected nozzle positions. The cutting conditions for the first step are shown in Table 5.1. To exclude the effect of tool wear, no tool was used for more than 90 mm of cutting in this step. The cutting forces and temperatures were measured, flank and rake tool wear were found to be negligible.

Table 5.1: Nozzle Orientation Study Parameters

Coolant Type	Pure Oil (MQL)
Nozzle Diameter (mm)	0.25
Va (l/min)	31
Vo (ml/min)	17.5
N (rpm)	10,000
Vf (mm/min)	1,000
Vc (m/min)	200
Chip Load (mm/tooth)	0.025
Cutting Length (mm)	30

The results in Figure 5.8 show the variation of mean forces and maximum tool temperatures, with the nozzle position. The lowest tool temperatures were obtained using nozzle positions #4 and #8. The feed force values obtained at those two positions were moderate, though not the lowest. In the analyses presented in this chapter, the mean forces in the machine's X axis direction were the basis of the evaluation (feed force), being the most representative of the cutting forces. Similarly, only the temperature of the tool at the end of each cut was taken into consideration, being typically the maximum temperature in that cut, as shown in Figure 5.9.

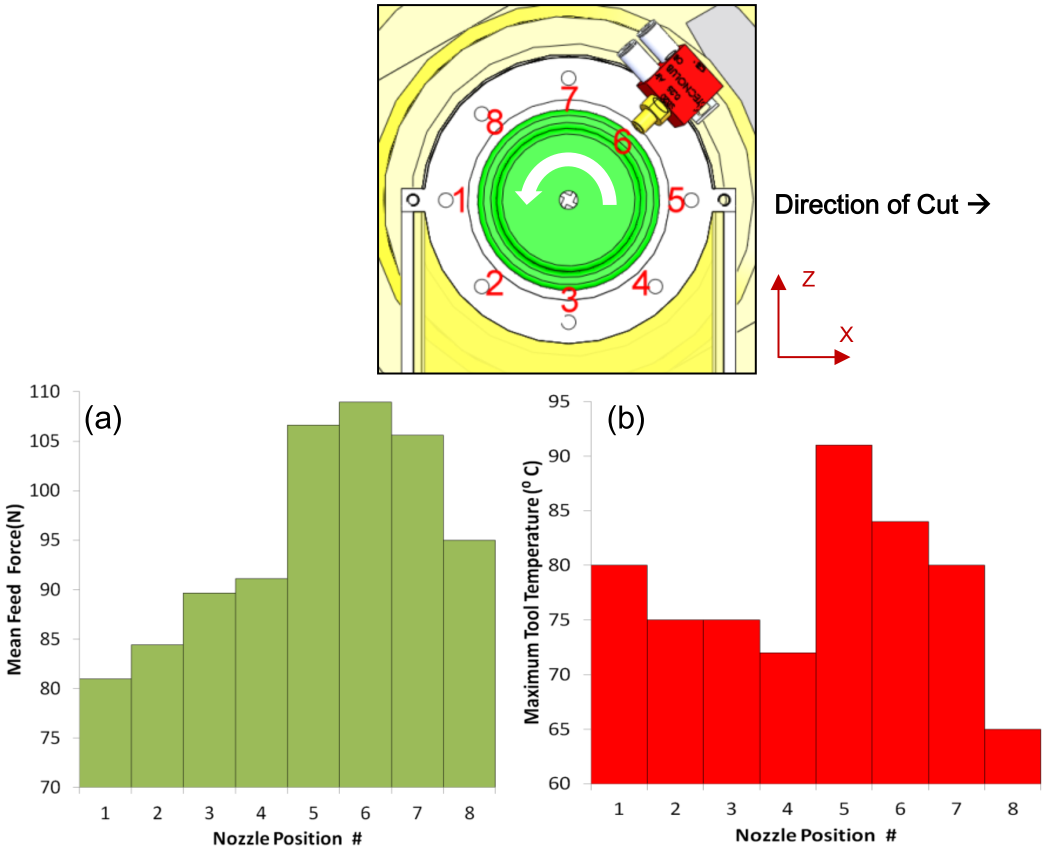

Figure 5.8: Force and maximum tool temperature comparison between the different nozzle positions. (a) Mean feed forces; (b) Maximum tool temperatures

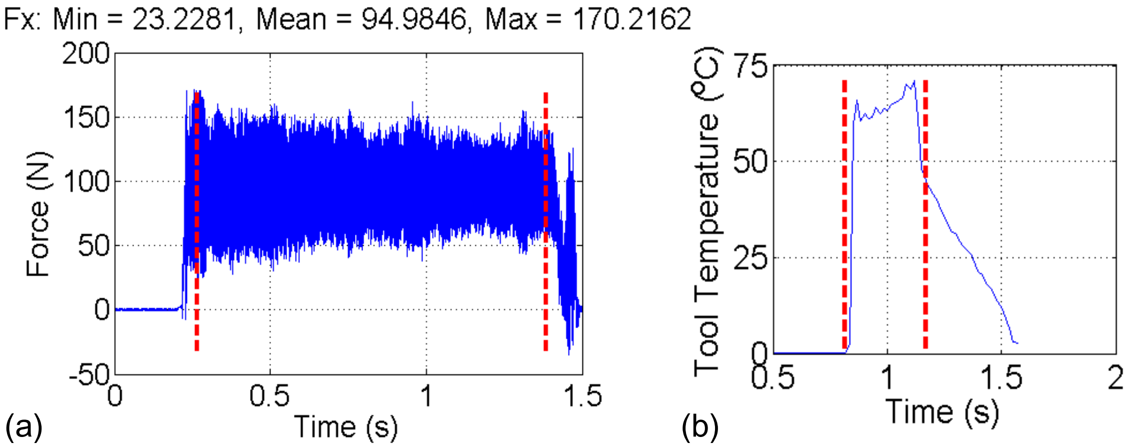

Figure 5.9: Typical feed force and tool temperature signals for position #8 (Vc = 200 m/min, Vf = 1,000 mm/min, N = 10,000 rpm). The dashed red lines represent the interval over which the mean forces and maximum temperatures were extracted. (a) Mean feed forces; (b) Tool temperatures

The next step in this study was to compare the best two nozzle positions in the previous step under prolonged cutting, in preparation of the second set of experiments. Here, the machining and lubrication parameters from the second set were used (N= 15,000 rpm, Vf= 1,500 mm/min, Va= 31 ml/min, Vo= 24 ml/min, coolant: 5% MECAGREEN 550 Emulsion (MQC)). Cutting was interrupted after 90 mm segments to record the tool wear. The results in Figure 5.10 show the flank wear measured after each segment. The tool wear trends were consistent with the values in the 30 mm tests, with position #8 resulting in slightly less overall flank wear than position #4. The force and temperature results for these two cuts are analyzed in detail in the next section.

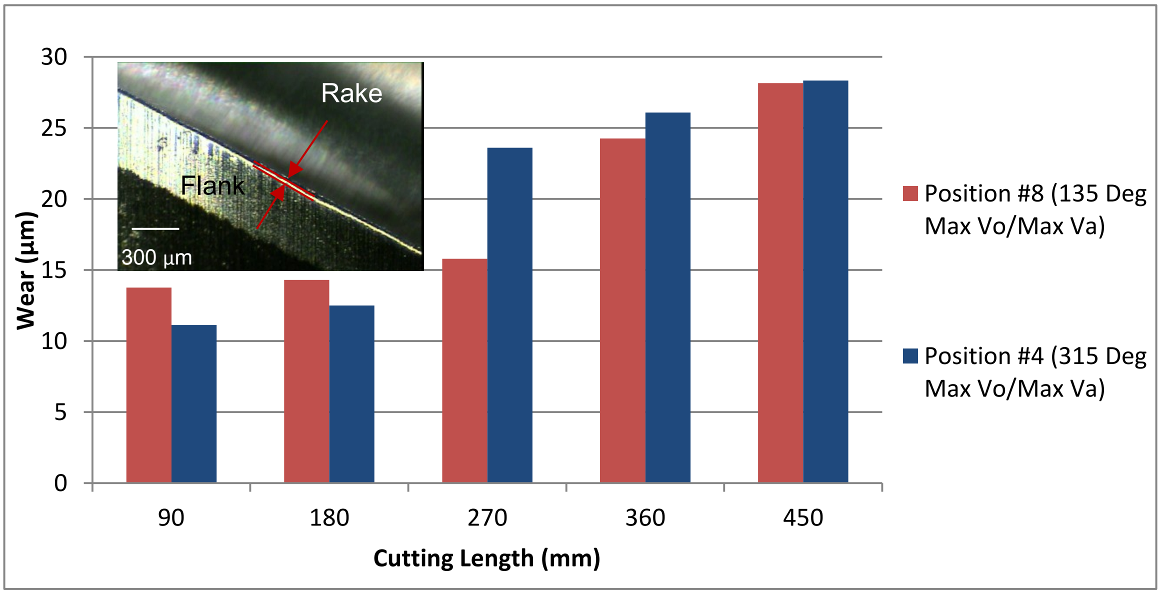

Figure 5.10: Flank wear progression for the 2 nozzle positions tested in the full length experiments

This result is a possible indication of the effect of Nusselt number variation around the periphery of the rotating tool, obtained in the flow behaviour study in section 4.7 (the difference in tool rotational speed between 10,000 and 15,000 rpm is not expected to shift the Nusselt number location significantly). If the workpiece was a metal, the maximum heat generation due to cutting would be expected in the center of the chip, where the maximum chip load exists. For CFRP’s no chips are formed, but the maximum load is expected to be in the same location, and thus the maximum heat generation. When the nozzle is in position #8, the flow direction is 135º from the positive cutting direction. At this position, and according to the CFD results in section 4.7 (Figure 4.14), the maximum Nu number should be located ~220º from the flow direction, measured in the direction of tool rotation, as shown in white in Figure 5.11 (a). This location coincides with the location of maximum chip load (Point “A” in Figure 5.11 (b)). Aligning the point where the maximum Nu number occurs, with the point of maximum chip load, could therefore be behind the more efficient cooling and lubrication around the surface of the tool. When the nozzle is in position #4, the flow direction is 315º from the positive cutting direction while the maximum Nu number is located in the center of the cut but, in this case, behind the tool (Point “B” in Figure 5.11 (b)). The low tool temperature and forces previously observed using position #4, in Figure 5.8, could be due to the fact that the maximum heat transfer was occurring in a location unobstructed by the workpiece. Since position #8 still outperformed position #4, position #8 was selected in all the subsequent experiments.

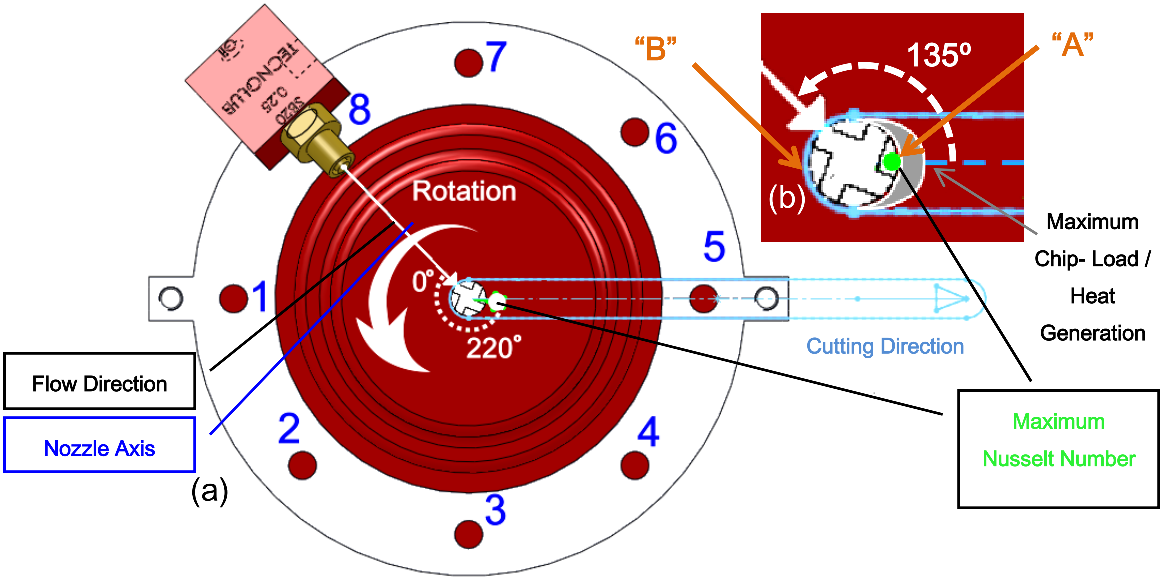

Figure 5.11: (a) Location of the Nusselt number for 10,000 rpm, Max Vo and Max Va, when the nozzle is in position #8; (b) Close-up on the tool showing the angle between the aerosol flow direction and the cutting direction, when the maximum Nu is aligned with the maximum cutting heat generation point

5.3.2 Comparison of the Effects of Cooling/Lubrication Modes (Experimental Set-2)

The second set of experiments was designed to examine the effect of the different lubrication conditions in cutting CFRP laminates. The purpose was to compare industrially common techniques of lubrication, such as dry and flood cooling, with MQC. This set was designed so that all machining parameters would be fixed with only the tribological conditions changing (see Table 5.2). Four MQC conditions were considered along with flood cooling, pressurized air, and dry.

Seven different conditions were compared in this study, as detailed in Table 5.2. Note that conditions 4 and 5 are identical to the last two tests in Set-1 of this experimental study and were, therefore, not repeated. Their force and temperature results are analyzed in this section with the rest of the conditions. With the exception of condition 4, all other MQC tests were conducted with the nozzle located in position #8. Condition 4 was conducted with the nozzle at position #4. All other parameters (tool rotational speed, nozzle diameter, coolant type) were fixed. The tool speed was 15,000 rpm and the cutting feed was fixed at 1,500 mm/min, resulting in a nominal chip load of 0.025 mm/tooth. MECAGREEN 550 was used to make a 5% concentration emulsion used in the MQC tests. The flank wear was measured at intervals of 90 mm of cutting length, for a total length of 450 mm. The maximum temperatures, the mean cutting forces, tool wear and geometric errors were evaluated.

Table 5.2: Tribological Study Conditions and Parameters

Condition	Coolant	Nozzle Diameter (μm)	Position	Va (l/min)	Vo (ml/min)
1	Air	N/A	#8	31 (Max Va)	N/A
2	Flood	N/A			
3	N/A (Dry)	N/A			
4	Emulsion (MQC)	250	#4	31 (Max Va)	24 (Max Vo)
5		250	#8	31 (Max Va)	24 (Max Vo)
6		250	#8	20 (Min Va)	24 (Max Vo)
7		250	#8	31 (Max Va)	10 (Min Vo)

5.3.2.1 Cutting Forces

Typical force signals captured by the dynamometer and converted into forces are shown in Figure 5.12. Mean forces were calculated over the second half of each cut. This was to exclude any potentially misleading measurements that were taken when the coolant had not fully reached the cutting zone yet. Again, only the forces in the feed direction (Fx) were considered in the comparisons.

The plot in Figure 5.13 shows the combined signals for the same condition over the whole cutting length. The observed decrease in forces during each segment can be attributed to the temperature increase. As the cutting progresses, the CFRP matrix softens under the effect of increased temperature in the cutting zone, and the forces that are needed to cut it are reduced. When the cutting is interrupted and the tool and workpiece are allowed to return to room temperature, the cutting forces increase once again, this time higher than before due to the added effect of tool wear. The effect of interrupting the cutting process can be seen in the form of a “jump” in the forces at the beginning of a new 90 mm segment in Figure 5.13.

.

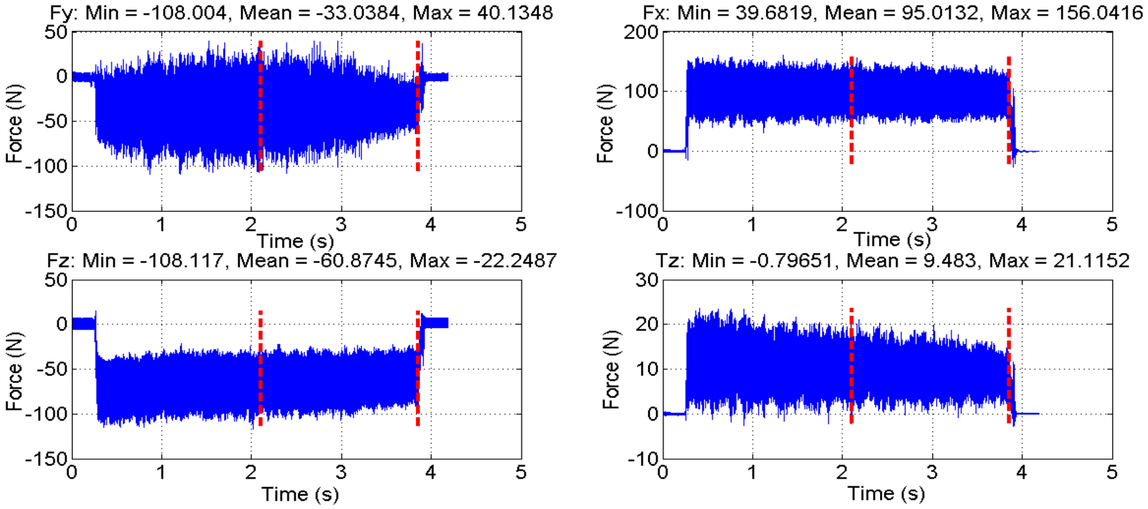

Figure 5.12: Dynamometer output signal for the first 90 mm of cutting for condition 7. The feed direction corresponds to Fx. The dashed red lines are the interval over which the mean forces were calculated.

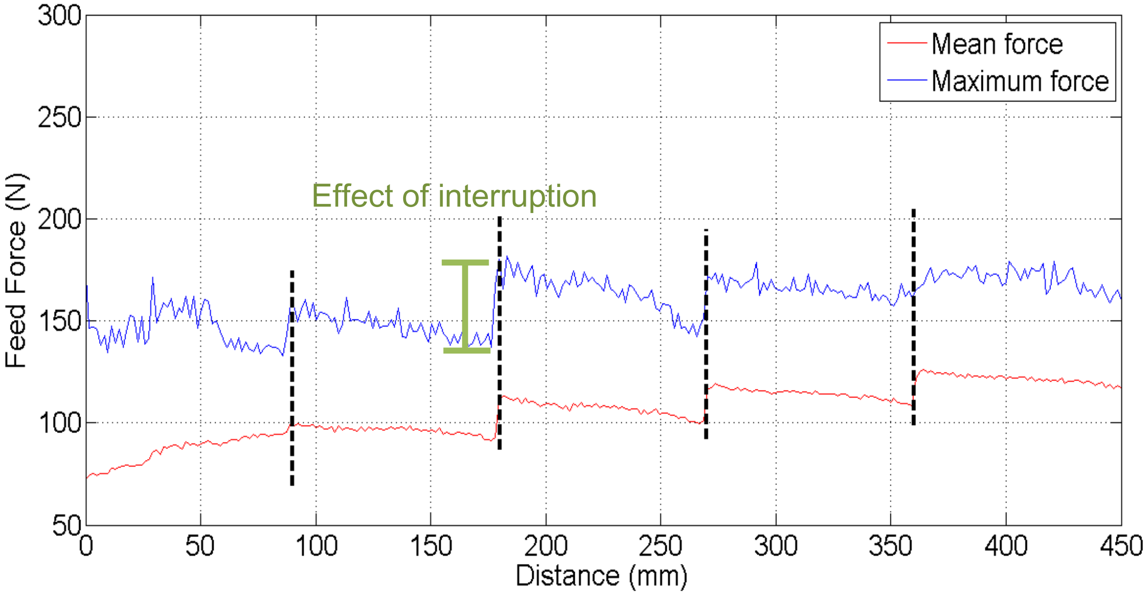

Figure 5.13: Combination of averaged maximum and mean force signals of the different segments for condition 3

The plot in Figure 5.14 shows the mean forces in the feed direction for all the cuts performed. Over the last two segments, the Min Vo/Max Va with pressurized air only (green) show about 20 N less mean forces over the other conditions. The lower forces under the pressurized air condition can be attributed to the cutting temperatures, which are higher in the case of pressurized air than in the MQC cases with the same air flow rate (see section 5.3.2.2). This observation supports the hypothesis of the CFRP softening effect. It is worth noting, however, that the forces for the MQC conditions and those for flood and dry cutting are within 10 N of each other, for all the segments. Comparing the three MQC conditions at 135º, it can be seen that the Max Vo/Min Va condition (orange), which has the same lubricant flow rate as the Max Vo/Max Va condition (red), seems to have the lowest forces throughout the tests. This condition has the highest predicted SMD and the lowest air and droplet velocity, as was shown in Section 3.4. The Min Vo/Max Va condition (light blue) resulted in higher cutting forces, as compared with the Max Vo/Max Va condition (red). This could be interpreted by less softening in the former case due to lower temperatures. Forces resulting from dry cutting (purple) were similar to those resulting from MQC, and lower than those with flood cooling (black). Flood cooling also resulted in higher cutting forces than all MQC conditions. This result, in particular, could be an indication that the flood coolant was not capable of penetrating to the cutting zone as efficiently as MQC. This can be confirmed by observing the tool wear results in section 5.3.2.3.

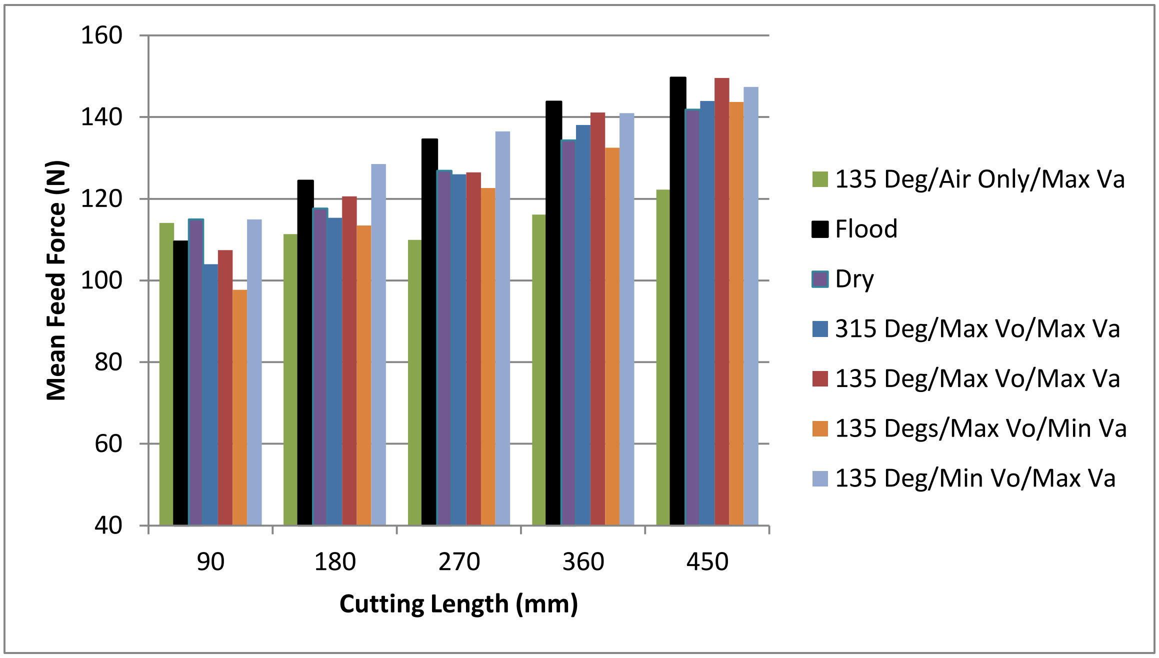

Figure 5.14: Mean force progression under different lubrication environments

5.3.2.2 Cutting Temperatures

As in the previous study, the maximum tool temperatures throughout the cut were used for comparison of the different lubrication modes. As discussed in section 5.3.1 and shown in Figure 5.15 having the MQCL nozzle in position #8 (135º/red) resulted in lower temperatures than when the nozzle was in position #4 (315º/dark blue). Pressurized air (green) resulted in substantially higher temperatures than all other conditions (including dry cutting). The higher temperatures obtained with pressurized air, however, could explain the lower mean forces obtained; higher temperatures soften the resin and thus reduce the required cutting force. This can be clearly seen by comparing the forces and temperatures obtained with pressurized air (green), with those with completely dry cutting (purple). Comparing the MQC conditions at 135º, it can be seen that the Max Vo/Max Va condition (red) resulted in the highest temperatures almost throughout all the tests; higher than the Min Vo/Max Va (light blue), which has less fluid for the same air flow rate. This improvement in lowering the temperature could be caused by lower SMD; the improved droplet penetration to the cutting zone enhances the heat exchange. In addition, MQC with the Max Vo/Min Va (orange) resulted in the lowest temperatures throughout, despite the higher SMD, compared with Min Vo/Max Va (light blue). This could be indicative that a higher emulsion flow rate was required, and that this requirement is more important than the effect of the SMD.

It can be also observed, based on these results, that the cooling effect of the carrying air (in the MQC and pressurized air cases) was lower than predicted in sections 4.7. The improved cooling discussed in section 5.3.1, which was observed in the case of position #8 (135º) over the other 7 positions, is likely due to the proper delivery of the fluid and reduced flow interference with cutting chips/dust, rather than the heat exchange. It is also worth noting that, due to the setup’s limitations, infrared temperature measurement was not possible while using flood cooling.

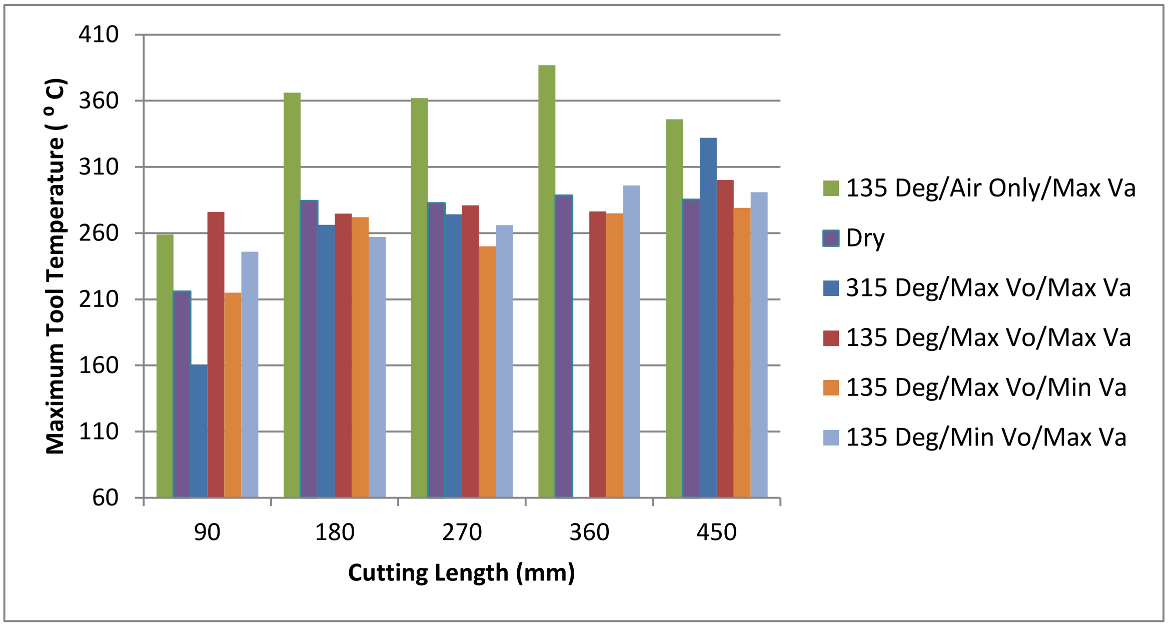

Figure 5.15: Progression of maximum tool temperature under different tribological environments

5.3.2.3 Tool Wear

The superior effect of MQC in controlling tool wear can be seen in Figure 5.16 (see Appendix C for measurement errors). All four MQC conditions resulted in lower tool wear than pressurized air, dry and flood cooling. Comparing MQC with Max Vo/Max Va (red), with Min Vo/Max Va (light blue), it can be seen that the lower SMD in the case of the latter was important in controlling tool wear, despite the reduced amount of coolant. It can also be observed that the slightly higher maximum temperatures, observed in the previous section, were beneficial in preventing excessive wear by softening the CFRP resin. The flank wear from MQC cuts with Max Vo/Min Va are higher than those of the Max Vo/Max Va MQC condition (red), except in the last two segments. The abrupt increase in the tool wear for the Max Vo/Max Va condition at the 4th cut segment (8 µm) was a breakage that was not consistent with the process, and is most likely a damage that took place during tool entry and retraction.

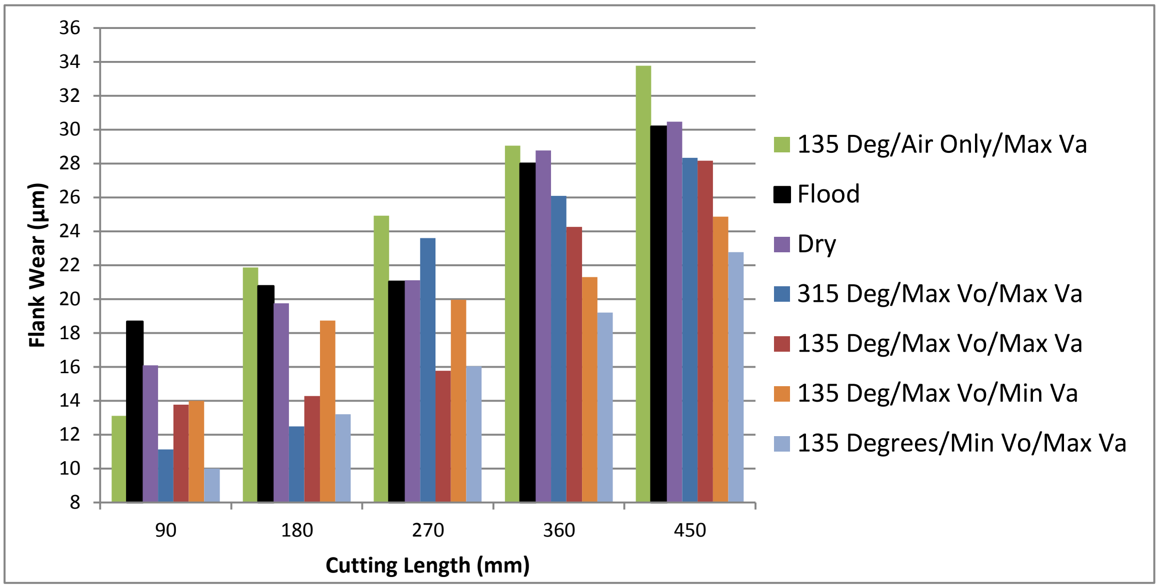

Figure 5.16: Flank wear progression under different lubrication environments

Flood cooling (black) and dry machining (purple) modes resulted in higher tool wear than MQC. The fact that flood cooling and dry machining showed similar results is the reason why dry machining is the most industrially employed method with CFRPs; the abundance of water and moisture has adverse effects on the matrix integrity. This is less likely under MQC since the dispensed lubricant amounts are substantially lower, and the incumbent pressurized air on the workpiece facilitates the rapid evaporation of the liquid. The flank wear after 450 mm of cutting for conditions 1 and 7 are shown in Figure 5.17.

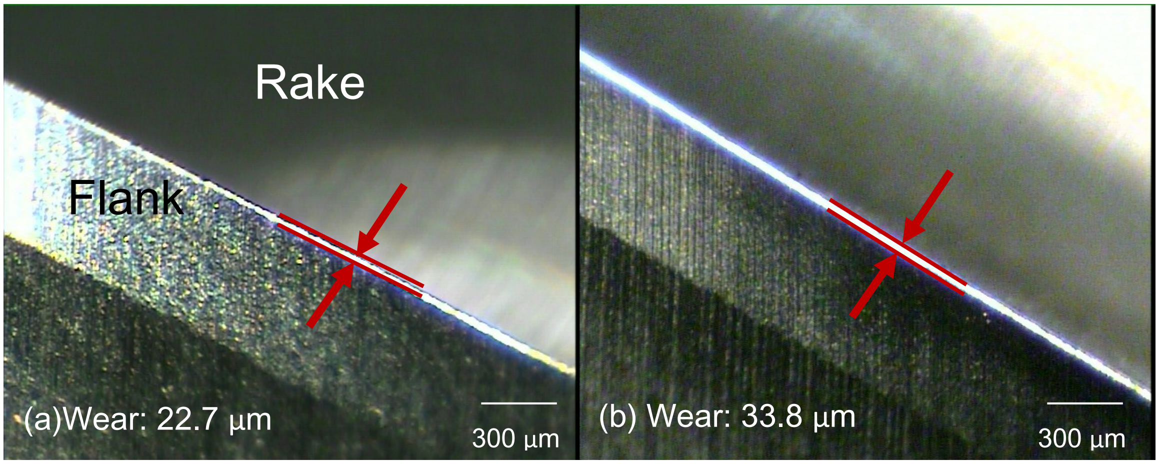

Figure 5.17: Flank wear after 450 mm of cutting. (a) Max Vo/Min Va; (b) Pressurized Air (Max Va); Magnification: 30X

5.3.2.4 Geometric Errors

The CFRP slots were analyzed for geometric accuracy using a Mitutoyo MACH806 coordinate measuring machine (see Appendix C for measurement errors). The width of cut, the straightness, and the parallelism errors were measured at two depths 4.35 mm apart for each cut, and on both sides of the slot (top and bottom). Figure 5.18 shows the measured geometrical features for condition 7 (Min Vo/Max Va). Comparing the different lubrication environments (see Appendix E), it can be observed that with the exception of condition 7 (Min Vo/Max Va), all initial segments had higher than nominal (6.35 mm) width of cuts. Dry mode, pressurized air mode, and MQC with high Vo and low Va resulted in higher than nominal widths of cut, compared with low Vo MQC, and flood cooling. This was clear in the initial segments, before the tool wear caused smaller and smaller widths in the subsequent segments. The abundance of air (Min Vo/Max Va), compared to lubricant in MQC machining, resulted in the most stable width of cut around the nominal, throughout the cut distance (Figure 5.18). These results are consistent with their corresponding low tool wear; the width of the cut decreased with the tool wear, beginning with a few tens of microns higher than the tool's nominal diameter to a few tens of microns lower, indicating the effect of the worn tool.

The apparent contradiction in results between the min Vo max Va combination, and combinations with higher Vo or flood cooling, is indicative of the better lubrication and cooling of minimal quantities, if the atomization quality is appropriate. The tribological conditions did not seem to have any remarkable effect on the straightness and parallelism errors over the distance of 450 mm. Instead, these errors showed a dependence on the workpiece orientation, despite the material's assumed near-isotropic properties. Cuts under the same tribological conditions, but performed on different plates, had sharp jumps in these errors depending on the sample's orientation during the tests, and were not valid for proper comparison (see Appendix E). In terms of geometric accuracy, the weave orientation of the workpiece had the predominant effect on the straightness and parallelism errors, but did not have any effect on the width of cut. The effect of tool length can be observed in the consistently higher errors at the deeper measurement location D2 (closer to the tool tip and further from the tool holder).

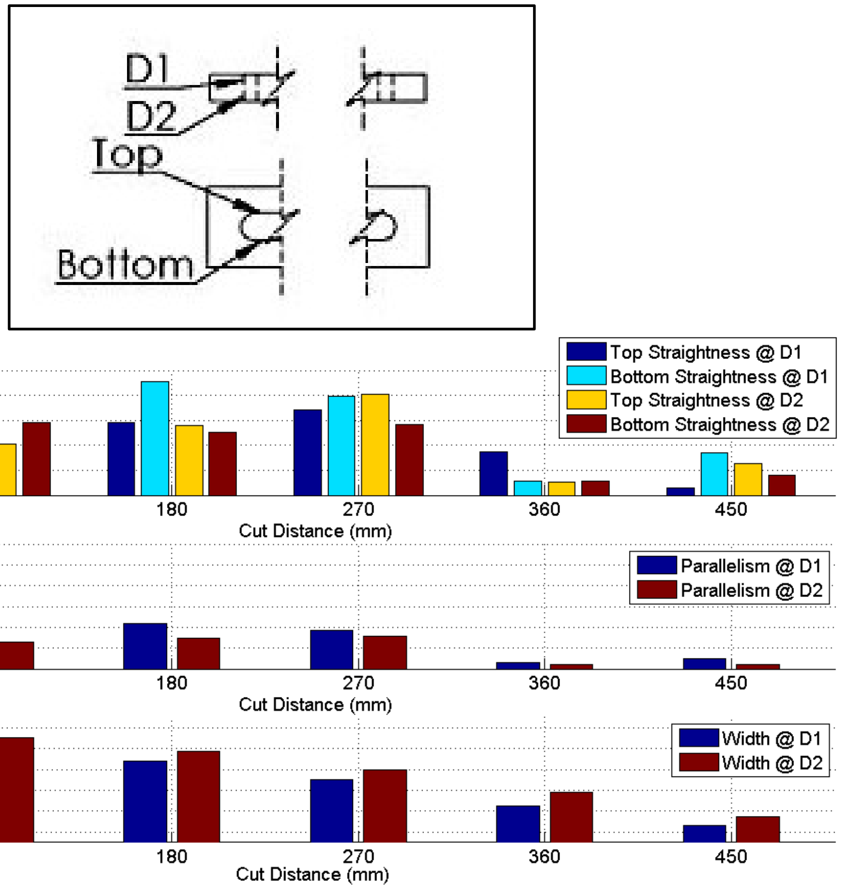

Figure 5.18: Geometric accuracy progression for condition 7 (Min Vo, Max Va)

5.3.3 Investigation of the Significance of the MQCL Parameters (Experimental Set-3)

The results obtained in Set-1 and Set-2 of this experimental study indicate the potential effect of the MQCL flow parameters on the cutting performance, in terms of cutting forces, cutting temperatures, tool wear and geometric accuracy. To further investigate the significance of each parameter on these effects and distinguish any interactions present, a multi-level experimental design had to be created. The design of this third set of experiments was to test the largest possible number of factors considered earlier, using the same levels employed. Analysis of the main effects by examining the signal-to-noise ratios of the factors could then be performed and interactions could be distinguished. This also allowed for several One-Way Analyses of Variance between the different factors and effects. All calculations were done using Minitab® 16 [59].

While a full factorial design would be the most informative, the large number of parameters/factors and levels was prohibitive due to the large cost and time needed. Instead, an L-18 orthogonal Taguchi array was found to be suitable (Table 5.3) in allowing an experiment with one 2-level factor (Nozzle Diameter) and four 3 -level factors (“Coolant Type”, air flow rate “Va”, oil flow rate “Vo”, and tool rotational speed “N”).

The cutting length for each cut was 30 mm, and the results of each cut were averaged over three repetitions. This was possible since the tool wear after 90 mm of cutting was shown to be negligible. The feed rate was varied with the tool rotational speed to maintain the chip load at 0.025 mm/tooth. This was necessary to minimize the variation of the feed forces with the tool rotational speed. A second nozzle, having an oil nozzle diameter of 0.35 mm, was also used in this study in addition to the previously used nozzle (0.25 mm). Water was also used as a third cutting fluid (MQC), in addition to 5% emulsion (MQC) and pure oil (MQL).

From the CFD results presented in the previous chapter, it was found that the variation of the separation point and the point of maximum heat transfer with the speed range employed in the current study was ± 5º, which is less than the nozzle position interval in the setup (45 º). The nozzle position was thus maintained to be #8 (135º from the cutting direction), as determined in the first experimental set.

Table 5.3: Taguchi L-18 Design

Condition	Coolant Type	Nozzle Diameter (mm)	Va (l/min)	Vo (ml/min)	N (rpm)	Feed (mm/min)
1	MQL: Pure Oil (PO)	0.35	20	24	15,000	1,500
2	MQL: Pure Oil (PO)	0.35	25	10	5,000	500
3	MQL: Pure Oil (PO)	0.35	31	24	15,000	1,500
4	MQL: Pure Oil (PO)	0.25	20	17.5	10,000	1,000
5	MQL: Pure Oil (PO)	0.25	25	17.5	10,000	1,000
6	MQL: Pure Oil (PO)	0.25	31	10	5,000	500
7	MQC: Water (W)	0.25	20	24	15,000	1,500
8	MQC: Water (W)	0.25	25	24	15,000	1,500
9	MQC: Water (W)	0.25	31	17.5	10,000	1,000
10	MQC: Water (W)	0.35	20	10	5,000	500
11	MQC: Water (W)	0.35	25	17.5	10,000	1,000
12	MQC: Water (W)	0.35	31	10	5,000	500
13	MQC: Emulsion (EM)	0.35	20	17.5	10,000	1,000
14	MQC: Emulsion (EM)	0.35	25	24	15,000	1,500
15	MQC: Emulsion (EM)	0.35	31	17.5	10,000	1,000
16	MQC: Emulsion (EM)	0.25	20	10	5,000	500
17	MQC: Emulsion (EM)	0.25	25	10	5,000	500
18	MQC: Emulsion (EM)	0.25	31	24	15,000	1,500

5.3.3.1 Main Effects of Process Parameters

The signal-to-noise (SN) ratio was used to evaluate the significance of each parameter on the responses. Three responses were used in this evaluation (maximum tool temperatures, mean feed forces, and tool wear for a given length of cut). Since it is practically more desirable to reduce each of these responses for better machining performance (i.e. lower tool temperatures, cutting pressures, and wear), the SN ratio formula used was for “smaller-is-better” response; a larger SN ratio is obtained when the response values are minimal. The calculation of the SN ratio for smaller-is-better response was calculated as follows:

$$\frac{S}{N} = -10 \times \log\left(\frac{\sum(Y^2)}{n}\right) \qquad 5.1$$

For each of the responses, a SN ratio was calculated at each factor level according to Equation 5.1. Then, the means of the three SN ratios per factor level were obtained, they are plotted in Figure 5.19. The slopes of the means of the SN ratio represent the magnitude of the effect. When there is a large slope, a significant effect is present. It can be observed that the nozzle diameter and the tool rotational speed have the greatest effect on the results. However, the oil and air flow rates, as well as the cutting fluid, show less significant effect on the cutting process.

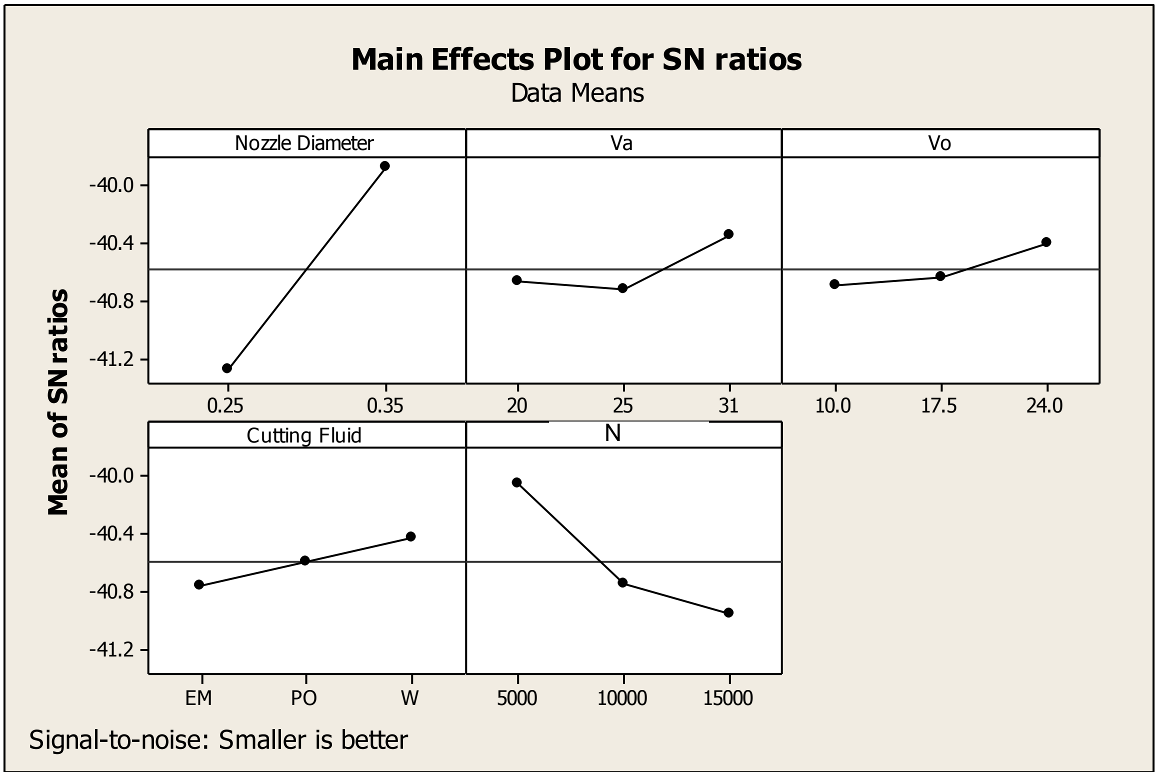

Figure 5.19: Main Effects plot for SN ratios – Smaller-Is-Better (Maximum Temperatures, Mean Forces, Tool Wear)

5.3.3.2 Interactions of Process Parameters

The plots in Figure 5.20 contain the interactions of the SN ratios between the nozzle diameter and the rotational speed, Va and Vo, and the nozzle diameter and cutting fluid, respectively. The plots show strong interactions between Va and Vo (shown by the strong non-parallelism of the SN ratios), and insignificant interactions between the nozzle diameter and cutting fluid. Some interactions also exist between the nozzle diameter and rotational speed, when increasing the rotational speed N from 5,000 rpm to 10,000 rpm. When no interactions are present, the main effects plots and response tables show how a change in one factor, while holding the other factors constant, affects the response characteristic. When there is an interaction, the main effects no longer reflect the actual effects of the factor because they are coupled. Further inspection was thus needed to confirm any existing factor significance.

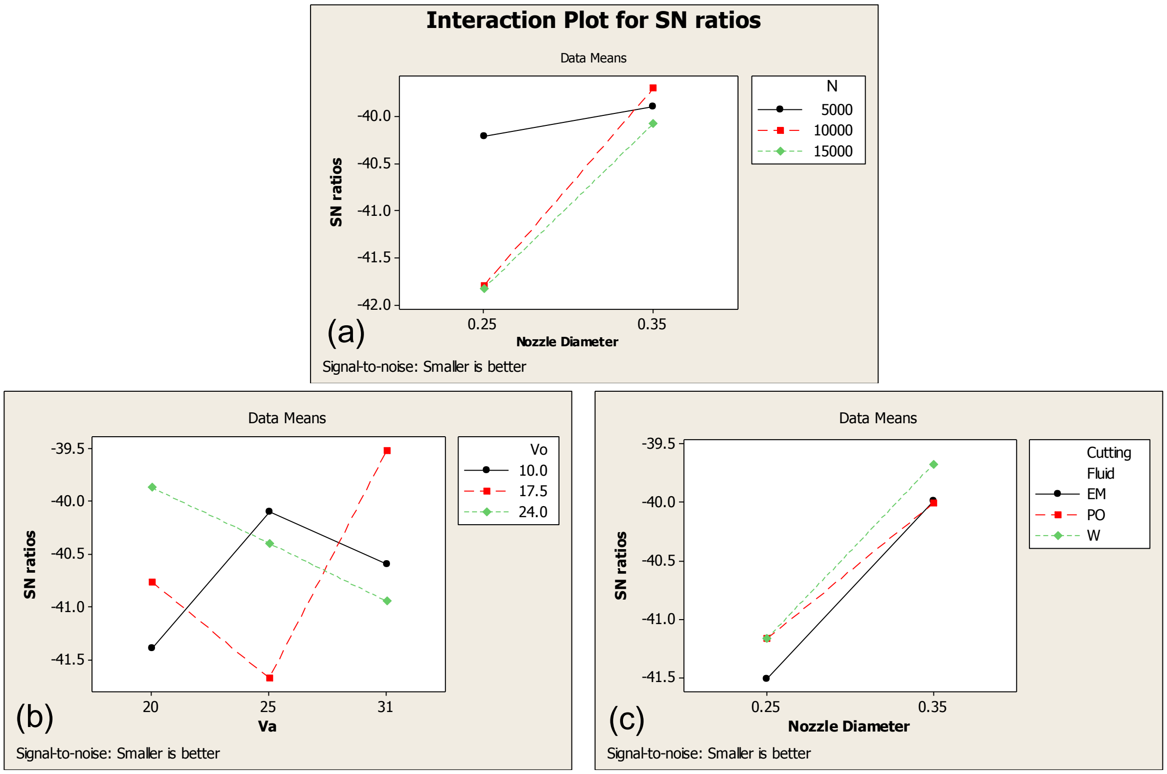

Figure 5.20: Interaction plots for SN ratios. (a) Nozzle Diameter and Tool Rotational Speed N; (b) Va and Vo; (c) Nozzle Diameter and Cutting Fluids

Because of the interactions present between the air and oil flow rates, the responses of the combinations of the air and oil flow rates (MQCL injection parameters) were therefore used to interpret the main effects. Nine combinations of injection parameters are present in the Taguchi design in Table 5.3, each combination was tested at 2 levels of Nozzle Diameter, for a total of 18 tests. Combining these injection parameters into one parameter results in a 9-level parameter, "Va-Vo Comb.". The plots in Figure 5.21 contain the signal-to-noise ratios for the main effects of the parameters on the maximum temperature, the mean feed force and the tool wear (smaller-is-better) with the new design. The values are detailed in Table 5.4. The plots show approximately the same responses in the cases of the rotational speed, coolant type and nozzle diameter. The slight differences between these SN ratio values and the values in the previous design (Figure 5.19) are due to the fact that the mean in the former case are calculated over 9 responses, while the means in the latter case are calculated over 3 responses only. The response of the new parameter "Va-Vo

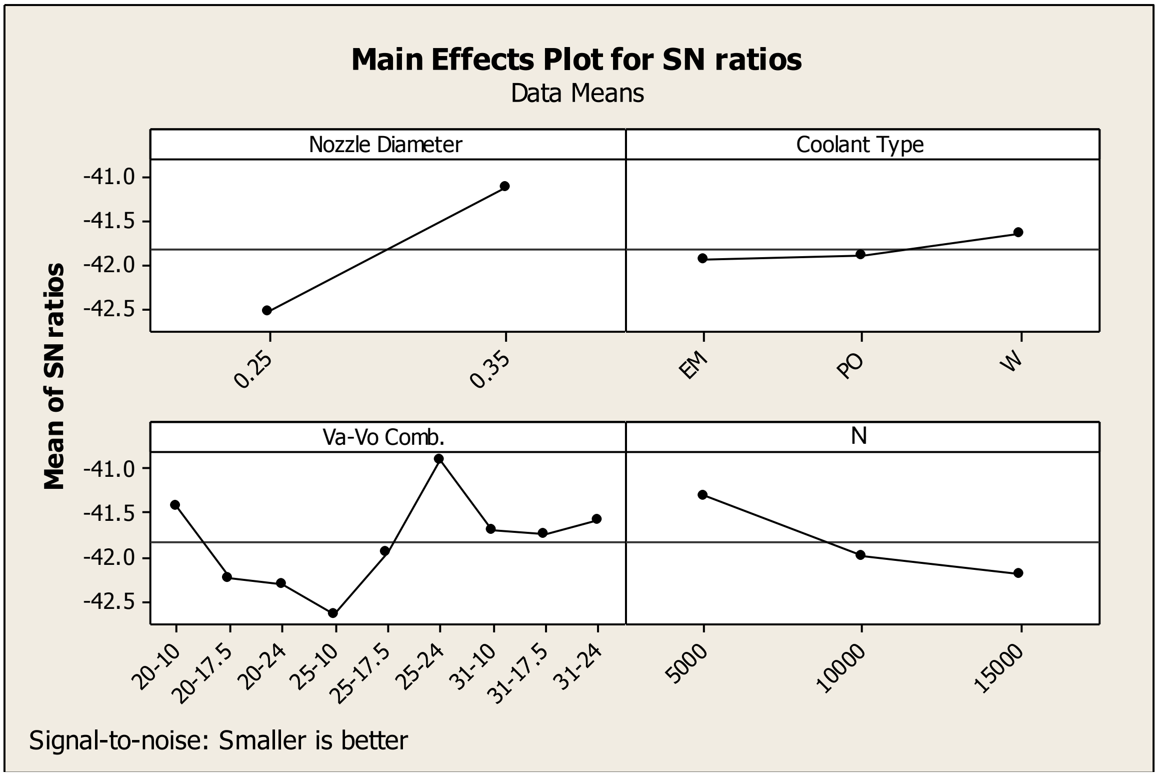

Figure 5.21: Main Effects plot of the new design, for SN ratios – Smaller-Is-Better (Maximum Temperatures, Mean Forces, Tool Wear)

Comb" shows a strong effect between the different levels used. This can be also observed in the "Delta" values shown in Table 5.4. The parameter "Delta" measures the size of the effect by taking the difference between the highest and lowest SN ratio value for each response characteristic. The order of the size from greatest effect to least effect is the "Rank".

Table 5.4: Response Table of SN ratios – Smaller-Is-Better

Level	Nozzle Diameter	Coolant Type	Va-Vo Comb.	N
1	-42.5	-41.92	-41.38	-41.3
2	-41.1	-41.87	-42.22	-42
3		-41.62	-42.29	-42.2
4			-42.63	
5			-41.92	
6			-40.86	
7			-41.66	
8			-41.7	
9			-41.56	
Delta	1.4	0.3	1.76	0.9
Rank	2	4	1	3

From the above results, one can observe the significance of the MQCL flow parameters, as compared to the tool rotational speed and the coolant type. To further investigate these observations, multiple One-Way ANOVA's were conducted to examine the significance of each of the parameters on each response.

5.3.3.3 One-Way Analysis of Variance

In the Analysis of Variance of this set of experiments, a higher importance was given to detecting all the effects of the used parameters, at the expense of the increased probability detecting effects that are non-existent. In other words, the ANOVA was in favor of making a Type I error (rejecting a true Null

Hypothesis), as opposed to a Type II error (accepting a false Null Hypothesis). An "α" of 0.15 was therefore used to evaluate the p-values. The p-values indicate whether an observed relationship has statistical significance on the results; a p-value smaller than or equal to "α" indicates a significant relationship and that the predictor does affect the response [60]. Therefore, with our selection of α =0.15, there exists a 15% chance that non existing effects are "detected".

This trade-off between the Type I and Type II error probabilities was permitted since the purpose of this study was to detect as many of the effects as possible, leaving the task of fully validating these detections to a more comprehensive experimental analysis. The p-values from the different ANOVA analyses were calculated and compared in Table 5.5. Upon observation of the p-values, the following can be concluded:

- A significant relationship between the nozzle diameter and the maximum temperature (p-value = 0.003).
- A significant relationship between the tool rotational speed and maximum temperatures(p-value = 0.046).
- A significant relationship between the air and oil flow rate combination (Va-Vo Comb.) with both the wear (p-value = 0.000) and the feed forces (p-value = 0.114).

Table 5.5: Comparison of p-values obtained in the ANOVA. Values in red are p-values below the "α" threshold of 0.15

Factor↓ /Response →	**Wear**	**Fr-mean**	**T-max**	**Width of Cut**
Nozzle Diameter	0.593	0.343	0.003	0.262
Coolant	0.811	0.812	0.903	0.941
N	0.177	0.736	0.046	0.263
Va-Vo	0.000	0.114	0.912	0.927

5.3.3.4 Effect of the Air Flow Rate – Oil Flow Rate (Va-Vo) Combination (MQCL Injection Parameters)

The plots in Figure 5.22 show the effect of the MQCL air and oil flow rates on the responses after 30 mm of cutting, under different cutting conditions, cutting fluids and nozzle diameters. The data mean values are shown by the blue dots while the red dots represent the data points. The first plot shows the strong temperature variation with the change in injection parameter combinations. The increase in oil flow rate seems to reduce temperatures, but only when atomization is adequate, as in the cases of Va= 25 l/min and Va= 31 l/min, but not for Va= 20 l/min. This is reflected in the cutting forces; lower forces are again expected when temperatures are high, due to ease of cutting. The superior lubrication of pure oil (PO), however, can be seen in the case of Va=25 l/min and Vo= 17.5 ml/min; although the temperature was higher than the case of water (for the same Va and Vo), the additional lubrication of the pure oil was capable of reducing the forces dramatically, this is also consistent throughout the cases of pure oil, as will be shown in section 5.3.3.7.The detected significance of the flow parameters on tool wear can be observed in the third graph; the overall trend shows a reduction in wear with the increase of both Va and Vo (larger SMD). The variance in the results for all responses was minimal for the mid-range air flow rate of 25 l/min, for both nozzle diameters. This can be best seen in the second and third plots of Figure 5.22. The higher variation in the 20 l/min air flow rate cuts is most likely due to the lower atomization quality, typical of the low air flow rate, as shown in section 3.4. MQCL with moderate air flow rate also seemed to result in the least variance of cut width, with all results falling lower than the desired width. This is preferred than the opposite case as it allows for finishing in a typical machining operation.

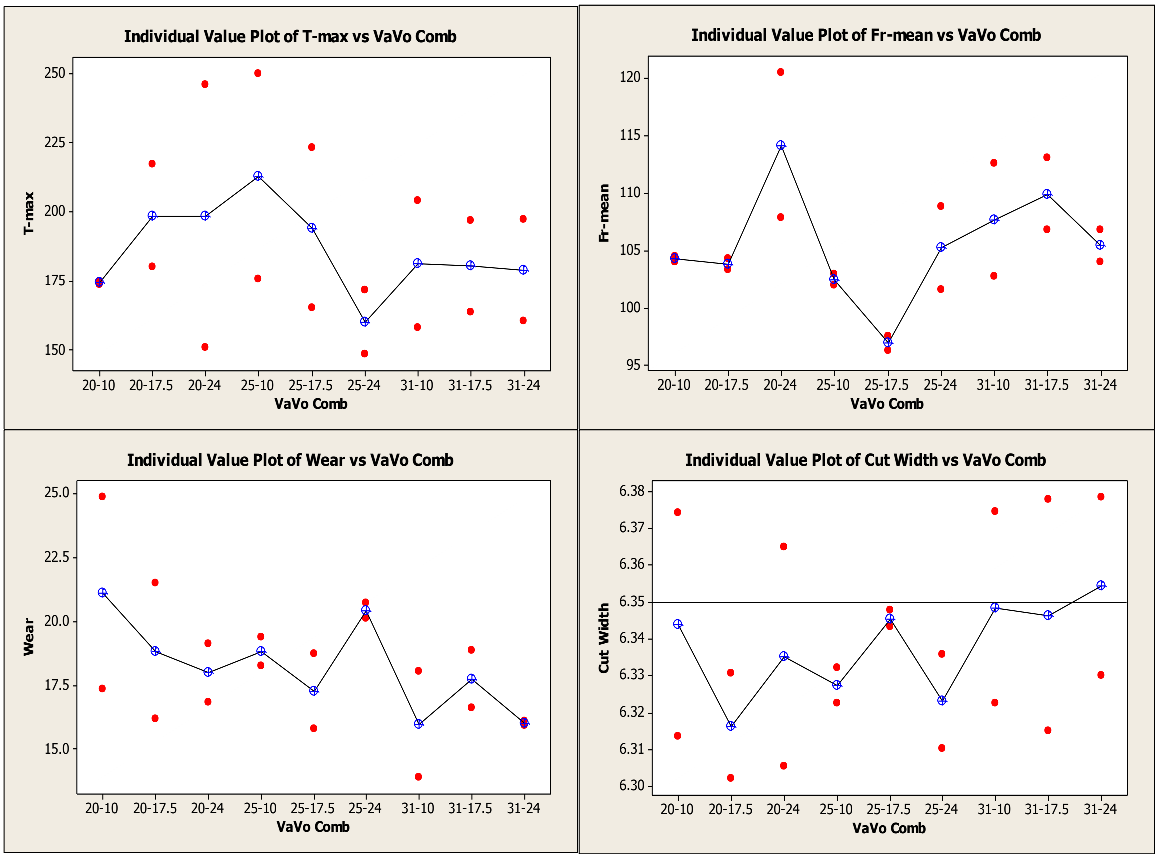
Individual Value Plot of T-max vs VaVo Comb

Individual Value Plot of Fr-mean vs VaVo Comb

Individual Value Plot of Wear vs VaVo Comb

Individual Value Plot of Cut Width vs VaVo Comb

Figure 5.22: Individual value plots showing the effect of the Va-Vo Comb. parameter on the outputs

5.3.3.5 Effect of the Tool Rotational Speed (N)

The first plot in Figure 5.23 shows an overall increase of maximum temperature with increasing tool rotational speed, despite the variable MQCL conditions. It is worth noting, however, that all temperatures were close to 200º C. While the rotational speed used in these tests was not constant, the feed per tooth was kept constant by varying the feed speed (mm/min) with the rotational speed. This helped maintain the cutting feed force levels around 105 (N), with slightly lower mean forces and mean tool wear for the 15,000 rpm cuts under the effect of increased temperatures.

Looking at the p-values of the ANOVA studies performed (Table 5.5), the only significant effect can be seen in the case of temperatures, meaning the effect of the rotational speed on temperature was more significant than its effect on either the resultant force or the tool wear. The softening of the matrix under increased temperature was present here as it was seen in section 5.3.2.1, but not as pronounced due to the shorter cutting length. Tool wear generally increased with the tool speed N. A striking similarity can be observed between the force and tool wear plots; cutting with lower mean forces resulted in lower tool wear. This observation seems logical. The increase in N (and consequently the cutting speed), produced generally smaller widths of cut due to the increased tool wear.

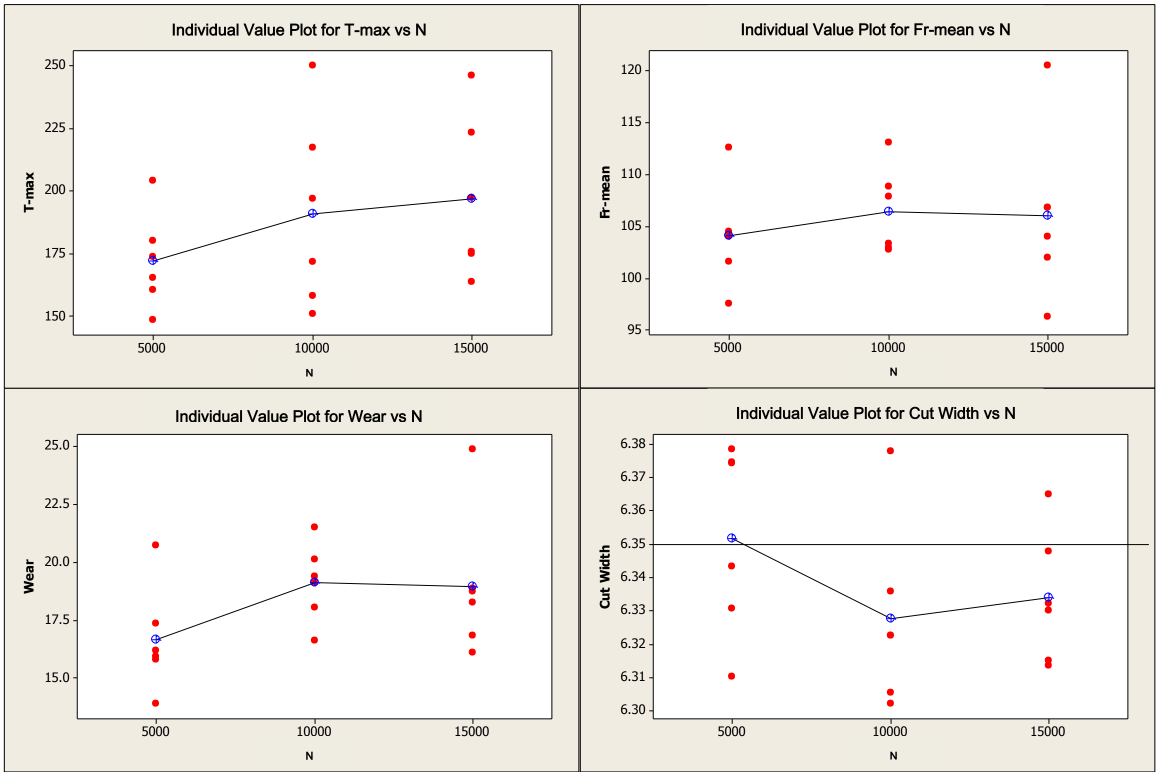

Figure 5.23: Individual value plots showing the effect of the tool speed N on the outputs

5.3.3.6 Effect of the Nozzle Diameter

The two nozzles used through the course of this set of experiments were identical in design with the exception of the different oil channel orifice diameter. Equation 3.5 examined in section 3.4 indicated that for the same fluid and flow rate, the larger diameter results in a smaller Sauter Mean Diameter (SMD). In the machining experiments, this diameter difference had an impact on all responses. This can be observed in the small p-value and in the response plots in the Figure 5.24. The maximum temperatures were around 50º C lower in the case of the 0.35 mm nozzle. Slightly lower mean forces can also be observed in this case. In terms of tool wear, the mean value was also slightly higher in the 0.35 mm nozzle case, though the variation was clearly lower and most results were close to the mean. This observation is the same in the case of the cut width, although the means of the 0.25 mm nozzle were closer to the nominal value. There is no surprise, however, to see a correlation between the tool wear and the accuracy of the cut width.

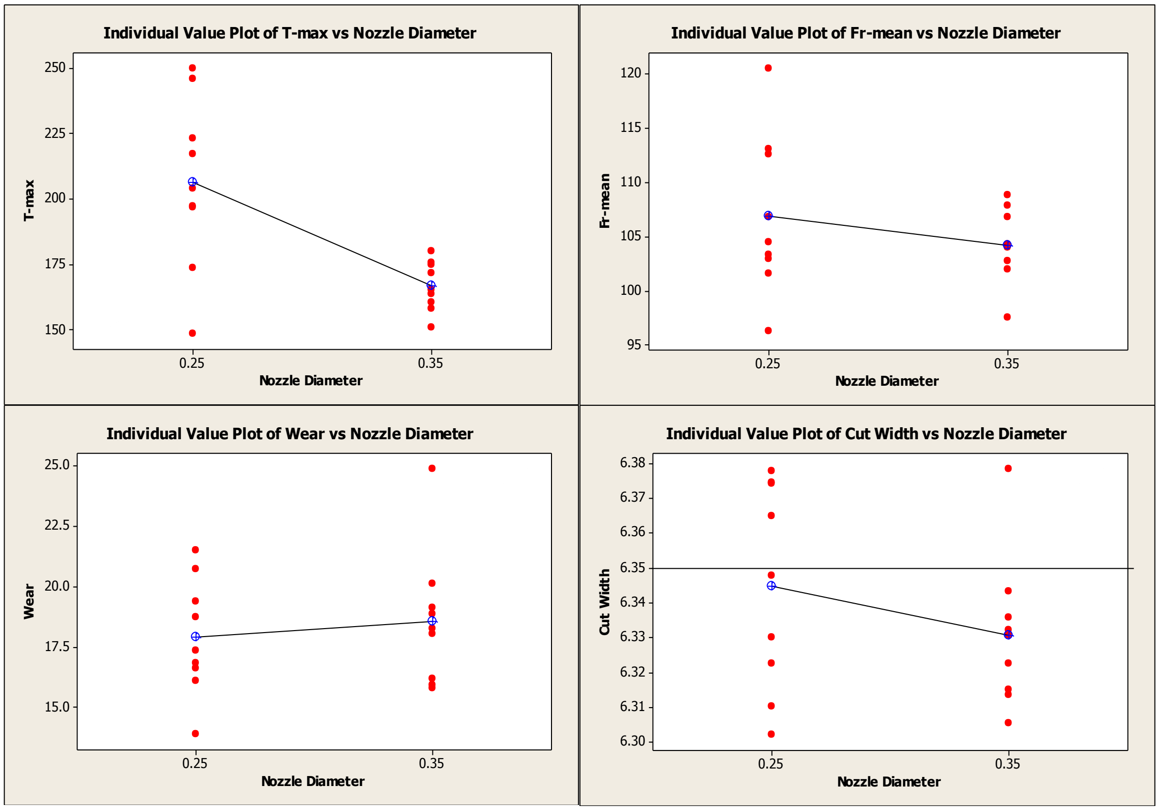

Figure 5.24: Individual value plots showing the effect of the nozzle diameter on the outputs

5.3.3.7 Effect of the Coolant Type

While the ANOVA p-values did not indicate any significance of the cutting fluid on the responses, it can be noted that the variance in the case of Water (cooling only, limited or no lubrication) was higher for most tests in all the examined responses (Figure 5.25). Water clearly resulted in the lowest temperatures, but the inadequate lubrication is easy to observe in the higher feed forces. Emulsion resulted in slightly lower feed forces indicating the importance of the oil lubricant, this trend continues with the lowest cutting forces and tool wear being in the cases of pure oil. In terms of geometric accuracy, the mean in the case of pure oil was closer to the desired width of cut, but the variance is higher which might not be appropriate from a practical manufacturing point of view.

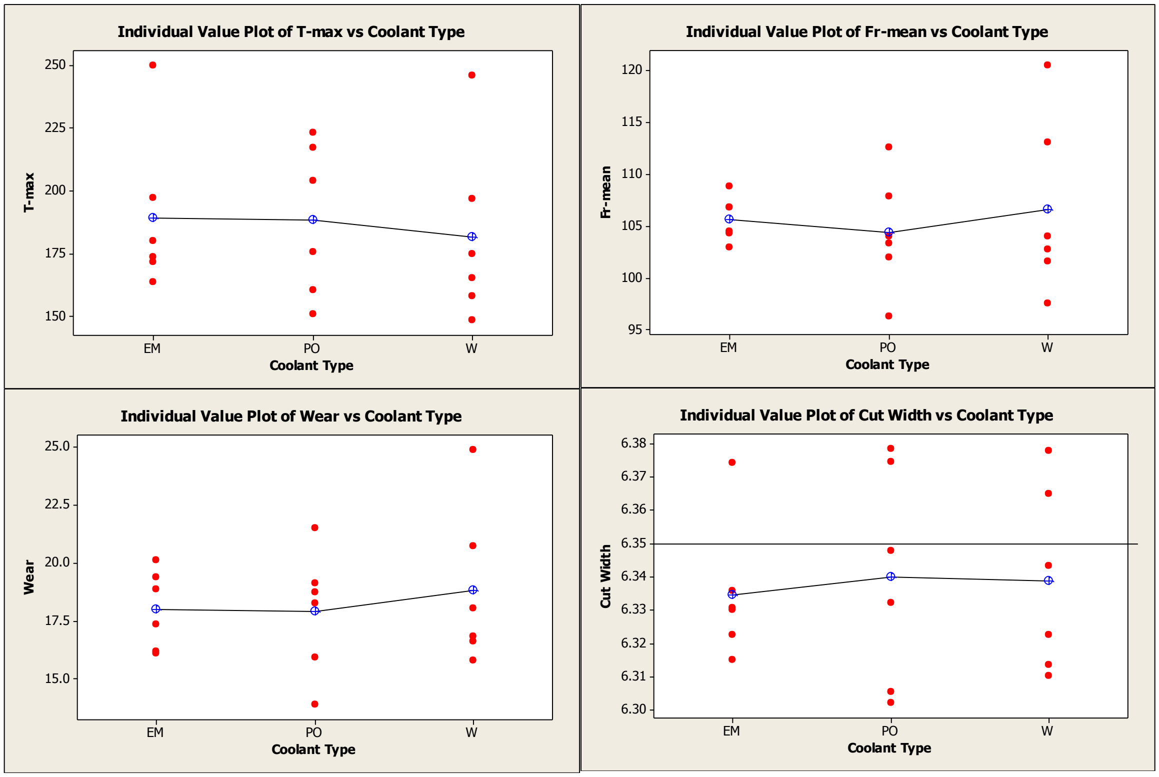

Figure 5.25: Individual value plots showing the effect of the nozzle diameter on the outputs

5.4 Conclusions

The applicability of MQCL in machining of CFRP was highly sensitive to the nozzle diameter and the MQCL injection parameters. The orientation of the nozzle and the direction of the flow had a practical importance, such as obstruction in the machining environment, but no significant effect the convection of the air flow with the tool surface. The variation of the Nusselt number around the rotating tool surface, as predicted in section 4.7 does not seem to impact temperatures, from a machining point of view.

While dry and flood cooling are more commonly used in industry, the benefit of employing MQCL, particularly in the machining of CFRPs, was shown in the lower tool wear under prolonged cutting. The importance of a liquid lubricant was relevant in controlling cutting temperatures, despite the “messy” lubricant-CFRP dust mixture that interferes with the tool and workpiece. The better results of lower tool wear and geometric error were obtained using MQCL, particularly with minimum oil flow rate and maximum air flow rate. This can be attributed to the more effective penetration of the lubricant under the elevated air pressure. This was only possible when the atomization is efficient, i.e. when the air flow rates were high enough to fully mystify the oil.

The cutting forces and temperatures, however, were not fully indicative of the quality of machining of CFRP with MQCL. While elevated temperatures could have adverse effects on tool wear, the material softening effect, due to this elevation, reduced the cutting forces required. This, in turn, helped minimize the tool wear, resulting in an overall lower tool wear than flood or MQCL with higher oil flow rates. The geometric errors in terms of parallelism and straightness were not dependent on forces and temperatures as much as on the laminate weave orientation. The width of cut was conversely affected by tribological conditions manifested in the flank wear in the tool. A low flank wear with no sharp increases during each cut resulted in the least variance in the widths of cuts throughout the prolonged experiments.

This significance of the oil/air flow rate ratio indicated the importance of the flow parameters on the performance of MQCL. This fact is not well investigated by most of the ongoing research where the MQCL parameters are often fixed, and nominal parameters suggested by the manufacturer are used.

The importance of the diameter of the lubricant nozzle was also higher than predicted. The lower speed of the fluid at the nozzle exit in the case of the larger diameter nozzle resulted in better machining quality for the same lubricant flow rate. The effect of the lubricant nozzle diameter, here, is best captured by equation 3.5 discussed in section 3.4. This equation shows that the SMDs of the droplets generated by the 0.35 mm nozzle are smaller than those generated by the 0.25 mm, for the same air and oil flow rates. This smaller SMD could help explain the variation in the machining quality of the two nozzles, but further investigation would be needed.

Chapter 6 Conclusions and Research Recommendations

6.1 Conclusions

The critical review of the literature shows that the applicability of MQCL in many machining operations could make it a valid replacement to traditional cooling methods.

In general, the experimental investigations conducted showed that the properties of the MQCL aerosol spray have a remarkable impact on its performance as a machining cooling/lubrication mode. The orientation of the nozzle and the direction of the flow were first shown to have a practical importance. The results of comparing MQCL machining with flood cooling or dry modes were consistent with the results available in the reviewed literature. Machining under MQCL is capable of leading to superior results than under conventional methods, provided certain conditions were met. Some of the advantages seen were attributed to the thermal characteristics of the CFRP material; the increased the higher temperatures led to increased material softening, and therefore lowered cutting forces and tool wear. The Analysis of Variance (ANOVA) showed that the most important factors in optimizing the performance of MQCL appear to be in the injection parameters. Since the injection parameters, in turn, govern the properties of the aerosol spray, it was possible to observe how the properties of the aerosol impact the machining process. Flow visualization experiments were performed to examine the impact of the injection parameters on the flow behaviour. The Particle Image Velocimetry experiments had shown that when a low SMD is predicted, the flow is generally more uniform. This, therefore, bridged the gap between the MQCL injection parameters and the properties of the aerosol itself. In other words, the properties of the flow had the effect of “intermediate parameters” controlling the MQCL performance in machining. The Computational Fluid Dynamics simulations allowed rapid computations of the flow behaviour in more complicated arrangements, difficult to replicate experimentally. The most important conclusion of CFD, however, was showing that single-phase (air only) simulations can be sufficiently accurate in describing the real flow (oil + air). This was found through the comparison of the model with the results of the PIV experiments performed before. This conclusion implies that a substantial amount of computational resources, required for a two-phase flow, could be saved, resulting in less timely computations.

Looking in retrospect, this superset of flow and machining experiments allows for observations beyond the limits of each individual study. The PIV experiments indirectly showed the importance of the droplet sizing, in addition to the oil and air velocities, on the nozzle’s performance. The behaviour of the nozzle at the extreme air and oil flow rate values also showed the nozzle’s limitations; for a specific nozzle, there exists an optimal range of liquid and air flow rates that would qualify as a jet, out of which an optimal range of flow rates might qualify for machining. The machining experiments, therefore, allowed for the investigation of such range. Finally, while the PIV experiments allowed for a partial visualization of the flow, they showed the aerosol velocities, but lacked droplet sizing information. The second limitation of PIV was that its application is restricted to “simple” flows, such as the unobstructed flow studied. However, this was partially surpassed though the use of single-phase CFD simulations.

In this second step, the use of CFD allowed the introduction of a model of the tool/workpiece into the overall external nozzle flow, thus, further simulating the real machining environment. The ability to simulate a more realistic machining environment, along with the simplicity as compared with visualization experiments, makes further investment in single-phase models worthy. These models, along with pre-existing correlations, might be useful in producing rapid flow predictions, but the conclusions of the PIV experiments showed the indispensability of accurate droplet sizing information. In the case of CFD, such information is only obtainable using two-phase simulations. Two-phase simulations could also provide more accurate predictions as to how the oil droplets behave in the vicinity of a rotating tool/workpiece.

Despite the limitations, the flow information available proved useful in the final section of this thesis. First, the CFD simulations prompted the investigation of the nozzle direction, providing the most suitable nozzle direction for the rest of the experiments. This also showed the significance of this parameter. Then, the extreme air and oil flow rate conditions examined in the PIV tests were applied in machining to compare MQCL with dry and flood conditions. This allowed for conclusions that took the flow behaviour into consideration, and confirmed the predictions in the PIV study regarding the importance of the droplet sizing, and all the parameters that control it. Further variations in the nozzle and flow parameters, in the last section of the machining experiments, further confirmed the same predictions. They also showed the importance of an oil lubricant or emulsion as opposed to pure water, from a machining quality perspective.

6.2 Recommendations for Future Research

The conclusions of this thesis allow for recommendations to further develop the MQCL technique, and its implementation in the machining operations:

1- Experimental or numerical investigation of the droplet sizing and distribution of the two-phase flow (oil + air). Such information could then be used to generate an accurate model, predicting the aerosol properties from the injection parameters. It could also be used to generate performance maps, showing the expected properties of the droplets based on the injection parameters. This model could, in turn, help in making predictions of the effects of this lubrication mode on machining. The high variability of nozzle designs on the market makes a purely experimental flow visualization approach counter-productive, since the results of costly experimentation will not be relevant for all nozzles. In such case, two-phase numerical models would be necessary. The higher computational costs are compensated for by the flexibility of the model and its ease of application to various nozzle designs, as compared with experimental visualization.

2- The study performed on the relative significance of various process parameters showed that more research is necessary to explain certain phenomena. For example, the mechanisms by which the smaller SMD of the MQCL droplets improves machining quality, over a large SMD. It is expected that an optimum combination of SMD, air velocity, and fluid flow rate (lubrication/cooling) exists, for a particular machining application. The common recommendation of the 0.25 mm nozzle by the manufacturer must also be reconsidered, since it implies a larger SMD than the 0.35 mm nozzles as seen in equation 3.5, for the same flow rates. The larger diameter nozzle also exhibited less hysteresis in the dispensed flow rate, when changing the pressures.

3- Further adaptations to the CFD model, which could help further simulate the real machining environment. If thermal simulation is possible, such model could be then used to investigate the evaporation of the droplets along the tool/workpiece surfaces (provided a two-phase model is present). Since the modelling of machining applications exists, they could complement such studies. It can be easily seen how an iterative process of machining, thermal, and flow simulations could take place along with experimental validation, for the benefit of an accurate model.

4- The CFRP milling experiments also showed signs of overlap between the cooling and lubrication effects of MQCL; the cause of lower temperatures was not always clear as to whether it was due to cooling or lubrication. Thermal exchange analysis can be used to make estimates on the cooling effects of the MQCL nozzle flow on hot surfaces, while tribological tests can be used to estimate the lubrication of the aerosol.

Appendix A Particle Image Velocimetry Instrumentation

A.1 PIV Instrumentation details

CCD Camera	
Model	Hamamatsu Photonics HiSense MkII
Resolution	1,344 pixels x 1,024 pixels
Pixels/interrogation region	16 pixels
Experimental field dimensions	513 mm x 391 mm
Total number of vectors	5,229
PC acquisition frequency	6Hz
Laser	
Model	NANO-L-200-15
Energy/pulse	65 mJ/pulse
Pulse frequency	15 HZ
Laser sheet thickness	1 mm
Δt	10 μs
EMULTEC VG	
ρ at 15º C	1006.5 kg/m3
Solution pH at 5%	9.67

Appendix B Machining Experiments Material Properties

B.1 Machining experiments material properties

CFRP Material	
Brand	J.D. Lincoln
Standard weight (Prepreg)	352g/m^2
Resin content (Prepreg)	45%
Ultimate tensile strength (Prepreg)	669 Mpa
Tensile modulus (Prepreg)	61 Gpa
Compression modulus (Prepreg)	57 Gpa
Weave style	8 Harness Satin (0º-45º-90º-45º)
MECAGREEN 550	
ρ at 15º C	934.3 kg/m^3
Solution pH at 5%	8.1
Cutting Tool	
Brand	SGS 30131 Endmill
Material	Tungsten-Carbide
Flutes	4 (Center-Cutting)
Diameter	1/4"
Cutting length	3/4"
Spiral	30º (Right-Hand)

Appendix C Machining Experiments Measurements Uncertainty

Table C.1 Uncertainty of measurements in the machining experiments

	Error	Source
Feed Force (Dynamometer)	±2 N linearity error (±1% of FS) and ±2 N cross-talk error (±1% of FS)	KISTLER 5255B datasheet
Temperature (Infrared Camera)	±15 °C for temperatures between 100° C -200° C	Emissivity calibration and FLIR ThermoVision™ A20M datasheet
Tool Wear (Microscope)	± 4.376 µm (at a 95% confidence interval)	Winslow Eng. Model 560 Tool Analyzer calibration
Geometric Accuracy (Coordinate-Measuring Machine)	Uncertainty of Error, U(MPEp)=0.14 µm Uncertainty of error of indication, U(MPEe) = ± (0.4 + 1.43 x (Measured Length)/1000) µm	Mitutoyo MACH806 calibration
Vo (Pressure-Flowrate Characteristic)	Maximum Error: ±2.04 ml/min (±8.5% of FS) Average Error: ±0.62 ml/min (±2.6% of FS)	Pressure - Flow-rate calibration (CECOMP® DPG1000B4BARGON)
Va (Air Flowmeter)	±2.7 l/min (± 3% of FS)	GAS-VIEW FLM30-10 datasheet

Appendix D Particle Image Velocimetry Q-Criterion Flow Field

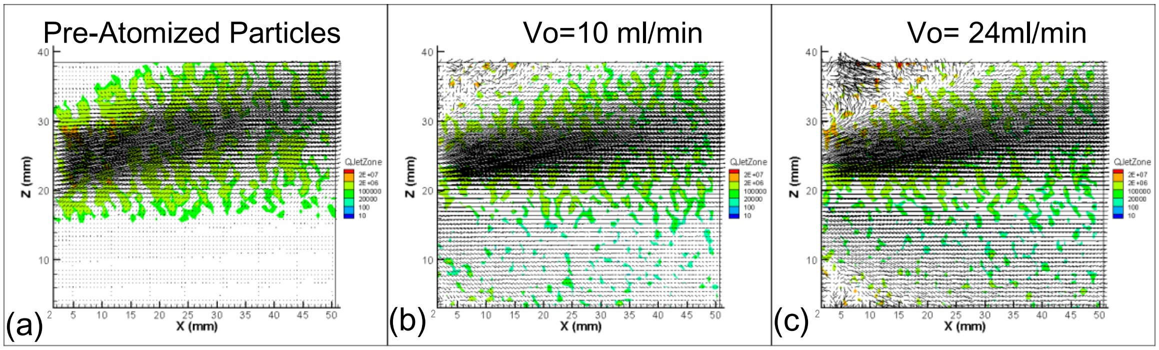

Figure D.1 Calculation of the second invariant of the velocity tensor, *Q*, in the flow field and velocity vectors when Va= 31 l/min:

(a) With pre-atomized particles; (b) Vo= 10 ml/min; (c) Vo= 24 ml/min

Appendix E Machining Geometric Accuracy (Set-2)

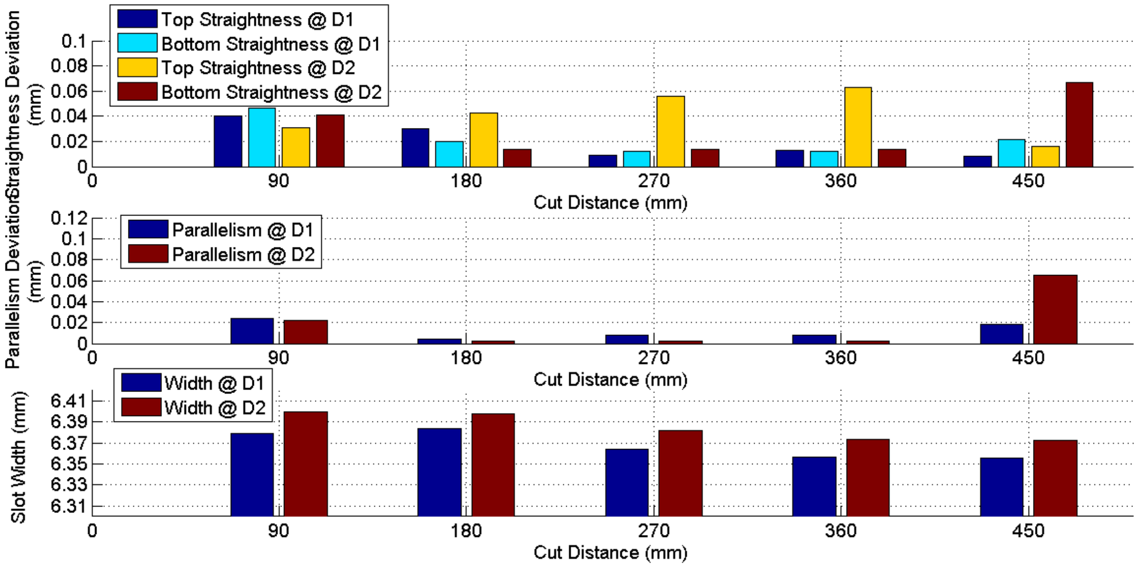

E.1: Geometric accuracy progression for condition 1 (Air Only, Max Va, Nozzle Position #8)

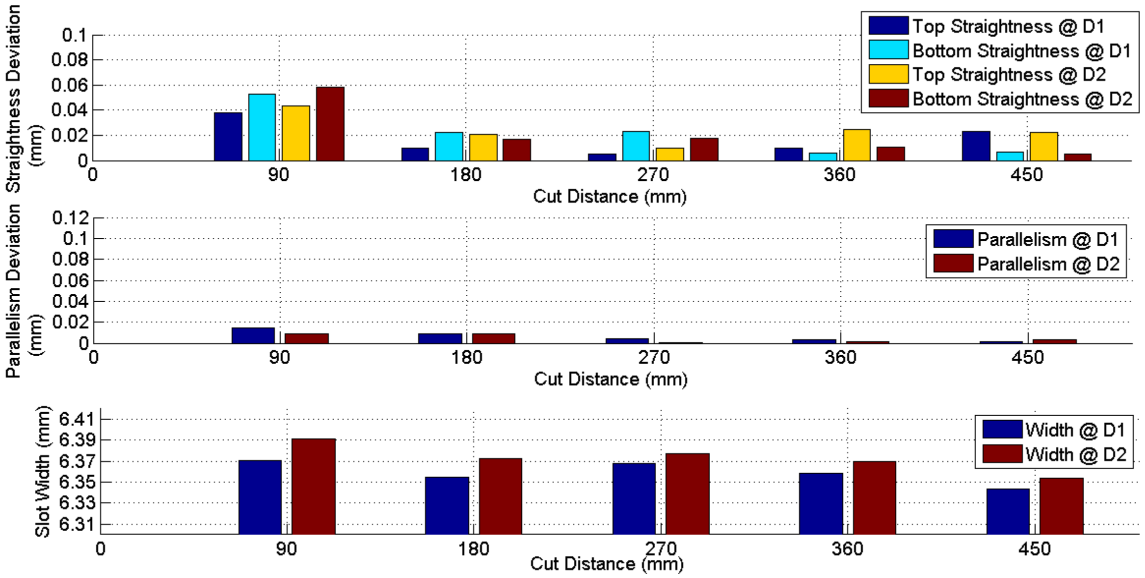

E.2: Geometric accuracy progression for condition 2 (Flood)

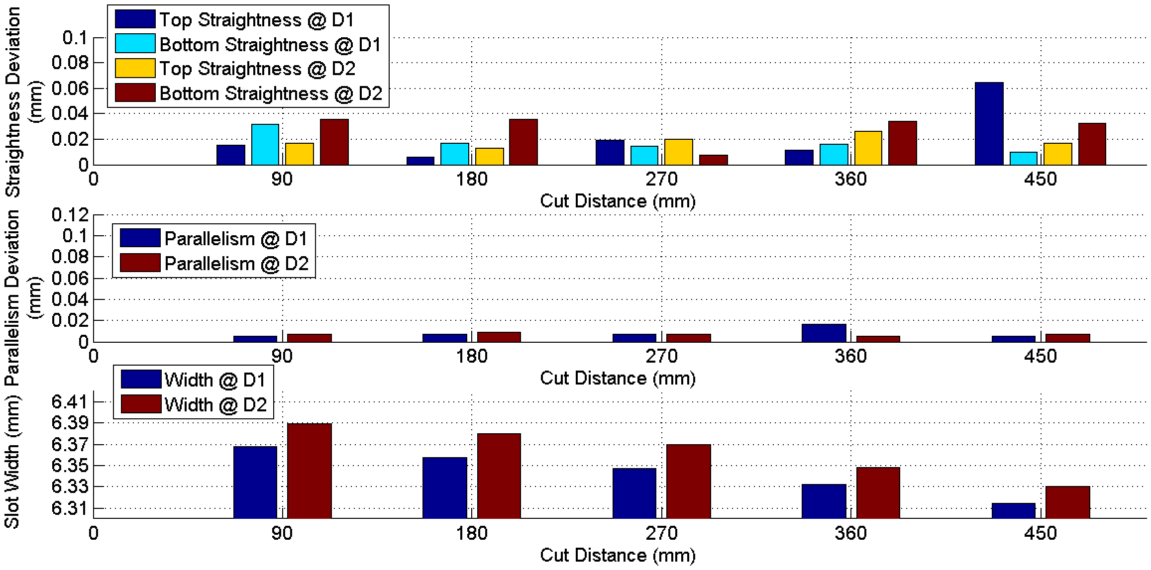

E.3: Geometric accuracy progression for condition 3 (Dry)

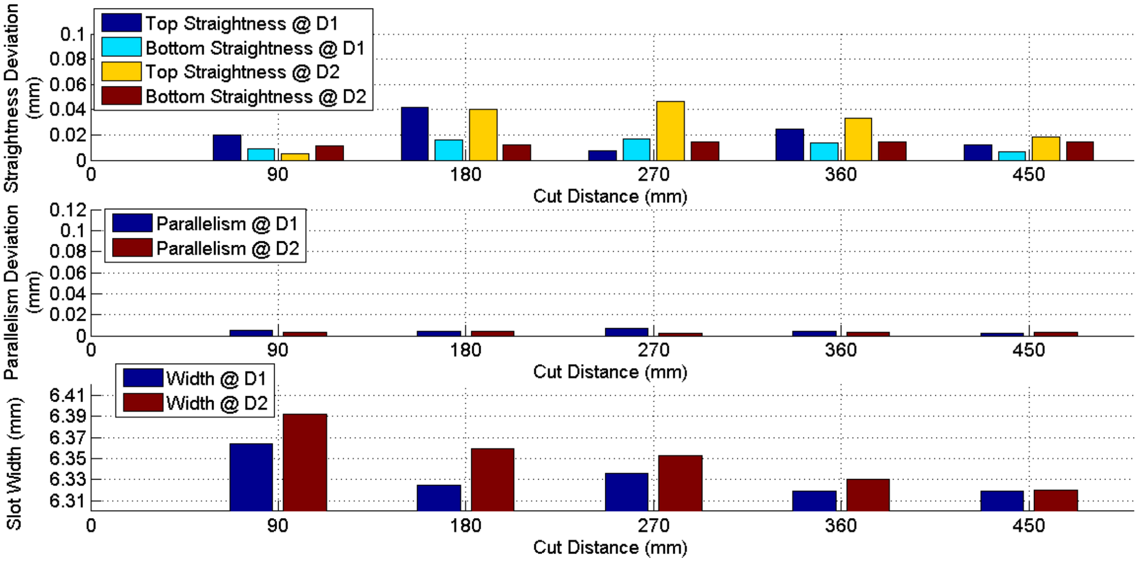

E.4: Geometric accuracy progression for condition 4 (Max Vo, Max Va, Nozzle Position #4)

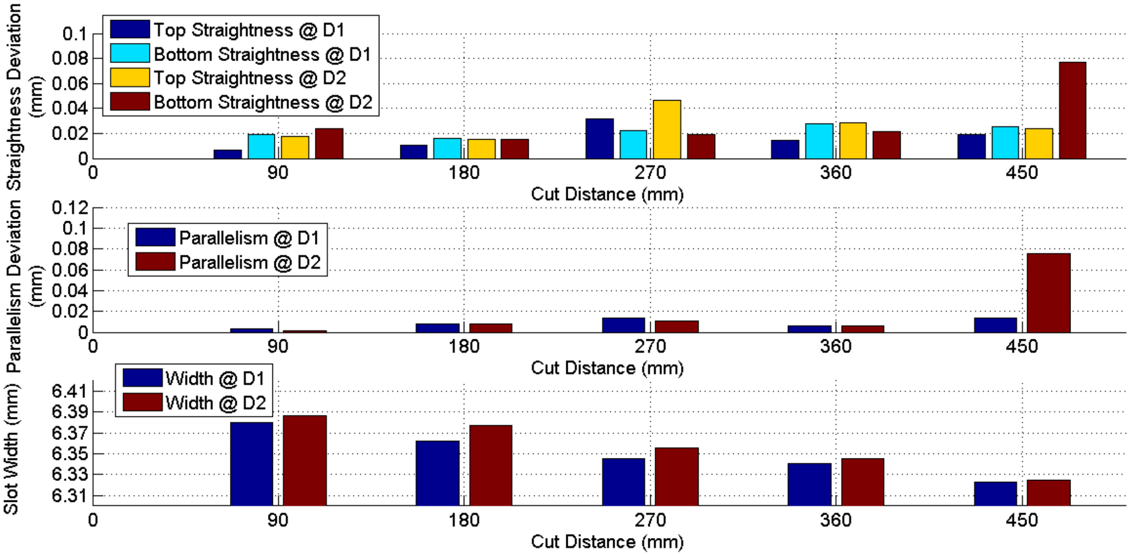

E.5 Geometric accuracy progression for condition 5 (Max Vo, Max Va, Nozzle Position #8)

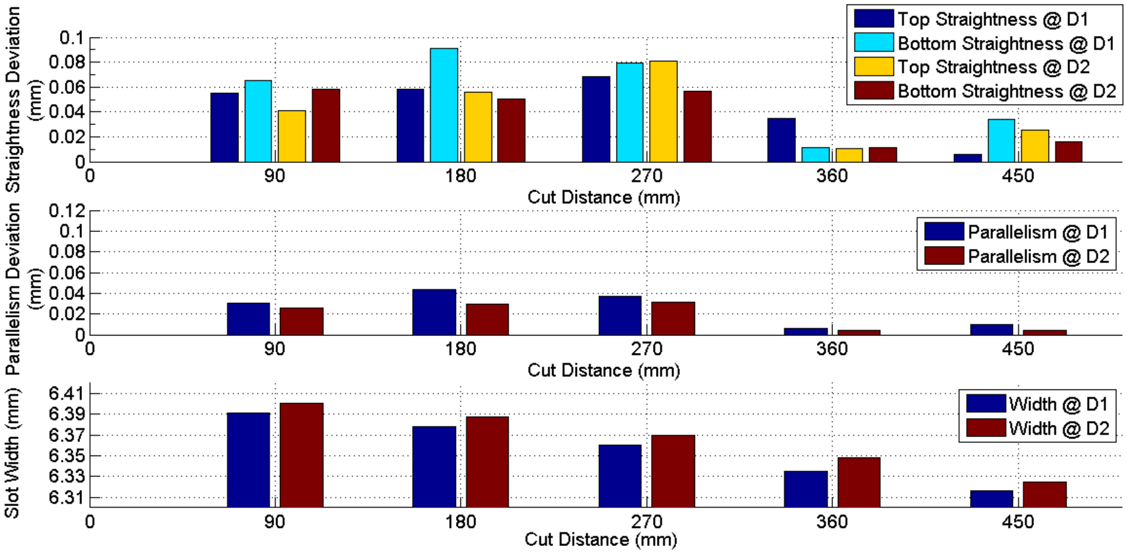

E.6: Geometric accuracy progression for condition 6 (Min Vo, Max Va, Nozzle Position #8)

References

1. Byrne, G., D. Dornfeld, and B. Denkena, *Advancing Cutting Technology.* CIRP Annals - Manufacturing Technology, 2003. **52**(2): p. 483-507.
2. Shaw, M.C., *Metal cutting principles*. Oxford series on advanced manufacturing, 31986, Oxford [Oxfordshire]; New York: Clarendon Press ; Oxford University Press.
3. Weinert, K., et al., *Dry machining and minimum quantity lubrication.* CIRP Annals - Manufacturing Technology, 2004. **53**(2): p. 511-537.
4. Klocke, F. and G. Eisenblaetter, *Dry cutting.* CIRP Annals - Manufacturing Technology, 1997. **46**(2): p. 519-526.
5. Khan, M.M.A., M.A.H. Mithu, and N.R. Dhar, *Effects of minimum quantity lubrication on turning AISI 9310 alloy steel using vegetable oil-based cutting fluid.* Journal of Materials Processing Technology, 2009. **209**(15-16): p. 5573-5583.
6. Liao, Y.S., H.M. Lin, and Y.C. Chen, *Feasibility study of the minimum quantity lubrication in high-speed end milling of NAK80 hardened steel by coated carbide tool.* International Journal of Machine Tools and Manufacture, 2007. **47**(11): p. 1667-1676.
7. López De Lacalle, L.N., et al., *Experimental and numerical investigation of the effect of spray cutting fluids in high speed milling.* Journal of Materials Processing Technology, 2006. **172**(1): p. 11-15.
8. Tawakoli, T., et al., *An experimental investigation of the effects of workpiece and grinding parameters on minimum quantity lubrication-MQL grinding.* International Journal of Machine Tools and Manufacture, 2009. **49**(12-13): p. 924-932.
9. McClure, T.F. and M.D. Gugger, *Microlubrication in metal machining operations.* Lubrication Engineering, 2002. **58**(12): p. 15-21.
10. Aoyama, T., *Development of a mixture supply system for machining with minimal quantity lubrication.* CIRP Annals - Manufacturing Technology, 2002. **51**(1): p. 289-292.

11. Wakabayashi, T., J.A. Williams, and I.M. Hutchings, *Action of gaseous lubricants in the orthogonal machining of an aluminum alloy by titanium nitride coated tools.* Surface and Coatings Technology, 1993. **57**(Compendex): p. 183-189.

12. Lefebvre, A.H., *Airblast atomization.* Progress in Energy and Combustion Science, 1980. **6**(3): p. 233-261.

13. Lefebvre, A., *Atomization and sprays*1989: Hemisphere Pub. Corp.

14. Rusk, T. and N. Rajagopalan, *Evaluation of aged and recycled metalworking fluids by the tapping torque.* 2003. **59**(2): p. 5.

15. Obikawa, T., Y. Kamata, and J. Shinozuka, *High-speed grooving with applying MQL.* International Journal of Machine Tools and Manufacture, 2006. **46**(14): p. 1854-1861.

16. Abukhshim, N.A., P.T. Mativenga, and M.A. Sheikh, *Heat generation and temperature prediction in metal cutting: A review and implications for high speed machining.* International Journal of Machine Tools and Manufacture, 2006. **46**(7-8): p. 782-800.

17. Li, K.M. and S.Y. Liang, *Modeling of cutting temperature in near dry machining.* Journal of Manufacturing Science and Engineering, Transactions of the ASME, 2006. **128**(2): p. 416-424.

18. Rowe, G.W. and E.F. Smart, *The importance of oxygen in dry machining of metal on a lathe.* British Journal of Applied Physics, 1963. **14**(12): p. 924-926.

19. Min, S., et al., *Investigation of adsorption behaviour of lubricants in near-dry machining.* Proceedings of the Institution of Mechanical Engineers, Part B: Journal of Engineering Manufacture, 2005. **219**(9): p. 665-671.

20. Wakabayashi, T., et al., *Tribological characteristics and cutting performance of lubricant esters for semi-dry machining.* CIRP Annals - Manufacturing Technology, 2003. **52**(1): p. 61-64.

21. Shen, B., A.J. Shih, and S.C. Tung, *Peer-reviewed: Application of nanofluids in minimum quantity lubrication grinding.* Tribology and Lubrication Technology, 2009. **65**(3): p. 73-80.
22. Bardeisky, A., H. Attia, and M. Elbestawi. *Evaluating of tool wear suppressive ability of lubricants used in minimum quantity of lubrication application in high speed machining of cast aluminum alloys*. 2005. Orlando, FL.
23. Bhowmick, S., M.J. Lukitsch, and A.T. Alpas, *Dry and minimum quantity lubrication drilling of cast magnesium alloy (AM60).* International Journal of Machine Tools and Manufacture, 2010. **50**(5): p. 444-457.
24. Kishawy, H.A., et al., *Effect of coolant strategy on tool performance, chip morphology and surface quality during high-speed machining of A356 aluminum alloy.* International Journal of Machine Tools and Manufacture, 2005. **45**(2): p. 219-227.
25. Clarens, A.F., et al. *Solubility of a metalworking lubricant in high-pressure CO₂ and effects in three machining processes*. 2009. Greenville, SC.
26. Sharma, V.S., M. Dogra, and N.M. Suri, *Cooling techniques for improved productivity in turning.* International Journal of Machine Tools and Manufacture, 2009. **49**(6): p. 435-453.
27. Heinemann, R., et al., *Effect of MQL on the tool life of small twist drills in deep-hole drilling.* International Journal of Machine Tools and Manufacture, 2006. **46**(1): p. 1-6.
28. Tasdelen, B., T. Wikblom, and S. Ekered, *Studies on minimum quantity lubrication (MQL) and air cooling at drilling.* Journal of Materials Processing Technology, 2008. **200**(1-3): p. 339-346.
29. Zeilmann, R.P. and W.L. Weingaertner, *Analysis of temperature during drilling of Ti6Al4V with minimal quantity of lubricant.* Journal of Materials Processing Technology, 2006. **179**(1-3): p. 124-127.

30. Bhowmick, S. and A.T. Alpas, *Minimum quantity lubrication drilling of aluminium-silicon alloys in water using diamond-like carbon coated drills.* International Journal of Machine Tools and Manufacture, 2008. **48**(12-13): p. 1429-1443.
31. Braga, D.U., et al., *Using a minimum quantity of lubricant (MQL) and a diamond coated tool in the drilling of aluminum-silicon alloys.* Journal of Materials Processing Technology, 2002. **122**(1): p. 127-138.
32. Yan, L., S. Yuan, and Q. Liu, *Influence of minimum quantity lubrication parameters on tool wear and surface roughness in milling of forged steel.* Chinese Journal of Mechanical Engineering, 2012. **25**(3): p. 419-429.
33. Rahman, M., A. Senthil Kumar, and S. Manzoor Ul, *Evaluation of minimal quantities of lubricant in end milling.* International Journal of Advanced Manufacturing Technology, 2001. **18**(4): p. 235-241.
34. Hwang, Y.K., C.M. Lee, and S.H. Park, *Evaluation of machinability according to the changes in machine tools and cooling lubrication environments and optimization of cutting conditions using Taguchi method.* International Journal of Precision Engineering and Manufacturing, 2009. **10**(3): p. 65-73.
35. Sun, J., et al., *Effects of Coolant Supply Methods and Cutting Conditions on Tool Life in End Milling Titanium Alloy.* Machining Science and Technology: An International Journal, 2006. **10**(3): p. 355 - 370.
36. Kamata, Y. and T. Obikawa, *High speed MQL finish-turning of Inconel 718 with different coated tools.* Journal of Materials Processing Technology, 2007. **192-193**: p. 281-286.
37. Varadarajan, A.S., P.K. Philip, and B. Ramamoorthy, *Investigations on hard turning with minimal cutting fluid application (HTMF) and its comparison with dry and wet turning.* International Journal of Machine Tools and Manufacture, 2002. **42**(2): p. 193-200.
38. Dhar, N.R., et al., *The influence of minimum quantity of lubrication (MQL) on cutting temperature, chip and dimensional accuracy in turning AISI-*

1040 steel. Journal of Materials Processing Technology, 2006. **171**(1): p. 93-99.

39. Dhar, N.R., M. Kamruzzaman, and M. Ahmed, *Effect of minimum quantity lubrication (MQL) on tool wear and surface roughness in turning AISI-4340 steel.* Journal of Materials Processing Technology, 2006. **172**(2): p. 299-304.
40. Jayal, A.D. and A.K. Balaji, *Effects of cutting fluid application on tool wear in machining: Interactions with tool-coatings and tool surface features.* Wear, 2009. **267**(9-10): p. 1723-1730.
41. Itoigawa, F., et al., *Effects and mechanisms in minimal quantity lubrication machining of an aluminum alloy.* Wear, 2006. **260**(3): p. 339-344.
42. Gaitonde, V.N., S.R. Karnik, and J.P. Davim, *Selection of optimal MQL and cutting conditions for enhancing machinability in turning of brass.* Journal of Materials Processing Technology, 2008. **204**(1-3): p. 459-464.
43. Sadeghi, M.H., et al., *Minimal quantity lubrication-MQL in grinding of Ti-6Al-4V titanium alloy.* International Journal of Advanced Manufacturing Technology, 2009. **44**(5-6): p. 487-500.
44. Kamata, Y., T. Obikawa, and J. Shinozuka, *Analysis of Mist Flow in MQL Cutting*, 2004. p. 339-344.
45. Obikawa, T., Y. Asano, and Y. Kamata, *Computer fluid dynamics analysis for efficient spraying of oil mist in finish-turning of Inconel 718.* International Journal of Machine Tools and Manufacture, 2009. **49**(12-13): p. 971-978.
46. Bailey, A.G., W. Balachandran, and T.J. Williams, *The rosin—rammler size distribution for liquid droplet ensembles.* Journal of Aerosol Science, 1983. **14**(1): p. 39-46.
47. Broniarz-Press, L., et al., *The atomization of water-oil emulsions.* Experimental Thermal and Fluid Science, 2009. **33**(6): p. 955-962.
48. *Dantec Dynamics*. Available from: www.dantecdynamics.com.

49. Tropea, C., A.L. Yarin, and J.F. Foss, *Springer Handbook of Experimental Fluid Mechanics* 2007.

50. Raffel, M., C.E. Willert, and J. Kompenhans, *Particle image velocimetry : a practical guide*. Experimental fluid mechanics 1998, Berlin; New York: Springer.

51. Liu, H.F., et al., *Effect of liquid jet diameter on performance of coaxial two-fluid airblast atomizers.* Chemical Engineering and Processing: Process Intensification, 2006. **45**(4): p. 240-245.

52. Batchelor, G.K., *An Introduction to Fluid Dynamics* 2000: Cambridge University Press.

53. Kolář, V., *Brief notes on vortex identification*, in *Proceedings of the 8th WSEAS international conference on fluid mechanics, 8th WSEAS international conference on Heat and mass transfer* 2011, World Scientific and Engineering Academy and Society (WSEAS): Puerto Morelos, Mexico. p. 23-28.

54. *HEXPRESSTM - Numeca International*. Available from: http://www.numeca.com.

55. Pope, S.B., *Turbulent Flows*2000: Cambridge University Press.

56. Yang, Z., et al., *A k-E [i.e. Kappa-Epsilon] calculation of transitional boundary layers* 1992: NASA.

57. Launder, B.E. and D.B. Spalding, *The numerical computation of turbulent flows.* Computer Methods in Applied Mechanics and Engineering, 1974. **3**(2): p. 269-289.

58. Lienhard, J.H., *A heat transfer textbook* 1981: Prentice-Hall.

59. *Minitab*. Available from: http://www.minitab.com.

60. Field, A., *Discovering Statistics Using SPSS* 2009: SAGE Publications.